

EUROPEAN ORGANISATION FOR NUCLEAR RESEARCH (CERN)



Phys. Rev. D 99 (2019) 072009
DOI: [10.1103/PhysRevD.99.072009](https://doi.org/10.1103/PhysRevD.99.072009)



CERN-EP-2018-331
May 7, 2019

Measurement of the $t\bar{t}Z$ and $t\bar{t}W$ cross sections in proton–proton collisions at $\sqrt{s} = 13$ TeV with the ATLAS detector

The ATLAS Collaboration

A measurement of the associated production of a top-quark pair ($t\bar{t}$) with a vector boson (W , Z) in proton–proton collisions at a center-of-mass energy of 13 TeV is presented, using 36.1 fb^{-1} of integrated luminosity collected by the ATLAS detector at the Large Hadron Collider. Events are selected in channels with two same- or opposite-sign leptons (electrons or muons), three leptons or four leptons, and each channel is further divided into multiple regions to maximize the sensitivity of the measurement. The $t\bar{t}Z$ and $t\bar{t}W$ production cross sections are simultaneously measured using a combined fit to all regions. The best-fit values of the production cross sections are $\sigma_{t\bar{t}Z} = 0.95 \pm 0.08_{\text{stat.}} \pm 0.10_{\text{syst.}} \text{ pb}$ and $\sigma_{t\bar{t}W} = 0.87 \pm 0.13_{\text{stat.}} \pm 0.14_{\text{syst.}} \text{ pb}$ in agreement with the Standard Model predictions. The measurement of the $t\bar{t}Z$ cross section is used to set constraints on effective field theory operators which modify the $t\bar{t}Z$ vertex.

1 Introduction

Properties of the top quark have been explored by the Large Hadron Collider (LHC) and previous collider experiments in great detail. The production cross sections of top-quark pairs and single top quarks, as well as the top-quark mass, spin correlations and W boson helicity fractions have all been measured. Other properties of the top quark are now becoming accessible, owing to the large center-of-mass energy and luminosity at the LHC. These include its coupling to the Higgs boson and electroweak neutral-current couplings, accessed by measurements of pair-produced top quarks in association with a Higgs boson [1–4] or a photon [5–8].

Measurements of top-quark pairs in association with a Z or W boson ($t\bar{t}Z$ and $t\bar{t}W$) provide a direct probe of the weak couplings of the top quark [9–11]. These couplings may be modified in the presence of physics beyond the Standard Model (BSM). Any deviations from the SM predictions due to BSM effects can be parameterized in a model-independent way using the framework of the Standard Model Effective Field Theory (SMEFT) [12–14]. If no deviations are observed, measurements of the $t\bar{t}Z$ and $t\bar{t}W$ production cross sections, $\sigma_{t\bar{t}Z}$ and $\sigma_{t\bar{t}W}$, can be used to set constraints on the weak couplings of the top quark in the SMEFT context. The $t\bar{t}Z$ and $t\bar{t}W$ processes were observed by ATLAS [15, 16] and CMS [17, 18], with measured cross sections compatible with the SM prediction. At 13 TeV, ATLAS analysed 3.2 fb^{-1} of data using the same-sign dimuon, trilepton and tetralepton channels, and measured $\sigma_{t\bar{t}Z} = 0.9 \pm 0.3 \text{ pb}$ and $\sigma_{t\bar{t}W} = 1.5 \pm 0.8 \text{ pb}$, while CMS analysed 35.9 fb^{-1} and measured $0.99^{+0.15}_{-0.13} \text{ pb}$ and $0.77^{+0.18}_{-0.16} \text{ pb}$, respectively.

The production of $t\bar{t}Z$ and $t\bar{t}W$ is often an important background in searches involving final states with multiple leptons and b -quarks. These processes also constitute an important background in measurements of the associated production of the Higgs boson with top quarks.

This paper presents measurements of the $t\bar{t}Z$ and $t\bar{t}W$ cross sections using proton–proton (pp) collision data at a center-of mass energy $\sqrt{s} = 13 \text{ TeV}$ corresponding to an integrated luminosity of 36.1 fb^{-1} , collected by the ATLAS detector in 2015 and 2016. The final states of top-quark pairs produced in association with a Z or a W boson contain up to four isolated, prompt leptons.¹ In this analysis, events with two opposite-sign (OS) or same-sign (SS) leptons, three leptons or four leptons are considered. The dominant backgrounds in these four channels are Z +jets and $t\bar{t}$, events with non-prompt or misidentified leptons, WZ , and ZZ production, respectively. An interpretation of the $t\bar{t}Z$ cross-section measurement in the SMEFT framework is also performed.

2 The ATLAS detector

The ATLAS detector [19] consists of three main subsystems: an inner tracking system, electromagnetic (EM) and hadronic calorimeters, and a muon spectrometer (MS). The inner detector (ID) consists of a high-granularity silicon pixel detector, including the insertable B-layer [20, 21], which is the innermost layer of the tracking system, and a silicon microstrip tracker, together providing precision tracking in

¹ In this paper, lepton is used to denote electron or muon, and prompt lepton is used to denote a lepton produced in a Z or W boson decay, or in the decay of a τ -lepton which arises from a Z or W boson decay.

the pseudorapidity² range $|\eta| < 2.5$, followed by a transition radiation tracker covering $|\eta| < 2.0$. All these systems are immersed in a 2 T magnetic field provided by a thin superconducting solenoid. The EM sampling calorimeter uses lead and liquid argon (LAr) and is divided into barrel ($|\eta| < 1.475$) and endcap ($1.375 < |\eta| < 3.2$) regions. Hadronic calorimetry is provided by a steel/scintillator-tile calorimeter, segmented into three barrel structures, in the range $|\eta| < 1.7$, and by two copper/LAr hadronic endcap calorimeters that cover the region $1.5 < |\eta| < 3.2$. The solid angle coverage is completed with forward copper/LAr and tungsten/LAr calorimeter modules, optimized for EM and hadronic measurements, respectively, covering the region $3.1 < |\eta| < 4.9$. The muon spectrometer measures the deflection of muons in the range $|\eta| < 2.7$ using multiple layers of high-precision tracking chambers located in toroidal magnetic fields. The field integral of the toroids ranges between 2.0 Tm and 6.0 Tm for most of the detector. The muon spectrometer is also instrumented with separate trigger chambers covering $|\eta| < 2.4$. A two-level trigger system [22], using custom hardware followed by a software-based trigger level, is used to reduce the event rate to an average of around 1 kHz for offline storage.

3 Data and simulated event samples

The data were collected with the ATLAS detector during 2015 and 2016 at a proton–proton (pp) collision energy of 13 TeV. The bunch spacing was 25 ns and the mean number of interactions per bunch crossing was 14 (25) in 2015 (2016). With strict data-quality requirements, the integrated luminosity considered corresponds to 36.1 fb^{-1} [23, 24].

Monte Carlo (MC) simulation samples are used to model the expected signal and background distributions in the different control, validation and signal regions described below. The heavy-flavor hadron decays involving b - and c -quarks, particularly important in this measurement, were modeled using EvtGEN [25] v1.2.0, except for those processes modeled using the SHERPA [26] generator, as described below. In all samples the top-quark mass was set to 172.5 GeV, and the Higgs boson mass was set to 125 GeV. The response of the detector to stable³ particles was emulated by a dedicated simulation [27] based either fully on GEANT [28], or on a faster simulation [29] using a parameterized calorimeter response and GEANT for other detector systems. To account for additional pp interactions from the same and nearby bunch crossings (pileup), minimum-bias interactions generated using PYTHIA v8.186 [30], referred to as PYTHIA 8 in the following, with the A2 [31] set of tuned MC parameters (A2 tune) were superimposed on the hard-scattering events.

Simulated events were corrected using per-event weights to describe the distribution of the average number of interactions per proton bunch-crossing as observed in data. All samples were processed through the same reconstruction software as used for the data. Simulated events were corrected so that the object identification, reconstruction and trigger efficiencies, energy scales and energy resolutions match those determined from data control samples.

The associated production of a top-quark pair with one or two vector bosons was generated at next-to-leading order (NLO) with MADGRAPH5_aMC@NLO [32] (referred to in the following as MG5_aMC) version 2.3.2 interfaced to PYTHIA 8. The cross sections for the $t\bar{t}Z$ and $t\bar{t}W$ processes at 13 TeV, computed including

² ATLAS uses a right-handed coordinate system with its origin at the nominal interaction point (IP) in the center of the detector and the z -axis along the beam pipe. The x -axis points from the IP to the center of the LHC ring, and the y -axis points upward. Cylindrical coordinates (r, ϕ) are used in the transverse plane, ϕ being the azimuthal angle around the z -axis. The pseudorapidity is defined in terms of the polar angle θ as $\eta = -\ln \tan(\theta/2)$.

³ A particle is considered stable if $c\tau \geq 1 \text{ cm}$.

NLO QCD and electroweak corrections using MG5_aMC, are $\sigma_{t\bar{t}Z} = 0.88$ pb and $\sigma_{t\bar{t}W} = 0.60$ pb with an uncertainty of $\sim 12\%$ [32–34]. The uncertainty is primarily due to higher-order QCD corrections, estimated by varying the renormalization (μ_R) and factorization (μ_F) scales. The γ^* contribution and the Z/γ^* interference were included in the $t\bar{t}Z$ samples, with the dilepton invariant mass ($m_{\ell\ell}$) required to be above 5 GeV. The NNPDF2.3NLO parton distribution function (PDF) set [35] was used in the matrix-element (ME) computation. The A14 [36] set of tuned MC parameters (A14 tune) was used together with the NNPDF2.3LO PDF set [37] in the parton shower.

The t -channel production of a single top quark in association with a Z boson (tZ) was generated at leading order (LO) using MG5_aMC v2.2.3 interfaced to PYTHIA v6.427 [38], referred to as PYTHIA 6 in the following, with the CTEQ6L1 [39] PDF set and the Perugia2012 [40] set of tuned MC parameters at NLO in QCD. The four-flavor scheme was used in the generation, and the sample was normalized using the cross section computed at NLO in QCD using MG5_aMC.

The production of a single top quark together with a W and a Z boson (tWZ) was generated with MG5_aMC v2.3.3 using the NNPDF3.0NLO PDF set [35]. The generation was performed at NLO in QCD using the five-flavor scheme. Diagrams containing a top-quark pair were removed to avoid overlap with the $t\bar{t}Z$ process. The parton shower was modeled by PYTHIA 8 with the A14 tune. The sample was normalized using the NLO cross section obtained from the generator.

Events containing Z or W bosons with associated jets were simulated using the SHERPA 2.2.1 event generator. The matrix-element calculation was performed using COMIX [41] and OPENLOOPS [42] for up to two partons at NLO and four partons at LO, and merged with the SHERPA parton shower [43] according to the ME+PS@NLO prescription [44]. The NNPDF3.0NNLO PDF set was used in conjunction with dedicated parton-shower tuning developed by the SHERPA authors. The $Z/W + \text{jets}$ samples were normalized to next-to-next-to-leading-order (NNLO) QCD cross sections for Z/W production calculated by the FEWZ program [45].

Diboson processes with four charged leptons (4ℓ), three charged leptons and one neutrino ($\ell\ell\ell\nu$) or two charged leptons and two neutrinos ($\ell\ell\nu\nu$) were simulated using the SHERPA 2.1.1 generator. The matrix elements included all diagrams with four electroweak vertices. They were calculated including up to three partons at LO, and the CT10 PDF set [46] was used in conjunction with a dedicated parton-shower tune developed by the SHERPA authors. The invariant mass of any two opposite-sign, same-flavor (OSSF) leptons was required to be greater than 5 GeV in the generated events.

The production of three massive vector bosons with subsequent leptonic decays of all three bosons was modeled at LO with the SHERPA 2.1.1 generator and the CT10 PDF set. Up to two additional partons were included in the matrix element at LO and the full NLO accuracy was used for the inclusive process.

Electroweak processes involving the vector-boson scattering (VBS) diagram and producing two same-sign leptons, two neutrinos and two partons were modeled using SHERPA 2.1.1 at LO accuracy and the CT10 PDF set. Processes of orders four and six in the electroweak coupling constant were considered, and up to one additional parton was included in the matrix element. Other VBS processes are found to be negligible in the analysis regions considered.

The PowHEG-Box [47–50] v2 generator with the NNPDF3.0NLO PDF set was used for the generation of $t\bar{t}$ events. The parton shower and the underlying event were simulated using PYTHIA 8 with the NNPDF2.3LO PDF set and the corresponding A14 tune. The h_{damp} parameter, which controls the transverse momentum of the first gluon emission beyond the Born configuration, was set to 1.5 times the top-quark mass. The $t\bar{t}$

samples were normalized to the NNLO cross-section predictions, including soft-gluon resummation to next-to-next-to-leading-logarithm order, as calculated with the `Top++2.0` [51] program.

Electroweak s -channel and t -channel single-top-quark events, and Wt final states, were generated with `POWHEG-Box v1`, and the parton shower modeled by `Pythia v6.428`. The `CT10` PDF set was used for s -channel production and Wt events, while for t -channel production the four-flavor scheme was used for the NLO matrix element calculations together with the fixed four-flavor PDF set `CT10f4`. Diagram removal was employed to remove the overlap between $t\bar{t}$ and Wt production [52]. The single-top-quark samples were normalized to the cross sections computed at NLO reported in Refs. [53, 54] for the s - and t -channels and at NLO with next-to-next-to-leading-logarithm soft-gluon corrections for Wt production [55].

Samples of $t\bar{t}$ events produced in association with a Higgs boson ($t\bar{t}H$) were generated using NLO matrix elements in `MG5_aMC` with the `NNPDF3.0NLO` PDF set and interfaced to `Pythia 8` for the modeling of the parton shower. Higgs boson production via gluon–gluon fusion (ggF) and vector-boson fusion (VBF) was generated using the `POWHEG-Box v2` generator with the `CT10` PDF set. The parton shower and underlying event were simulated using `Pythia 8` with the `CTEQ6L1` PDF set and `AZNLO` tune. Higgs boson production with a vector boson was generated at LO using `Pythia 8` with the `NNPDF2.3LO` PDF. All Higgs boson samples were normalized using theoretical calculations presented in Ref. [34].

The SM production of three and four top quarks was generated at LO with `MG5_aMC+Pythia 8`, using the `A14` tune together with the `NNPDF2.3LO` PDF set. The samples were normalized using cross sections computed at NLO [56, 57].

The events with a Z or W boson in association with a photon were simulated with up to three partons at LO using `SHERPA 2.1.1` (ME+PS mode) and the `CT10` PDF set. They were normalized to the LO cross section obtained from the generator. The $t\bar{t}\gamma$ process was generated at LO with `MG5_aMC+Pythia 8`, using the `A14` tune together with the `NNPDF2.3LO` PDF set and normalized to the NLO cross section. Events in the $t\bar{t}$ sample with radiated photons of high transverse momentum were vetoed to avoid overlap with those from the $t\bar{t}\gamma$ sample.

4 Object reconstruction

Electron candidates [58] are reconstructed from energy deposits (clusters) in the EM calorimeter that are associated with reconstructed tracks in the ID. Electrons are required to pass the ‘medium’ likelihood identification requirements described in Ref. [58]. In the SS dilepton channel, the ‘tight’ likelihood requirement is used instead. The electrons are also required to have transverse momentum $p_T > 7 \text{ GeV}$ and $|\eta_{\text{cluster}}| < 2.47$, where η_{cluster} is the pseudorapidity of the calorimeter energy deposit associated with the electron candidate. Candidates in the EM calorimeter barrel/endcap transition region $1.37 < |\eta_{\text{cluster}}| < 1.52$ are excluded.

Muon candidates are reconstructed from a fit to track segments in the various layers of the muon spectrometer, matched with tracks identified in the inner detector. Muons are required to have $p_T > 7 \text{ GeV}$ and $|\eta| < 2.5$ and to pass the ‘medium’ identification requirements defined in Ref. [59]. The ‘medium’ criteria include requirements on the numbers of hits in the ID and MS as well as a compatibility requirement between momentum measurements in the ID and MS. They provide a high efficiency and purity of selected muons. Electron candidates sharing a track with a muon candidate are removed.

To reduce the background due to non-prompt leptons from hadron decays, photon conversions or jets misidentified as leptons (labeled as “fake leptons” throughout this paper), electron and muon candidates are required to be isolated. In the OS dilepton and the tetralepton channels, as well as in those trilepton regions that target the $t\bar{t}Z$ process, the total sum of the track transverse momenta in a surrounding cone of size $\Delta R_\eta \equiv \sqrt{(\Delta\eta)^2 + (\Delta\phi)^2} = \min(10\text{ GeV}/p_T, r_{e,\mu})$, excluding the track of the candidate, is required to be less than 6% of the candidate p_T , where $r_e = 0.2$ and $r_\mu = 0.3$. In addition, the sum of the cluster transverse energies in the calorimeter within a cone of size $\Delta R_\eta = 0.2$ around any electron candidate, excluding energy deposits of the candidate itself, is required to be less than 6% of the candidate p_T .

In the SS dilepton channel and those trilepton regions targeting the $t\bar{t}W$ process, where the fake-lepton background is particularly important, tighter isolation requirements are imposed on candidate leptons. A multivariate discriminant is built to distinguish prompt leptons from leptons arising from heavy-hadron decays inside jets [1]. The discriminant uses information from charged-particle tracks in a cone around the lepton candidate. Jets are reconstructed from these tracks to obtain a track-jet, and the discriminant is constructed from information such as the angular distance between the lepton and the track-jet, the number of tracks in the track-jet and the ratio of the lepton candidate p_T to the track-jet p_T . The rejection factor obtained for leptons from b -hadron decays is about 20, while the prompt-lepton efficiency is about 85% (80%) for $p_T \sim 20\text{ GeV}$ and reaches a plateau of $\sim 98\%$ (96%) for muons (electrons) at high p_T . Simulated events are corrected to account for differences in the prompt-lepton tagging discriminant between data and simulation.

Another important background in the SS dilepton channel arises from electrons with misidentified charge. To suppress this background, another multivariate discriminant is used, which takes as inputs various track and cluster properties of the electron candidates [1]. The discriminant provides a 95% efficiency for electrons with correct charge reconstruction while achieving a rejection factor of ~ 17 for electrons with misidentified charge that pass the ‘tight’ likelihood identification requirement. Correction factors are applied to selected electrons to match the efficiency of the discriminant in simulation to that measured in data.

For both the electrons and muons, the longitudinal impact parameter of the associated track relative to the primary vertex,⁴ z_0 , is required to satisfy $|z_0 \sin \theta| < 0.5\text{ mm}$. The significance of the transverse impact parameter d_0 is required to satisfy $|d_0|/\sigma(d_0) < 5$ for electrons and $|d_0|/\sigma(d_0) < 3$ for muons, where $\sigma(d_0)$ is the uncertainty in d_0 .

Jets are reconstructed using the anti- k_t algorithm [60, 61] with radius parameter $R = 0.4$, starting from topological energy clusters in the calorimeters [62]. The effect of pileup on jet energies is accounted for by a jet-area-based correction [63] and the energy resolution of the jets is improved by using global sequential corrections [64]. Jets are calibrated to the hadronic energy scale using energy- and pseudorapidity-dependent calibration factors derived from data. Jets are accepted if they fulfill the requirements $p_T > 25\text{ GeV}$ and $|\eta| < 2.5$. To reduce the contribution from jets associated with pileup, jets with $p_T < 60\text{ GeV}$ and $|\eta| < 2.4$ are required to satisfy pileup rejection criteria (JVT), based on a multivariate combination of track-based variables [65].

Jets are tagged as likely to contain b -hadrons (b -tagged) with a multivariate discriminant making use of the long lifetime, large decay multiplicity, hard fragmentation and high mass of b -hadrons [66]. For the working point used in this analysis, the average efficiency for correctly tagging a b -jet is approximately 77%, as determined in simulated $t\bar{t}$ events. In simulation, the tagging algorithm gives a rejection factor of

⁴ A primary vertex candidate is defined as a vertex with at least two associated tracks, consistent with the beam collision region. The vertex candidate with the largest sum of squared transverse momenta of its associated tracks is taken as the primary vertex.

134 against light-quark and gluon jets, and 6.2 against charm-quark jets. The b -tagging efficiency and mistagging rates in simulation are corrected to reproduce those in data [66].

The missing transverse momentum $\mathbf{p}_T^{\text{miss}}$, with magnitude E_T^{miss} , is a measure of the transverse momentum imbalance due to particles escaping detection. It is computed [67] as the negative sum of the transverse momenta of all electrons, muons and jets and an additional soft term. The soft term is constructed from all tracks that are associated with the primary vertex but not with any lepton or jet. In this way, the E_T^{miss} is adjusted for the best calibration of the jets and the other identified objects, while maintaining pileup independence in the soft term [67, 68].

To prevent double-counting of electron energy deposits as jets, the closest jet within $\Delta R_y = 0.2$ of a reconstructed electron is removed, where $\Delta R_y \equiv \sqrt{(\Delta y)^2 + (\Delta\phi)^2}$ and y is the rapidity of the electron. If the nearest jet surviving the above criterion is within $\Delta R_y = 0.4$ of an electron, the electron is discarded to ensure that selected electrons are sufficiently separated from nearby jet activity. To reduce the background from muons originating from heavy-flavor particle decays inside jets, muons are removed if they are separated from the nearest jet by $\Delta R_y < 0.4$. However, if this jet has fewer than three associated tracks, the muon is kept and the jet is removed instead; this ensures that high-energy muons undergoing significant energy loss in the calorimeter are retained.

5 Event selection and background estimation

Table 1 lists the analysis channels and the targeted decay modes of the $t\bar{t}Z$ and $t\bar{t}W$ processes. Each channel is divided into multiple analysis regions in order to enhance the sensitivity to the signal. Simultaneous fits to the signal regions and dedicated control regions are performed to extract the cross sections for $t\bar{t}Z$ and $t\bar{t}W$ production.

Table 1: List of $t\bar{t}W$ and $t\bar{t}Z$ decay modes and analysis channels targeting them. The symbols b and ν denote a bottom quark or antiquark and neutrino or antineutrino, respectively, with charge conjugation implied.

Process	$t\bar{t}$ decay	Boson decay	Channel
$t\bar{t}W$	$(\ell^\pm \nu b)(q\bar{q}b)$	$\ell^\pm \nu$	SS dilepton
	$(\ell^\pm \nu b)(\ell^\mp \nu b)$	$\ell^\pm \nu$	Trilepton
$t\bar{t}Z$	$(q\bar{q}b)(q\bar{q}b)$	$\ell^+ \ell^-$	OS dilepton
	$(\ell^\pm \nu b)(q\bar{q}b)$	$\ell^+ \ell^-$	Trilepton
	$(\ell^\pm \nu b)(\ell^\mp \nu b)$	$\ell^+ \ell^-$	Tetralepton

Only events collected using single-electron or single-muon triggers are accepted. Events are required to have at least one reconstructed primary vertex. In all regions considered, at least one reconstructed lepton with $p_T > 27 \text{ GeV}$ is required to match ($\Delta R_\eta < 0.15$) a lepton with the same flavor reconstructed by the trigger algorithm. Four channels are defined: same-sign dilepton, opposite-sign dilepton, trilepton and tetralepton.

The shapes of background distributions containing prompt leptons are modeled by simulation. The normalizations for the WZ and ZZ processes, as well as the production of a Z boson in association with heavy-flavor (HF) jets, are taken from data control regions as defined in this section and which are included in the fit discussed in Section 7. The yields in these data control regions are extrapolated to the signal

regions using simulation. Systematic uncertainties in the extrapolation are taken into account in the overall uncertainty in the background estimate.

The contribution from events containing an electron with misidentified charge (referred to as “charge-flip” in the following) is estimated from data. The charge-flip probability is extracted in events containing a pair of electrons with $m_{\ell\ell}$ close to the Z boson mass. It is parameterized in p_T and η and is found to range from around 0.01% to 2%, increasing with p_T and η , for electrons passing the identification and isolation criteria applied in the SS dilepton channel. The probability is extracted by maximizing a likelihood which relates the number of events in which the two electrons have the same charge to the total number of observed events. The background contribution from events other than charge-flip electrons in the same-sign region is estimated from a sideband of the $m_{\ell\ell}$ distribution and subtracted before performing the likelihood fit.

The charge-flip background contribution in any SS dilepton region is estimated by constructing a control region with identical requirements, but without any requirement on the lepton charge, and applying the appropriate charge-flip probabilities.

Background sources involving one or more fake leptons are modeled using data events from dedicated regions. For the SS dilepton (2ℓ -SS) and trilepton channels the fake-lepton background is estimated using the matrix method [69]. The matrix method makes use of events with the same selection as the region of interest, but for which the electron identification criteria are relaxed to the ‘loose’ likelihood requirement of Ref. [58], and neither electrons nor muons are required to be isolated. These leptons are referred to as loose leptons, whereas leptons satisfying the full set of identification and isolation criteria of Section 4 are referred to as tight leptons. The fake-lepton background in any region of interest is obtained from the aforementioned events using efficiencies for prompt and fake leptons to satisfy the tight criteria.

The lepton efficiencies are extracted in control regions with a likelihood fit, by using the model of the matrix method, and assuming that the number of events with two fake leptons is negligible. The control regions are defined in dilepton events, separately for events with exactly one b -tagged jet and ≥ 2 b -tagged jets. The prompt lepton efficiencies are measured in inclusive OSSF events, while fake-lepton efficiencies are measured in events with same-sign leptons. Both the prompt and fake-lepton efficiencies are parameterized as a function of the lepton p_T . The measurement of fake-lepton efficiencies is performed after subtracting the estimated contribution from charge-flip events. Contributions from processes with two prompt same-sign leptons or one real lepton and a photon conversion (arising mainly from $t\bar{t}\gamma$ production) are estimated from simulation and are also subtracted. The prompt and fake-lepton efficiencies are extracted separately for the regions targeting $t\bar{t}Z$ and those targeting $t\bar{t}W$, due to the different lepton isolation requirements applied in the two sets of regions.

In the tetralepton channel, the matrix method is not used due to the small number of events in data with four selected leptons. Instead, the contribution from backgrounds containing fake leptons is estimated from simulation and corrected with scale factors determined in control regions. The contributions from events containing a photon conversion (denoted by $\gamma + X$) in the SS dilepton and trilepton channels are estimated from simulation and scaled with these correction factors, obtained separately for lepton type and origin.

5.1 Opposite-sign dilepton analysis

The OS dilepton analysis targets the $t\bar{t}Z$ process, where both top quarks decay hadronically and the Z boson decays to a pair of leptons (electrons or muons). Events are required to have exactly two OSSF leptons. Events with additional isolated leptons are rejected. The invariant mass of the lepton pair is required to be

in the Z boson mass window, $|m_{\ell\ell} - m_Z| < 10$ GeV. The leading (subleading) lepton is required to have a transverse momentum of at least 30 (15) GeV.

The OS dilepton analysis is affected by large backgrounds from Z -jets or $t\bar{t}$ production, both characterized by the presence of two leptons. In order to improve the signal-to-background ratio and constrain these backgrounds from data, three separate analysis regions are considered, depending on the number of jets (n_{jets}) and number of b -tagged jets ($n_{b\text{-tags}}$): 2ℓ -Z-5j2b, 2ℓ -Z-6j1b and 2ℓ -Z-6j2b. The signal region requirements are summarized in Table 2. In signal region 2ℓ -Z-5j2b, exactly five jets are required, of which at least two must be b -tagged. In 2ℓ -Z-6j1b (2ℓ -Z-6j2b), at least six jets are required with exactly one (at least two) being b -tagged jets.

Table 2: Summary of the event selection requirements in the OS dilepton signal regions.

Variable	2ℓ -Z-6j1b	2ℓ -Z-5j2b	2ℓ -Z-6j2b
Leptons	= 2, same flavor and opposite sign		
$m_{\ell\ell}$		$ m_{\ell\ell} - m_Z < 10$ GeV	
p_T (leading lepton)		> 30 GeV	
p_T (subleading lepton)		> 15 GeV	
$n_{b\text{-tags}}$	1	≥ 2	≥ 2
n_{jets}	≥ 6	5	≥ 6

In order to separate signal from background, boosted decision trees (BDTs) are used. The BDTs are constructed and trained separately for each region against all the contributing backgrounds, using as input 15, 14 and 17 variables for 2ℓ -Z-6j1b, 2ℓ -Z-5j2b and 2ℓ -Z-6j2b, respectively. Fourteen of the variables are common to the three regions. The details of the variables used are given in Table 11 in the Appendix. In all three regions, the variables with the largest discriminative power are found to be:

- the η of the dilepton system,
- the scalar sum of transverse momenta of all jets divided by the sum of their energies,
- the first Fox–Wolfram moment H_1 [70].

Each of the signal regions is further divided into 19 equal-size bins of the BDT distribution. To avoid relying on simulation for the normalization of Z -HF jet production, the Z -jets background is constrained by using events with low values of the BDT discriminant. The simulated Z -jets background is split into three components, $Z+0\text{HF}$, $Z+1\text{HF}$ and $Z+2\text{HF}$, depending on the number of reconstructed jets which are matched to a generator-level b - or c -hadron (heavy-flavor, or HF jets). The normalization factors of the $Z+1\text{HF}$ and $Z+2\text{HF}$ components of the Z -jets background are determined from the fit to data, as described in Section 7, while the normalization of the $Z+0\text{HF}$ component is taken from simulation.

A data-driven method is used to estimate the $t\bar{t}$ background in the OS dilepton signal regions. Control regions are defined which are identical to the signal regions, except that the requirement of two leptons with the same flavor and opposite sign is replaced by the requirement of two leptons with different flavors and opposite sign. In this manner, three regions enriched in $t\bar{t}$ background are obtained. The number of $t\bar{t}$ events in each same-flavor dilepton region is estimated from corresponding opposite-flavor regions, corrected for non- $t\bar{t}$ backgrounds and differences in contributions from leptonic τ -lepton decays. This procedure is

applied to each bin of the distribution under consideration. Figure 1 shows the BDT distributions for the $t\bar{t}$ control regions. Agreement between the data and the expectation is observed.

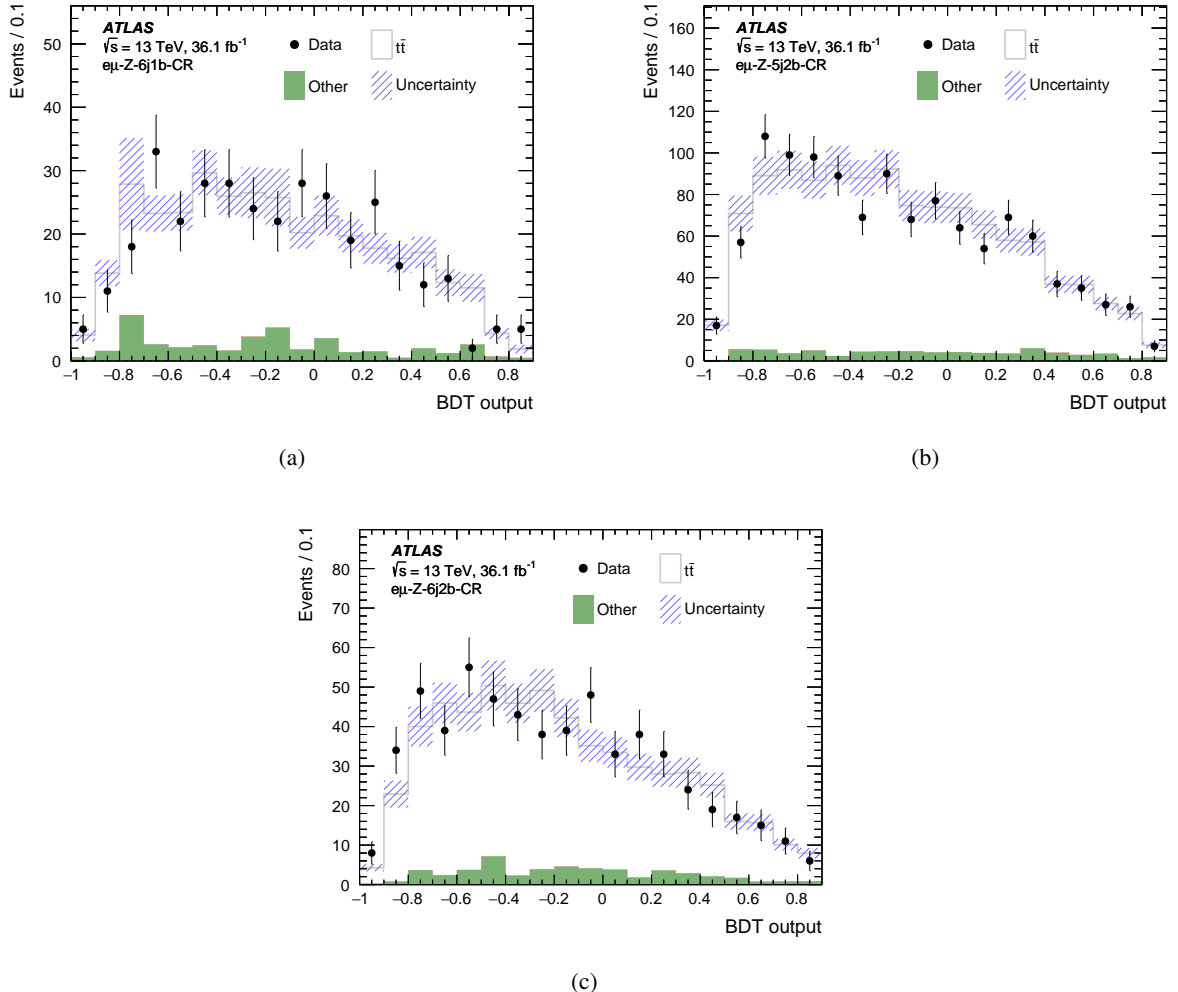


Figure 1: The BDT distributions for the $t\bar{t}$ control regions (a) 2 ℓ -Z-6j1b, (b) 2 ℓ -Z-5j2b, (c) 2 ℓ -Z-6j2b. The shaded band represents the total uncertainty. The ‘Other’ background contains SM processes with small cross sections producing two opposite-sign prompt leptons, including the $t\bar{t}Z$ process, whose contribution is negligible.

5.2 Same-sign dilepton analysis

The SS dilepton signal regions target the $t\bar{t}W$ process. Events are required to have two lepton candidates with the same sign and $p_T > 27 \text{ GeV}$. The scalar sum of the p_T of selected leptons and jets, H_T , is required to be above 240 GeV . Events containing additional loose leptons (with $p_T > 7 \text{ GeV}$) are vetoed. Twelve signal regions are defined in total, categorized by the number of b -tagged jets (one or ≥ 2) as well as the charge and the flavor of the selected leptons. The signal regions are denoted by 2 ℓ -SSp-1b, 2 ℓ -SSm-1b, 2 ℓ -SSp-2b and 2 ℓ -SSm-2b, where “p” or “m” indicates the charge of the selected leptons. Considering separate signal regions for positive and negative charges of the leptons increases the sensitivity

of the analysis since $t\bar{t}W$ events are preferentially produced with positively charged W bosons, while the fake-lepton background and other processes such as $t\bar{t}Z$ and $t\bar{t}H$ are expected to be charge symmetric.

The event selection requirements in the SS dilepton regions are summarized in Table 3. The presence of at least four jets and $E_T^{\text{miss}} > 40 \text{ GeV}$ is required in all signal regions except $2\mu\text{-SSp-}2b$ and $2\mu\text{-SSm-}2b$. In these regions, the E_T^{miss} requirement is loosened to $E_T^{\text{miss}} > 20 \text{ GeV}$, and at least two jets are required. In the $2e$ and 2μ signal regions, events containing a pair of leptons whose invariant mass is within 10 GeV of the Z boson mass are vetoed.

Table 3: Summary of the event selection requirements in the SS dilepton signal regions.

Requirement	$2\ell\text{-SS(p,m)-}1b$	$2e\text{-SS(p,m)-}2b$	$e\mu\text{-SS(p,m)-}2b$	$2\mu\text{-SS(p,m)-}2b$
$n_b\text{-tags}$	=1	≥ 2	≥ 2	≥ 2
E_T^{miss}	$> 40 \text{ GeV}$	$> 40 \text{ GeV}$	$> 40 \text{ GeV}$	$> 20 \text{ GeV}$
H_T		$> 240 \text{ GeV}$		
p_T (leading lepton)		$> 27 \text{ GeV}$		
p_T (subleading lepton)		$> 27 \text{ GeV}$		
n_{jets}	≥ 4	≥ 4	≥ 4	≥ 2
Z veto		$ m_{\ell\ell} - m_Z > 10 \text{ GeV}$ in the $2e$ and 2μ regions		

The control regions used to measure the fake-lepton efficiencies, as explained at the beginning of this section, are defined to be orthogonal to the SS dilepton signal regions: either the E_T^{miss} , H_T or jet multiplicity requirements of the signal regions are not satisfied. The $t\bar{t}W$ signal contribution in the control regions where both leptons satisfy the “tight” criteria is found to be non-negligible. To enhance the sensitivity of the analysis, the latter regions are also included in the final fit used to measure the $t\bar{t}W$ cross section, as discussed in Section 7. These six regions are further split according to the charge of the leptons, and the resulting twelve regions are denoted by $2\ell\text{-SS(p,m)-(1,2)b-CR}$, following the same notation as for the signal regions defined above. In each control region, both leptons are required to have $p_T > 27 \text{ GeV}$, and at least one (two) jets are required in the $1b$ ($2b$) regions. In addition, events containing a pair of leptons whose invariant mass is compatible with the Z boson mass are vetoed. The largest contamination from $t\bar{t}W$ is found to be 25%, in the region $2\mu\text{-SSp2b-CR}$.

The dominant background in the $2\ell\text{-SS}$ signal regions arises from events containing fake leptons. Backgrounds from the production of prompt leptons with correctly identified charge come primarily from $t\bar{t}H$ and WZ production. The charge-flip background is also significant in signal regions with two electrons. In regions with two muons, this background is negligible as the probability of misidentifying the charge of a muon in the relevant p_T range is very small. To validate the charge-flip background, a validation region called $2e\text{-SS-}1b\text{-VR}$ is constructed similarly to the $2e\text{-SS}$ signal regions, except that the number of jets is required to be between one and three, to ensure orthogonality with the signal regions. The requirement on H_T is also removed, exactly one jet is required to be b -tagged, and the invariant mass of the lepton pair is required to be greater than 15 GeV . The distributions of $m_{\ell\ell}$ and the leading lepton p_T are shown in Figure 2, demonstrating good modeling of the charge-flip background.

Figure 3 shows the distributions of H_T , E_T^{miss} and the subleading lepton p_T , for the control regions $2e\text{-SS-}2b\text{-CR}$, $e\mu\text{-SS-}1b\text{-CR}$ and $2\mu\text{-SS-}1b\text{-CR}$. The data and the expectation agree well, demonstrating the validity of the description of the fake-lepton background determined by the matrix method.

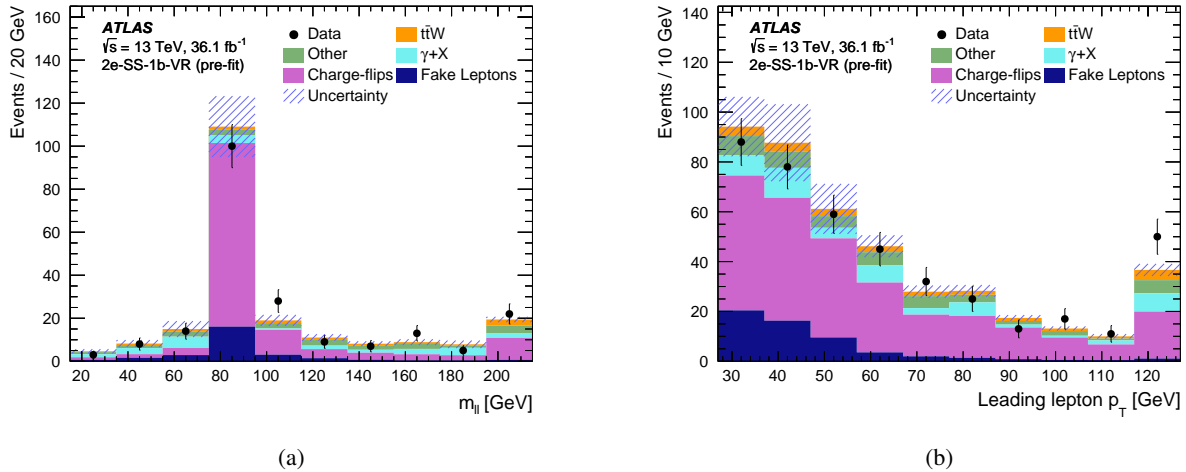


Figure 2: Distributions in the 2e-SS-1b-VR validation region: (a) the invariant mass $m_{\ell\ell}$ of the lepton pair and (b) leading lepton transverse momentum p_T . The shaded band represents the total uncertainty. The ‘Other’ background contains SM processes with small cross sections producing two same-sign prompt leptons. The last bin in each of the distributions includes the overflow.

To facilitate comparisons of data with the expectation, three regions 2e-SS, $e\mu$ -SS and 2μ -SS are formed by combining all the same-sign signal regions corresponding to a given lepton flavor combination. The distributions of E_T^{miss} and the number of jets for these three regions are shown in Figure 4.

5.3 Trilepton analysis

Eight signal regions with exactly three leptons are considered, four of them targeting the $t\bar{t}Z$ and four targeting the $t\bar{t}W$ process, as defined in Tables 4 and 5, respectively. The regions are divided into two groups depending on whether or not a pair of OSSF leptons with invariant mass within 10 GeV of the Z boson mass is present. The signal regions are further categorized according to jet and b -tagged jet multiplicities.

The four signal regions in the first group are sensitive to $t\bar{t}Z$. In the 3ℓ -Z-1b4j region, at least four jets are required, exactly one of which is b -tagged. In the 3ℓ -Z-2b3j region, exactly three jets with at least two b -tagged jets are required. In the 3ℓ -Z-2b4j region, at least four jets are required, of which at least two are b -tagged. In the 3ℓ -noZ-2b4j region, targeting events with an off-shell Z^* or γ^* , at least four jets are required, of which at least two are b -tagged; no OSSF lepton pair is allowed in the Z boson mass window. The sum of the lepton charges must be ± 1 .

The remaining four trilepton signal regions target the $t\bar{t}W$ process. These regions require two or three jets and veto events that contain an OSSF pair of leptons whose invariant mass is within 10 GeV of the Z boson mass. In the first two regions, 3ℓ p-noZ-2b2j and 3ℓ m-noZ-2b2j, at least two jets are required to be b -tagged. In the other two regions, 3ℓ p-noZ-1b2j and 3ℓ m-noZ-1b2j, exactly one jet is required to be b -tagged. The sum of lepton charges is required to be +1 (-1) in 3ℓ p-noZ-2b2j and 3ℓ p-noZ-1b2j (3ℓ m-noZ-2b2j and 3ℓ m-noZ-1b2j). In regions 3ℓ p-noZ-1b2j and 3ℓ m-noZ-1b2j, $H_T > 240$ GeV is also required. The signal region definitions for the trilepton channel are summarized in Tables 4 and 5 for the signal regions targeting $t\bar{t}Z$ and $t\bar{t}W$, respectively.

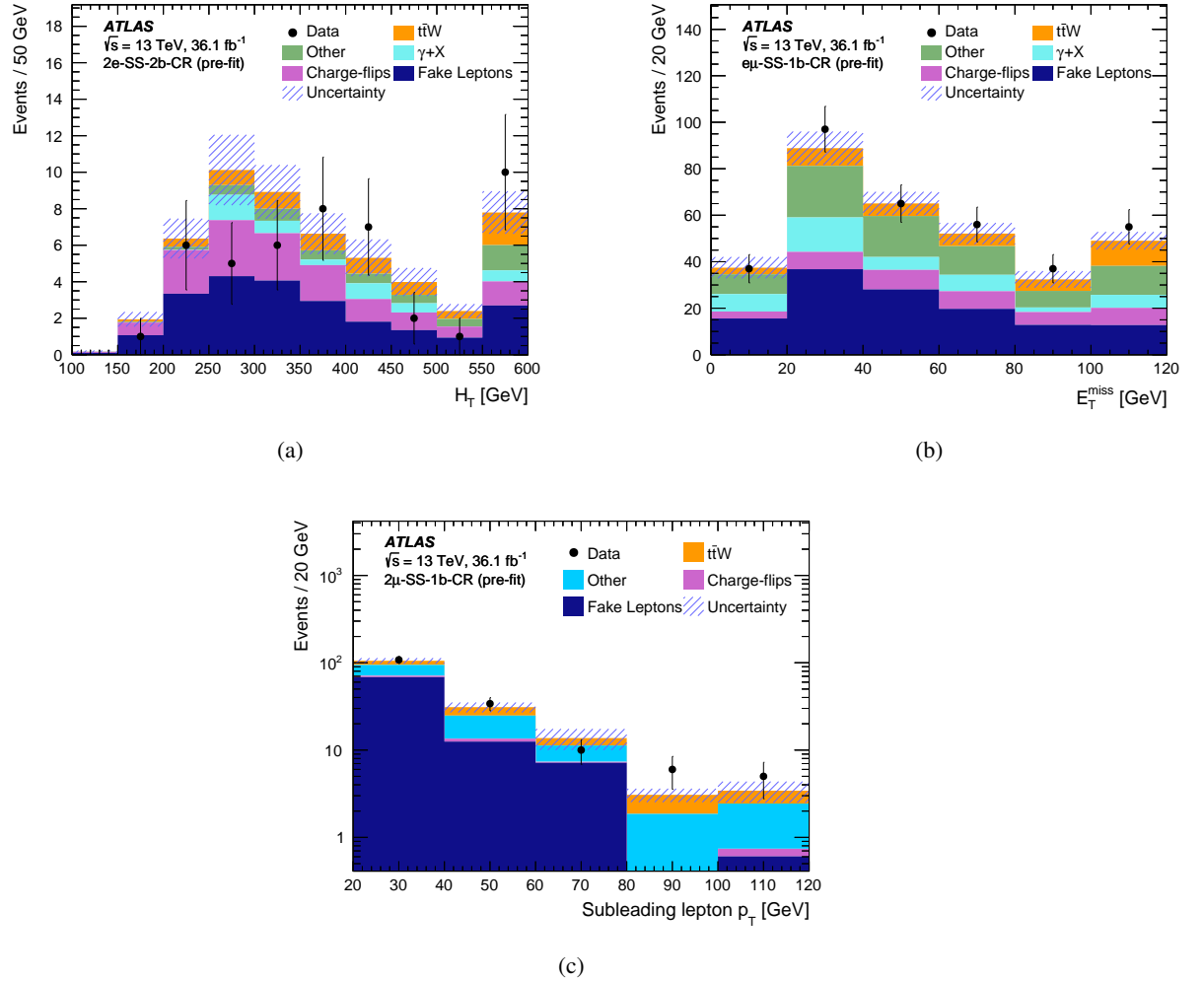


Figure 3: Distributions in fake-lepton control regions: (a) scalar sum of transverse momenta of leptons and jets, H_T , in the $2e$ -SS- $2b$ -CR region, (b) missing transverse momentum, E_T^{miss} , in the $e\mu$ -SS- $1b$ -CR region and (c) subleading lepton transverse momentum, p_T , in the 2μ -SS- $1b$ -CR region. The shaded band represents the total uncertainty. The ‘Other’ background contains SM processes with small cross sections producing two same-sign prompt leptons. The last bin in each of the distributions includes the overflow.

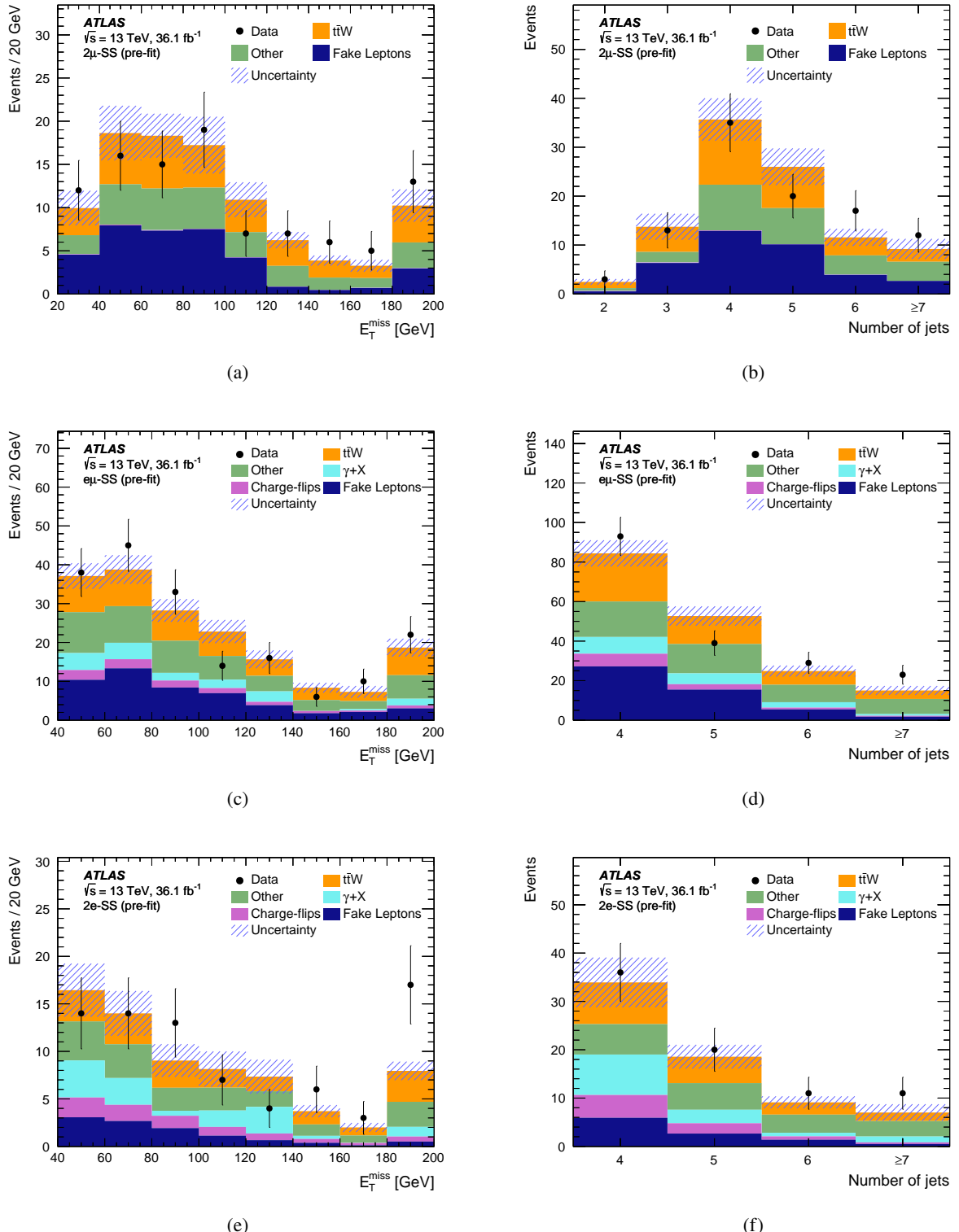


Figure 4: Distributions in the 2μ -SS, $e\mu$ -SS and $2e$ -SS regions of (a) (c) (e) the missing transverse momentum E_T^{miss} and (b) (d) (f) the jet multiplicity. The shaded band represents the total uncertainty. The ‘Other’ background contains SM processes with small cross sections producing two same-sign prompt leptons. The last bin in each of the distributions includes the overflow.

The dominant backgrounds in the 3ℓ -Z-1b4j, 3ℓ -Z-2b3j and 3ℓ -Z-2b4j signal regions arise from diboson production, the production of a single top quark in association with a Z boson (tZ and tWZ) and Z+jets production with a fake lepton.

Table 4: Summary of event selection requirements in the trilepton signal regions targeting the $t\bar{t}Z$ process.

Variable	3ℓ -Z-1b4j	3ℓ -Z-2b3j	3ℓ -Z-2b4j	3ℓ -noZ-2b4j
Leading lepton			$p_T > 27 \text{ GeV}$	
Other leptons			$p_T > 20 \text{ GeV}$	
Sum of lepton charges			± 1	
Z requirement (OSSF pair)		$ m_{\ell\ell} - m_Z < 10 \text{ GeV}$		$ m_{\ell\ell} - m_Z > 10 \text{ GeV}$
n_{jets}	≥ 4	3	≥ 4	≥ 4
$n_{b\text{-tags}}$	1	≥ 2	≥ 2	≥ 2

Table 5: Summary of event selection requirements in the trilepton signal regions targeting the $t\bar{t}W$ process.

Variable	$3\ell p$ -noZ-2b2j	$3\ell m$ -noZ-2b2j	$3\ell p$ -noZ-1b2j	$3\ell m$ -noZ-1b2j
All leptons			$p_T > 27 \text{ GeV}$	
Z veto (OSSF pair)			$ m_{\ell\ell} - m_Z > 10 \text{ GeV}$	
n_{jets}			2 or 3	
H_T	–			$> 240 \text{ GeV}$
Sum of lepton charges	+1	-1	+1	-1
$n_{b\text{-tags}}$	≥ 2	≥ 2	1	1

A control region is used to determine the normalization of the WZ +jets background in data. Exactly three leptons are required, at least one pair of which must be an OSSF pair with an invariant mass within 10 GeV of the Z boson mass. There must be exactly three jets, none of which pass the b -tagging requirement. This region is referred to as 3ℓ -WZ-CR and it is included in the fit. Distributions comparing data with SM predictions in 3ℓ -WZ-CR are shown in Figure 5, demonstrating good modeling of the WZ background.

Figure 6 shows the leading lepton p_T and E_T^{miss} for events belonging to any of the four trilepton regions targeting $t\bar{t}W$. Distributions of the number of jets, the p_T and mass of the reconstructed Z boson candidate in the signal region most sensitive to $t\bar{t}Z$, 3ℓ -Z-2b4j, are shown in Figure 7.

5.4 Tetralepton analysis

The tetralepton channel targets the $t\bar{t}Z$ process for the case where both W bosons, resulting from top-quark decays, and the Z boson decay leptonically. Events with two pairs of opposite-sign leptons are selected, and at least one pair must have the same flavor. The OSSF lepton pair with reconstructed invariant mass closest to m_Z is attributed to the Z boson decay and denoted in the following by Z_1 . The two remaining leptons are used to define Z_2 . The signal region definitions for the tetralepton channel are summarized in Table 6. Four signal regions are defined according to the relative flavor of the two Z_2 leptons, different flavor (DF) or same flavor (SF), and the number of b -tagged jets: one, or at least two (1b, 2b). The signal regions are thus 4ℓ -DF-1b, 4ℓ -DF-2b, 4ℓ -SF-1b and 4ℓ -SF-2b.

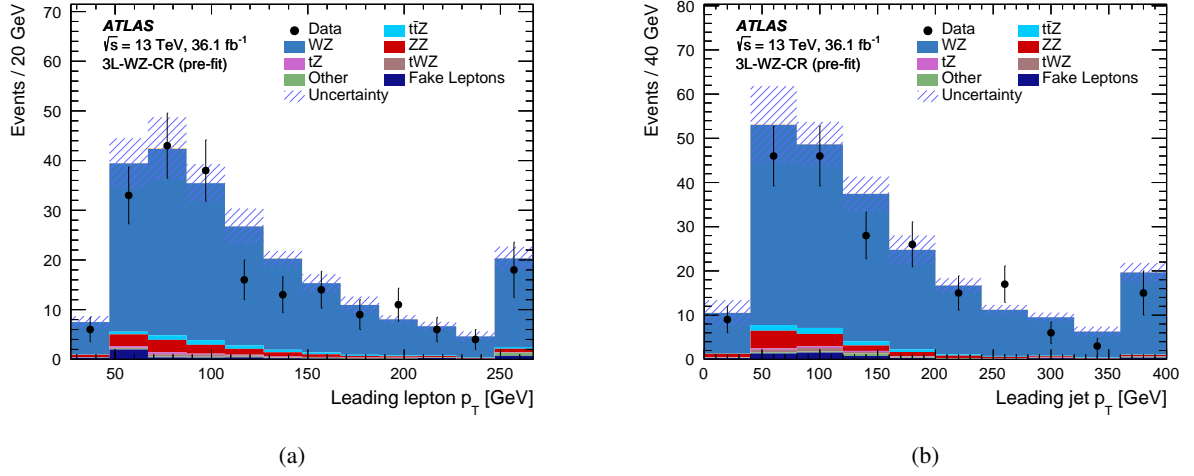


Figure 5: Distributions of (a) the leading lepton transverse momentum p_T and (b) the leading jet p_T in the 3ℓ -WZ-CR control region before the fit. The ‘Other’ background contains SM processes with small cross sections producing three prompt leptons. The shaded band represents the total uncertainty. The last bin in each of the distributions includes the overflow.

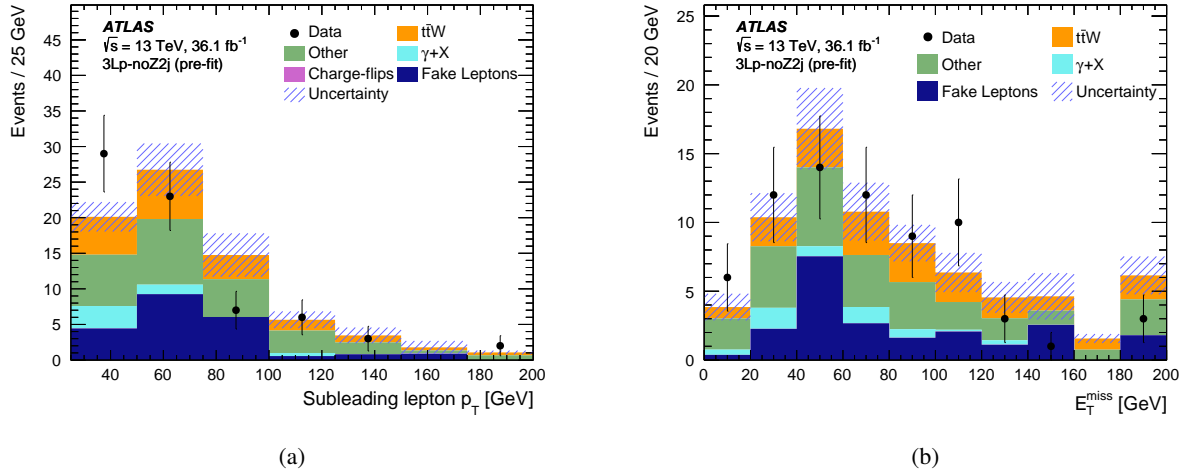


Figure 6: Distributions of (a) the subleading lepton transverse momentum p_T and (b) missing transverse momentum E_T^{miss} for events belonging to any of the four trilepton regions targeting the $t\bar{t}W$ process. The distributions are shown before the fit. The ‘Other’ background contains SM processes with small cross sections producing three prompt leptons. The shaded band represents the total uncertainty. The last bin in each of the distributions includes the overflow.

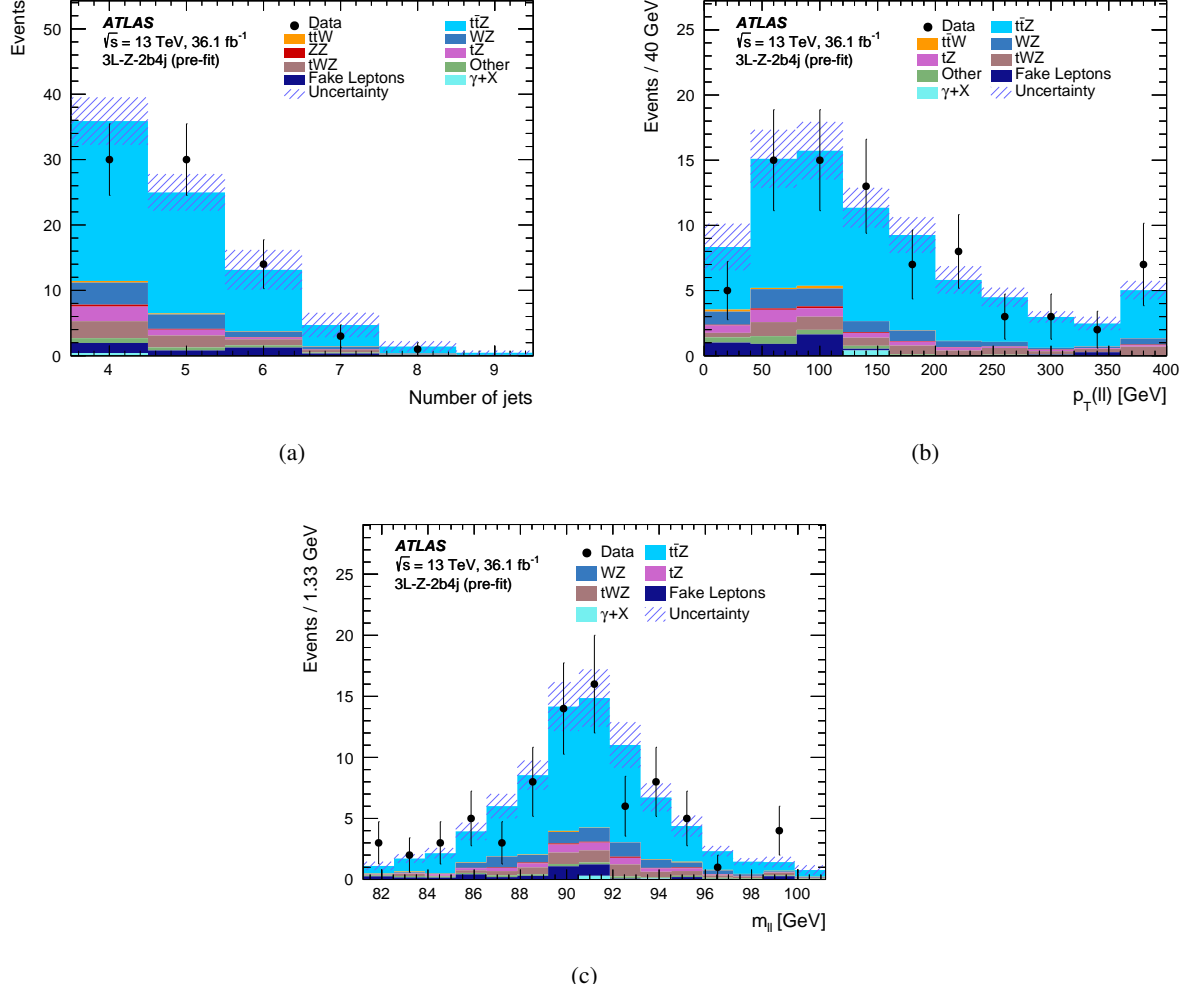


Figure 7: Distributions of (a) the number of jets, (b) the transverse momentum $p_T(\ell\ell)$ and (c) the mass $m_{\ell\ell}$ of the reconstructed Z boson candidate for events in 3L-Z-2b4j. The distributions are shown before the fit. The ‘Other’ background contains SM processes with small cross sections producing three prompt leptons. The shaded band represents the total uncertainty. The last bin in each of the distributions includes the overflow.

In the same-flavor regions, requirements on E_T^{miss} are applied to suppress the ZZ background. In the 4ℓ -SF-1b signal region, the E_T^{miss} is required to be greater than 80 GeV (40 GeV) for events with $|m_{Z_2} - m_Z| < 10$ GeV ($|m_{Z_2} - m_Z| > 10$ GeV). In the 4ℓ -SF-2b signal region, a requirement of $E_T^{\text{miss}} > 40$ GeV is applied for events with $|m_{Z_2} - m_Z| < 10$ GeV.

To suppress events with fake leptons in the $1-b$ -tag multiplicity regions, additional requirements on the scalar sum of the transverse momenta of the third and fourth leptons (p_{T34}) are imposed. In the 4ℓ -SF-1b and 4ℓ -DF-1b regions, events are required to satisfy $p_{T34} > 25$ GeV and $p_{T34} > 35$ GeV, respectively, while in the other regions all leptons are required to satisfy $p_T > 10$ GeV.

Table 6: Definitions of the four signal regions in the tetralepton channel.

Region	Z_2 leptons	p_{T4}	p_{T34}	$ m_{Z_2} - m_Z $	E_T^{miss}	$n_{b\text{-tags}}$
4ℓ -DF-1b	$e^\pm \mu^\mp$	–	> 35 GeV	–	–	1
4ℓ -DF-2b	$e^\pm \mu^\mp$	> 10 GeV	–	–	–	≥ 2
4ℓ -SF-1b	$e^\pm e^\mp, \mu^\pm \mu^\mp$	–	> 25 GeV	$\begin{cases} > 10 \text{ GeV} \\ < 10 \text{ GeV} \end{cases}$	$\begin{cases} > 40 \text{ GeV} \\ > 80 \text{ GeV} \end{cases}$	1
4ℓ -SF-2b	$e^\pm e^\mp, \mu^\pm \mu^\mp$	> 10 GeV	–	$\begin{cases} > 10 \text{ GeV} \\ < 10 \text{ GeV} \end{cases}$	$\begin{cases} - \\ > 40 \text{ GeV} \end{cases}$	≥ 2

A control region used to determine the ZZ normalization, referred to as 4ℓ -ZZ-CR, is included in the fit and is defined to have exactly four reconstructed leptons, a Z_2 pair with OSSF leptons, the value of both m_{Z_1} and m_{Z_2} within 10 GeV of the mass of the Z boson, and $20 \text{ GeV} < E_T^{\text{miss}} < 40 \text{ GeV}$. The leading lepton p_T and the jet multiplicity in this control region are shown in Figure 8, and good agreement is seen between data and prediction.

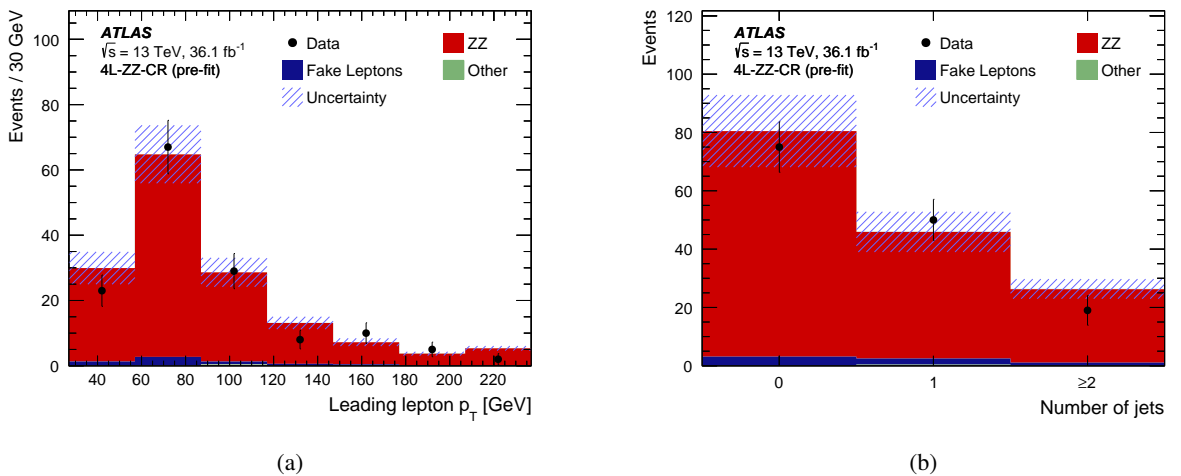


Figure 8: Distribution of (a) the leading lepton transverse momentum p_T and (b) jet multiplicity in the 4ℓ -ZZ-CR control region. The distributions are shown before the fit. The shaded band represents the total uncertainty. The last bin in each of the distributions includes the overflow.

The contribution from backgrounds containing fake leptons is estimated from simulation and corrected

with scale factors determined in two control regions: one region enriched in $t\bar{t}$ events and one region enriched in $Z+jets$ events. The scale factors are extracted and applied separately for electron and muon fake-lepton candidates, and for leptons arising from heavy-flavor hadrons and other sources. Therefore, a total of four scale factors are determined. The scale factors are applied to all MC simulation events with fewer than four prompt leptons according to the number, flavor and origin of the fake leptons. It is verified that the scale factors for different generators used in the simulation are consistent with each other.

Figure 9 compares the data with the expected distributions for all four signal regions combined, showing good agreement between data and expectation.

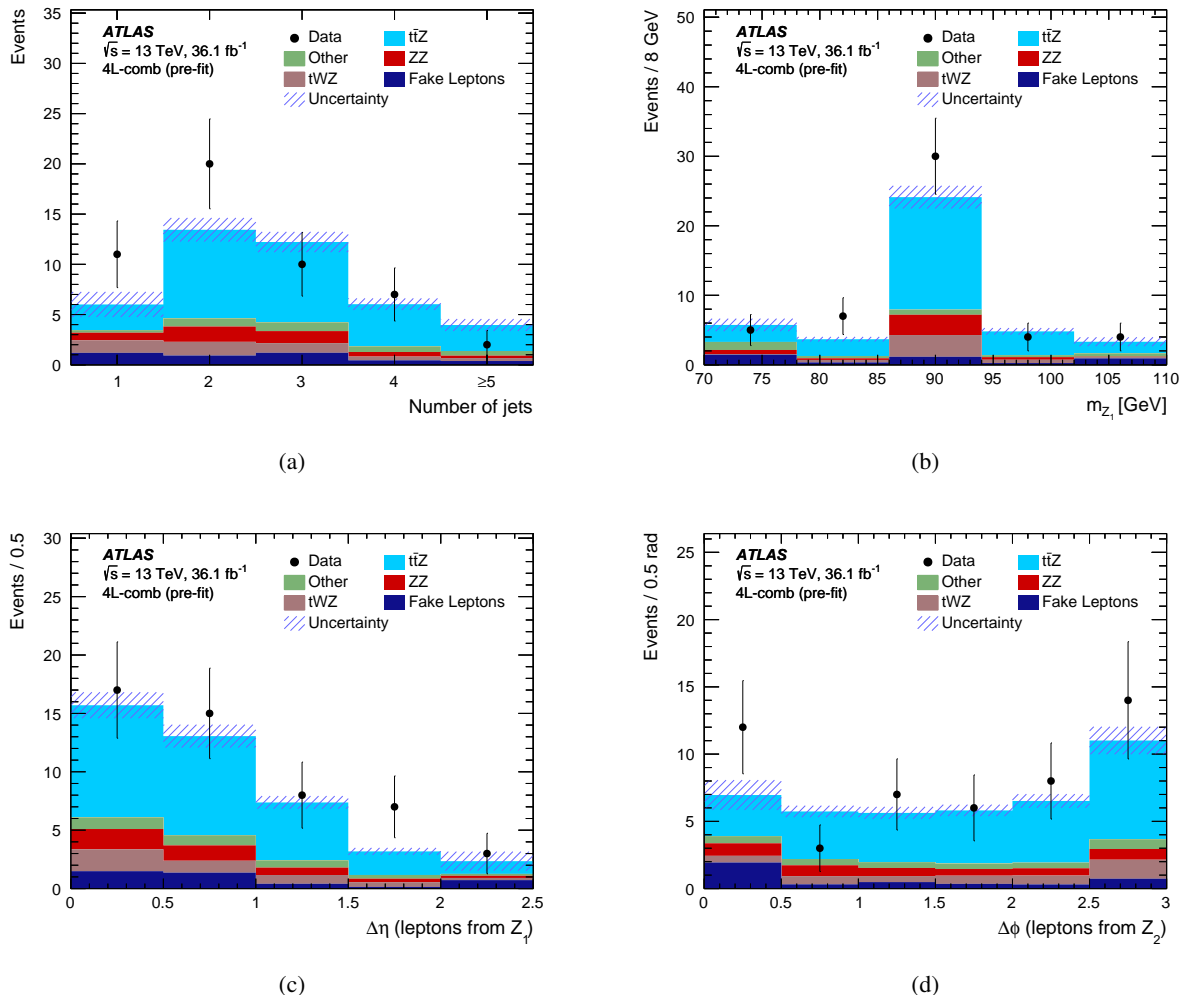


Figure 9: Distributions, for all tetralepton signal regions combined, of (a) the number of jets, (b) the invariant mass of the OSSF lepton pair closest to the Z boson mass, m_{Z_1} , (c) the pseudorapidity separation $\Delta\eta$ for that pair of leptons and (d) the azimuthal angle $\Delta\phi$ between the remaining two leptons. The ‘Other’ background contains SM processes with small cross sections producing four prompt leptons. The distributions are shown before the fit. The shaded band represents the total uncertainty. The first and last bin include the underflow and overflow, respectively.

6 Systematic uncertainties

The signal and background yields in each signal and control region may be affected by several sources of systematic uncertainty. These are implemented as nuisance parameters in the fit, explained in Section 7, are constrained by Gaussian probability density functions and are described in the following subsections.

6.1 Luminosity

The uncertainty in the integrated luminosity of the dataset is 2.1%. It is derived, following a methodology similar to that detailed in Ref. [23], and using the LUCID-2 detector for the baseline luminosity measurements [24], from a calibration of the luminosity scale using x - y beam-separation scans. This systematic uncertainty affects all processes modeled using Monte Carlo simulations, apart from $Z+1\text{HF}$, $Z+2\text{HF}$, WZ and ZZ , whose normalizations are taken from data control regions.

6.2 Uncertainties associated with reconstructed objects

Uncertainties associated with the lepton selection arise from the trigger, reconstruction, identification and isolation efficiencies, and lepton momentum scale and resolution [59, 71–73].

Uncertainties associated with the jet selection arise from the jet energy scale (JES), the JVT requirement and the jet energy resolution (JER). The JES and its uncertainty are derived by combining information from test-beam data, collision data and simulation [64]. The uncertainties in the JER and JVT have a significant effect at low jet p_{T} .

The efficiency of the flavor-tagging algorithm is measured for each jet flavor using control samples in data and in simulation. From these measurements, correction factors are derived to correct the tagging rates in the simulation. In the case of b -jets, correction factors and their uncertainties are estimated from data using dileptonic $t\bar{t}$ events [66]. In the case of c -jets, they are derived using jets from W boson decays in $t\bar{t}$ events [74]. In the case of light-flavor jets, correction factors are derived using dijet events [75]. Sources of uncertainty affecting the b - and c -tagging efficiencies are considered as a function of jet p_{T} , including bin-to-bin correlations [76]. The uncertainty in the efficiency for tagging light-flavor jets depends on the jet p_{T} and on η . These systematic uncertainties are taken as uncorrelated between b -jets, c -jets, and light-flavor jets. An additional uncertainty is assigned to account for the extrapolation of the b -tagging efficiency measurement from the p_{T} region used to determine the correction factors to regions with higher transverse momentum.

The treatment of the uncertainties associated with reconstructed objects is common to all analysis channels, and thus these are considered as fully correlated among different analysis regions.

6.3 Uncertainties in the signal modeling

Four sources of systematic uncertainties in the theoretical predictions of the $t\bar{t}Z$ and $t\bar{t}W$ processes are considered. These signal modeling uncertainties are treated as uncorrelated between the two processes, and correlated among channels. Taking instead the uncertainties as correlated between the two processes has a negligible impact on the results. Acceptance effects due to the choice of scale and PDF in the nominal

`MG5_aMC+PYTHIA` 8 (A14 tune) sample are considered. The renormalization and factorization scales $\mu_R = \mu_F$ are varied simultaneously by factors 2.0 and 0.5. In addition, the effects of a set of variations in the tune parameters (A14 eigentune variations), sensitive to initial- and final-state radiation, multiple parton interactions and color reconnection, are evaluated [36]. Studies performed at particle level show that the largest impact comes from variations in initial-state radiation [77]. The systematic uncertainty due to the choice of generator for the $t\bar{t}Z$ and $t\bar{t}W$ acceptance is estimated by comparing the nominal sample with one generated with `SHERPA` v2.2. The `SHERPA` sample uses the LO matrix element with up to one (two) additional parton(s) included in the matrix element calculation for $t\bar{t}Z$ ($t\bar{t}W$) and merged with the `SHERPA` parton shower [43] using the ME+PS@LO prescription. The NNPDF3.0NLO PDF set is used in conjunction with a dedicated parton-shower tune developed by the `SHERPA` authors.

6.4 Uncertainties in the background modeling

The Z +jets process is, together with $t\bar{t}$ production, the dominant background in the OS dilepton channel. Its normalization is extracted from data as described in Section 5.1, but the shape of the BDT distribution is obtained from simulation. To assess the systematic uncertainty in the shape, the renormalization, factorization and resummation scales used in the MC generation are varied by a factor of two with respect to the nominal values.

The normalization and shape of the $t\bar{t}$ background in the OS dilepton channel is obtained using the data-driven method detailed in Section 5.1. A systematic uncertainty arises from the factor used to obtain $t\bar{t}$ background yields in the same-flavor signal regions from corresponding opposite-flavor dilepton control regions. The uncertainty is due to the finite size of the samples of simulated events used, and the difference between the values of the factor obtained with the nominal PowHEG-Box+`PYTHIA` 8 sample and an alternative sample generated using `MG5_aMC+PYTHIA` 8. The total uncertainty in the factor is found to be 3%.

In the trilepton regions sensitive to $t\bar{t}Z$, the normalization of the WZ background is treated as a free parameter in the fit used to extract the $t\bar{t}Z$ and $t\bar{t}W$ signals. The uncertainty in the extrapolation of the WZ background estimate from the control region to signal regions with specific jet and b -tag multiplicities is evaluated by comparing predictions obtained by varying the renormalization, factorization and resummation scales used in MC generation. The uncertainties vary from 30% to 50%, depending on the signal region.

The normalization of the ZZ background is treated as a free parameter in the fit. An additional uncertainty arises from the extrapolation from the 4ℓ - ZZ -CR control region to the signal regions. It is assessed by varying the renormalization, factorization and resummation scales used in MC generation, and found to be in the range 20–40%.

The uncertainty in the $t\bar{t}H$ background is evaluated by varying the factorization and renormalization scales up and down by a factor of two with respect to the nominal values. It is found to be around 10%.

An overall normalization uncertainty of 30% is assigned to the tZ background, motivated by the measurements of this process presented in Refs. [78, 79]. An additional uncertainty affecting the distribution of this background as a function of jet and b -tagged jet multiplicities is evaluated by varying the factorization and renormalization scales, as well as the amount of radiation in the Perugia2012 parton-shower tune.

An uncertainty of 10% is assigned to the tWZ background cross section, resulting from different prescriptions for removing the interference with the $t\bar{t}Z$ process. The shape uncertainty is evaluated by

varying the factorization and renormalization scales up and down by a factor of two with respect to the nominal value.

For other prompt-lepton backgrounds, uncertainties of 20% are assigned to the normalizations of the WH and ZH processes, based on calculations from Ref. [34]. An uncertainty of 50% is considered for triboson and same-sign WW processes.

A 10% uncertainty is applied to the charge-flip background, resulting from uncertainties in the charge-flip rates extracted from a control sample as described in Section 5.

A 30% uncertainty is assigned to the contribution from events with two prompt leptons or one prompt lepton and a photon conversion in the control regions used to measure the fake-lepton efficiency. In the SS dilepton channel regions and trilepton regions targeting $t\bar{t}W$, there are 22 nuisance parameters corresponding to the statistical uncertainty in the measurement of the fake-lepton efficiencies. One nuisance parameter is used for each p_T bin used in the measurement of the fake-lepton efficiencies. For fake-lepton efficiencies in events with one (at least two) b -tagged jet(s), seven (four) bins are used, and there is one nuisance parameter for each of the two lepton flavors. In the trilepton signal regions targeting $t\bar{t}Z$, where the fake-lepton background is less important, a simplified description of the fake-lepton uncertainties is used, with one nuisance parameter for each of the two lepton flavors. These nuisance parameters correspond to the maximum of the up and down shifts of the fake-lepton efficiencies resulting from statistical uncertainties and the prompt lepton background subtraction in the control regions used to measure the fake-lepton efficiency. The uncertainties in the fake-lepton background in the $t\bar{t}Z$ and $t\bar{t}W$ analysis regions are considered to be uncorrelated, due to the different lepton selection requirements used in the two sets of regions.

Uncertainties in scale factors applied to the fake-lepton background are taken into account in the fake-lepton background yield in the tetralepton channel and the $t\bar{t}\gamma$ background contribution in the trilepton and 2ℓ -SS channels. These uncertainties are associated with reconstructed objects and the limited sizes of control regions in which the scale factors are obtained. The scale factors have uncertainties between 10% and 50%, depending on the fake-lepton flavor and source. The 2ℓ -SS and trilepton fake-lepton systematic uncertainties from the matrix method are assumed to be uncorrelated with the systematic uncertainties in the fake-lepton scale factors.

7 Results

The signal strengths $\mu_{t\bar{t}Z}$ and $\mu_{t\bar{t}W}$, defined as the ratios of the measured values of the inclusive production cross sections to the corresponding SM predictions discussed in Section 3, are extracted simultaneously using a binned maximum-likelihood fit to the numbers of events in the dilepton, trilepton and tetralepton signal and control regions. In the OS dilepton channel signal regions 2ℓ -Z-6j1b, 2ℓ -Z-5j2b and 2ℓ -Z-6j2b, the BDT output distribution is fitted. In the SS dilepton channel, the twelve signal regions 2ℓ -SSp-1b, 2ℓ -SSm-1b, 2ℓ -SSp-2b and 2ℓ -SSm-2b are fitted together with the twelve control regions 2ℓ -SSp-1b-CR, 2ℓ -SSm-1b-CR, 2ℓ -SSp-2b-CR and 2ℓ -SSm-2b-CR defined in Section 5. The contribution from the $t\bar{t}W$ signal in the SS dilepton control regions is taken into account in the fit. The dependence of the fake-lepton background in these regions on the $t\bar{t}W$ signal strength is also taken into account. In the trilepton channel, the eight signal regions described in Section 5 are included in the fit, as is the 3ℓ -WZ-CR control region. Finally, in the tetralepton channel, the four signal regions 4ℓ -DF-1b, 4ℓ -DF-2b, 4ℓ -SF-1b and 4ℓ -SF-2b and the control region 4ℓ -ZZ-CR are included in the fit.

The fit is based on the profile-likelihood technique, where systematic uncertainties are included in the fit as nuisance parameters constrained by Gaussian functions. None of the uncertainty parameters are found to be significantly constrained or pulled in the fit. The calculation of confidence intervals and hypothesis testing is performed using a modified frequentist method as implemented in RooStats [80, 81].

Figure 10 shows the BDT output distribution in signal regions 2ℓ -Z-6j1b, 2ℓ -Z-5j2b and 2ℓ -Z-6j2b after performing the fit. Figures 11 and 12 summarize the comparison between data and the post-fit signal and background yields for regions sensitive to $t\bar{t}Z$ and $t\bar{t}W$ production, together with the relevant control regions. In all cases, good agreement between observed values and the expectation is seen. The normalization corrections for the WZ and ZZ backgrounds with respect to the predictions are obtained from the fits as described in Section 5 and found to be compatible with unity: 0.91 ± 0.10 for the WZ background and 1.11 ± 0.17 for the ZZ background. The normalizations of the $Z+1HF$ and $Z+2HF$ backgrounds are mainly constrained in the low BDT output bins of the OS dilepton channel signal regions, where the signal contamination is low. Their values are found to be 1.19 ± 0.25 and 1.09 ± 0.13 , respectively.

In addition to the combined fit described above, fits in individual channels are performed. The $t\bar{t}Z$ signal strength is extracted through fits to the opposite-sign dilepton regions alone, to the trilepton channel regions alone and to the tetralepton channel signal regions alone. The $t\bar{t}W$ signal strength is extracted using the four trilepton signal regions targeting $t\bar{t}W$ and the same-sign dilepton regions considered in the combined fit. The measured values of the signal strengths $\mu_{t\bar{t}Z}$ and $\mu_{t\bar{t}W}$ are reported in Table 7 for each channel separately and for the combined fit. Agreement is observed for the measured values between all the different fit configurations.

Table 7: Measured signal strengths of $t\bar{t}Z$ and $t\bar{t}W$ for different fit configurations and the combined fit. The uncertainties include statistical and systematic components.

Fit configuration	$\mu_{t\bar{t}Z}$	$\mu_{t\bar{t}W}$
Combined	1.08 ± 0.14	1.44 ± 0.32
2ℓ -OS	0.73 ± 0.28	–
$3\ell t\bar{t}Z$	1.08 ± 0.18	–
2ℓ -SS and $3\ell t\bar{t}W$	–	1.41 ± 0.33
4ℓ	1.21 ± 0.29	–

The measured signal strengths from the combined fit and their uncertainties are converted to inclusive cross-section measurements using the signal simulation described in Section 3 and the central values of the theoretical predictions. The results are: $\sigma_{t\bar{t}Z} = 0.95 \pm 0.08_{\text{stat.}} \pm 0.10_{\text{syst.}}$ pb = 0.95 ± 0.13 pb and $\sigma_{t\bar{t}W} = 0.87 \pm 0.13_{\text{stat.}} \pm 0.14_{\text{syst.}}$ pb = 0.87 ± 0.19 pb. Figure 13 shows a comparison of the fit results with theoretical predictions, $\sigma_{t\bar{t}Z}^{\text{th}} = 0.88^{+0.09}_{-0.11}$ pb and $\sigma_{t\bar{t}W}^{\text{th}} = 0.60^{+0.08}_{-0.07}$ pb, demonstrating good agreement between the measured and predicted cross sections.

For the $t\bar{t}Z$ process, both the observed and the expected significances are found to be much larger than five standard deviations. For the $t\bar{t}W$ process, an excess of events over the expected background-only hypothesis is found with an observed (expected) significance of 4.3 (3.4) standard deviations. The significance values are computed using the asymptotic approximation described in Ref. [82].

Table 8 shows the uncertainties in the measured $t\bar{t}Z$ and $t\bar{t}W$ cross sections, grouped in categories, along with the total uncertainties. For both processes, the precision of the measurement is affected by statistical

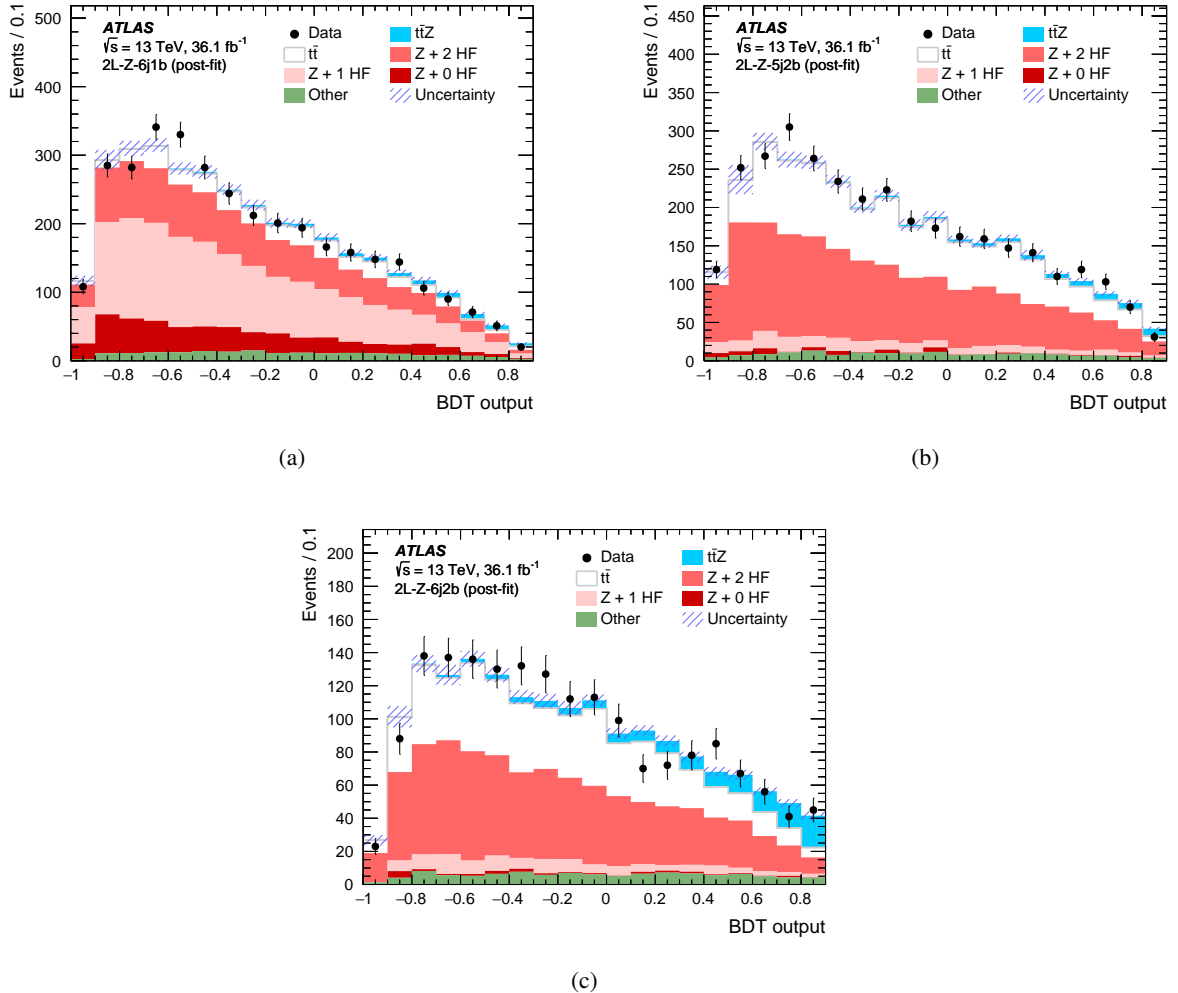


Figure 10: The BDT distributions for the OS dilepton signal regions, (a) 2ℓ -Z-6j1b, (b) 2ℓ -Z-5j2b, (c) 2ℓ -Z-6j2b. The distributions are shown after the fit. The ‘Other’ background contains SM processes with small cross sections producing two opposite-sign prompt leptons. The shaded band represents the total uncertainty. The last bin of each distribution contains the overflow.

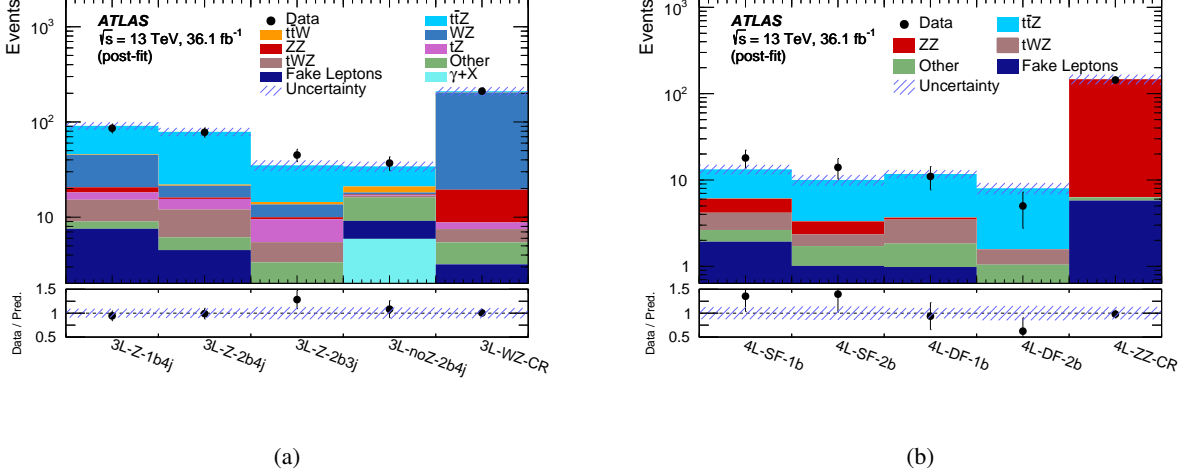


Figure 11: Event yields in data compared with the results of the fit that extracts $\sigma_{t\bar{t}Z}$ and $\sigma_{t\bar{t}W}$ simultaneously in the (a) trilepton and (b) tetralepton signal regions targeting the $t\bar{t}Z$ process. Yields for the control regions used to extract the normalization of the WZ and ZZ backgrounds are also shown. The ‘Other’ background summarizes all small SM backgrounds described in Section 3. The shaded band represents the total uncertainty.

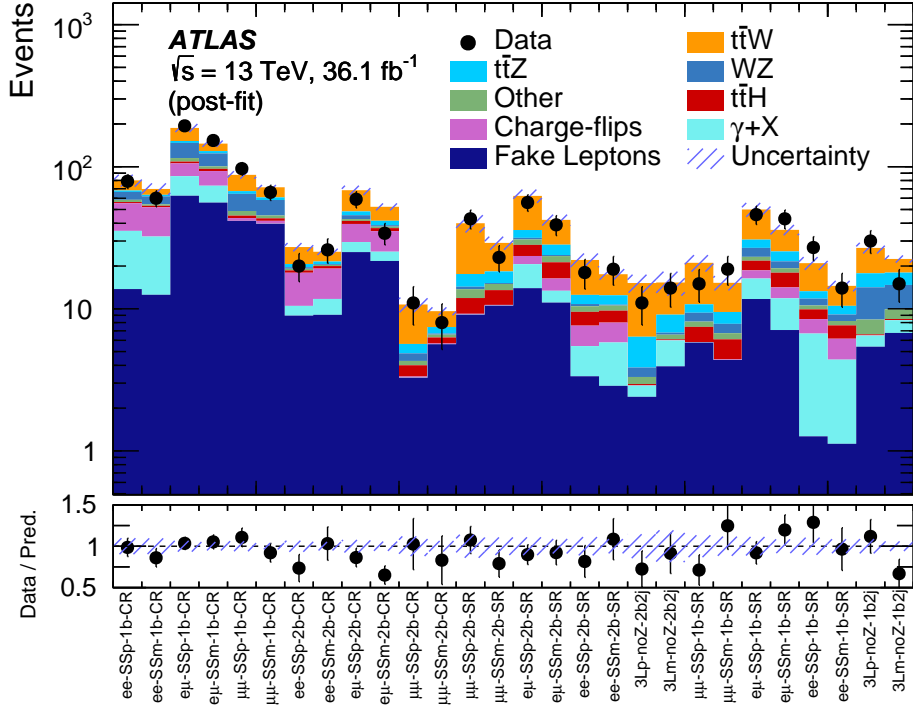


Figure 12: Event yields in data compared with the results of the fit that extracts $\sigma_{t\bar{t}Z}$ and $\sigma_{t\bar{t}W}$ simultaneously in the regions targeting the $t\bar{t}W$ process. The ‘Other’ background summarizes all small SM backgrounds described in Section 3. The shaded band represents the total uncertainty.

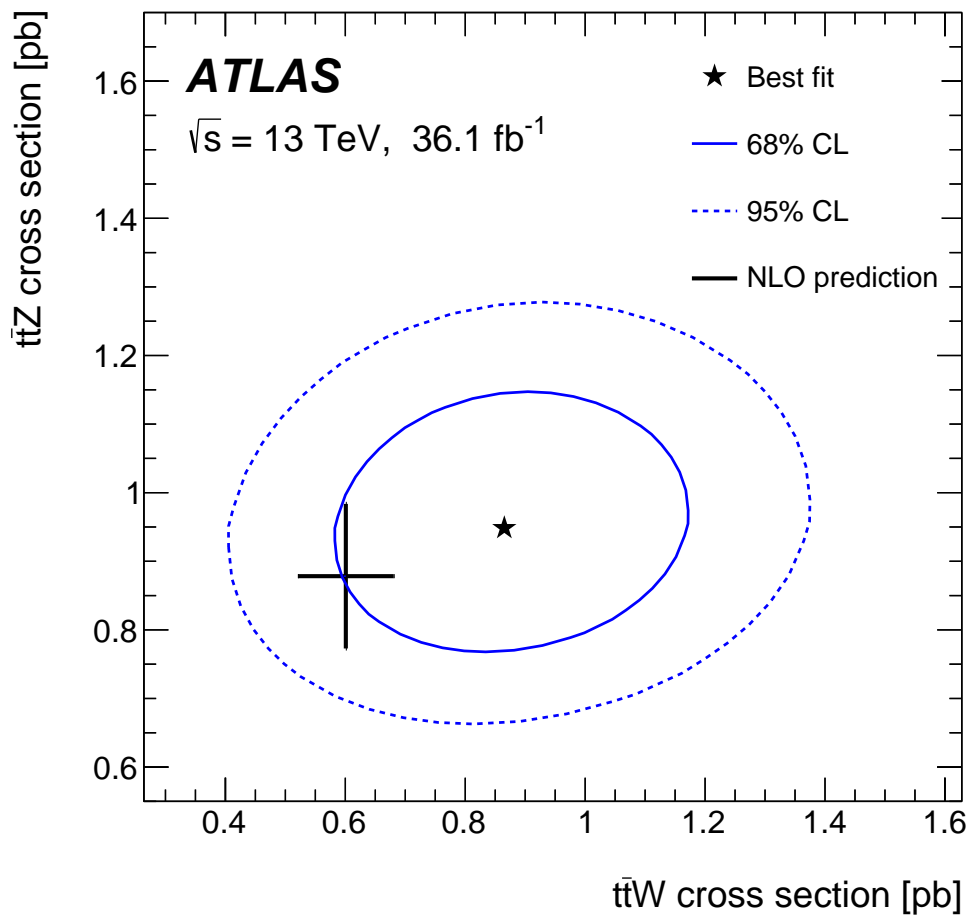


Figure 13: The result of the simultaneous fit to the $t\bar{t}Z$ and $t\bar{t}W$ cross sections along with the 68% and 95% confidence level (CL) contours. The cross shows the SM calculations and their uncertainties, including renormalization and factorization scale uncertainties as well as uncertainties including α_S variations.

and systematic uncertainties in similar proportions. For the $t\bar{t}Z$ determination, the dominant systematic uncertainty sources are the modeling of the backgrounds and of the signal. For the $t\bar{t}W$ determination, the dominant systematic uncertainty sources are the modeling of the signal and the limited amount of data available in the control regions and simulated event samples.

Table 8: List of relative uncertainties in the measured cross sections of the $t\bar{t}Z$ and $t\bar{t}W$ processes from the fit, grouped in categories. All uncertainties are symmetrized. The sum in quadrature may not be equal to the total due to correlations between uncertainties introduced by the fit.

Uncertainty	$\sigma_{t\bar{t}Z}$	$\sigma_{t\bar{t}W}$
Luminosity	2.9%	4.5%
Simulated sample statistics	2.0%	5.3%
Data-driven background statistics	2.5%	6.3%
JES/JER	1.9%	4.1%
Flavor tagging	4.2%	3.7%
Other object-related	3.7%	2.5%
Data-driven background normalization	3.2%	3.9%
Modeling of backgrounds from simulation	5.3%	2.6%
Background cross sections	2.3%	4.9%
Fake leptons and charge misID	1.8%	5.7%
$t\bar{t}Z$ modeling	4.9%	0.7%
$t\bar{t}W$ modeling	0.3%	8.5%
Total systematic	10%	16%
Statistical	8.4%	15%
Total	13%	22%

8 Interpretation

The effective field theory (EFT) framework provides a model-independent approach to the parameterization of possible deviations from the SM predictions. In this framework, effects due to BSM physics are described by adding additional operators of dimension six or higher to the SM Lagrangian. Each EFT operator O_i is associated with a Wilson coefficient C_i , and the operators enter the modified Lagrangian in the form $(C_i/\Lambda^2)O_i$, where Λ is the characteristic energy scale of the BSM physics.

The complete set of independent, gauge-invariant and baryon-number conserving EFT operators at dimension six contains 59 different operators [83, 84]. In the present analysis, five of these operators are considered, all of which modify the $t\bar{t}Z$ vertex: $O_{\phi Q}^{(3)}, O_{\phi Q}^{(1)}, O_{\phi t}, O_{tW}, O_{tB}$. The operators are defined in Table 9, following Ref. [85]. The first two operators enter the $t\bar{t}Z$ vertex as a linear combination, such that the measurement is sensitive to the difference $C_{\phi Q}^{(3)} - C_{\phi Q}^{(1)}$. For this paper, the effect of this combination is evaluated by varying $C_{\phi Q}^{(3)}$ with $C_{\phi Q}^{(1)}$ set to zero.

Table 9: Effective field theory operators considered and their form in terms of SM fields. The notation of Ref. [85] is used.

Operator	Expression
$O_{\phi Q}^{(3)}$	$(\phi^\dagger i \overleftrightarrow{D}_\mu^I \phi)(\bar{Q} \gamma^\mu \tau^I Q)$
$O_{\phi Q}^{(1)}$	$(\phi^\dagger i \overleftrightarrow{D}_\mu \phi)(\bar{Q} \gamma^\mu Q)$
$O_{\phi t}$	$(\phi^\dagger i \overleftrightarrow{D}_\mu \phi)(\bar{t} \gamma^\mu t)$
O_{tW}	$(\bar{Q} \sigma^{\mu\nu} \tau^I t) \tilde{\phi} W_{\mu\nu}^I$
O_{tB}	$(\bar{Q} \sigma^{\mu\nu} t) \tilde{\phi} B_{\mu\nu}$

Considering only one EFT operator at a time, any observable, such as the $t\bar{t}Z$ event rate in a certain signal region, can be expressed as a quadratic function of the coefficient C_i :

$$\sigma_{\text{tot},i} = \sigma_{\text{SM}} + \frac{C_i}{(\Lambda/1\text{TeV})^2} \sigma_i^{(1)} + \frac{C_i^2}{(\Lambda/1\text{TeV})^4} \sigma_{ii}^{(2)}. \quad (1)$$

The term linear in C_i on the right-hand side of Eq. (1) results from the interference of the BSM operators with the SM. For C_i/Λ^2 of order 1 TeV^{-2} , the interference term dominates in Eq. (1) for $O_{\phi Q}^{(3)}$ and $O_{\phi t}$, while the quadratic term dominates for O_{tW} and O_{tB} .

The values of $\sigma_i^{(1)}$ and $\sigma_{ii}^{(2)}$ are computed using simulated event samples generated with MG5_aMC interfaced to PYTHIA 8 [11, 86, 87]. The computation is performed at NLO, separately for all trilepton and tetralepton signal regions. The detector reconstruction efficiency is verified to be compatible between SM $t\bar{t}Z$ samples and samples with non-zero values of C_i , for ranges of C_i considered here.

A fit is then performed to extract C_i/Λ^2 . The fit is similar to the one described in Section 7, except that only the four trilepton and four tetralepton signal regions targeting $t\bar{t}Z$ are used and a normalization uncertainty of 12%, corresponding to the uncertainty in the NLO cross-section computation, is applied to the SM $t\bar{t}Z$ prediction. Uncertainties resulting from the limited sizes of MC samples used to derive the values of $\sigma_i^{(1)}$ and $\sigma_{ii}^{(2)}$ are propagated to the measured values of C_i/Λ^2 .

The profile-likelihood test statistic is defined as $-\Delta \log(L) = \log(\mathcal{L}(\hat{C}_i)/\mathcal{L}(C_i))$, where \mathcal{L} is the profile likelihood as a function of the Wilson coefficient C_i , and \hat{C}_i is the best-fit value of C_i . Approximate confidence intervals for the Wilson coefficients are computed using the formula $-\Delta \log(L) = \varepsilon$, where the threshold ε is set to 0.5 and 1.92 for the 68% (1σ) and 95% confidence levels (CL), respectively.

The confidence intervals for C_i are computed considering only the minimum of $\lambda(C_i)$ near $C_i = 0$. For coefficient $C_{\phi Q}^{(3)}$ ($C_{\phi t}$), another, deeper minimum exists for negative values of $C_i \sim 30$ (20), which is excluded by previous constraints. The 68% and 95% confidence intervals are shown in Table 10, together with previous constraints on the EFT coefficients obtained from Refs. [10, 88–90]. The lower boundary of the 95% confidence interval for $C_{\phi t}$ is at large negative values, which are excluded by indirect constraints. The $t\bar{t}Z$ measurement provides competitive constraints for positive $C_{\phi t}$ values. The full likelihood scans are shown in Figure 14 in the Appendix.

The fits are repeated while assuming that the quadratic terms are zero, and the results of these fits are also reported in Table 10. For C_{tW} and C_{tB} , where the quadratic terms dominate, the fits do not converge. Compared with the nominal fits for $C_{\phi Q}^{(3)}$ and $C_{\phi t}$, the limits shift to larger values, consistent with removing

a positive term from the prediction. The most notable change is the improvement in the lower limit for $C_{\phi t}$ at 95% CL, as the second minimum disappears when a linear expression is assumed.

Table 10: The expected and observed 68% and 95% confidence intervals, which include the value 0, for C_i/Λ^2 for the EFT coefficients $C_{\phi Q}^{(3)}$, $C_{\phi t}$, C_{tB} and C_{tW} . The intervals for $C_{\phi Q}^{(3)}$ are derived setting $C_{\phi Q}^{(1)}$ to zero; the measurement is sensitive to the difference $C_{\phi Q}^{(3)} - C_{\phi Q}^{(1)}$. All results are obtained by varying one coefficient at the time and are given in units of $1/\text{TeV}^2$. Previous indirect 68% CL constraints [88] are also quoted. The previous direct constraints at 95% CL are obtained from Ref. [10] for $C_{\phi t}$ and C_{tB} and from Refs. [89, 90] for $C_{\phi Q}^{(3)}$ and C_{tW} , using Ref. [83] to translate the measurements into limits on the coefficients. Limits from fits for the EFT coefficients with only the linear term are also shown.

Coefficients	$C_{\phi Q}^{(3)}/\Lambda^2$	$C_{\phi t}/\Lambda^2$	C_{tB}/Λ^2	C_{tW}/Λ^2
Previous indirect constraints at 68% CL	[−4.7, 0.7]	[−0.1, 3.7]	[−0.5, 10]	[−1.6, 0.8]
Previous direct constraints at 95% CL	[−1.3, 1.3]	[−9.7, 8.3]	[−6.9, 4.6]	[−0.2, 0.7]
Expected limit at 68% CL	[−2.1, 1.9]	[−3.8, 2.7]	[−2.9, 3.0]	[−1.8, 1.9]
Expected limit at 95% CL	[−4.5, 3.6]	[−23, 4.9]	[−4.2, 4.3]	[−2.6, 2.6]
Observed limit at 68% CL	[−1.0, 2.7]	[−2.0, 3.5]	[−3.7, 3.5]	[−2.2, 2.1]
Observed limit at 95% CL	[−3.3, 4.2]	[−25, 5.5]	[−5.0, 5.0]	[−2.9, 2.9]
Expected limit at 68% CL (linear)	[−1.9, 2.0]	[−3.0, 3.2]	—	—
Expected limit at 95% CL (linear)	[−3.7, 4.0]	[−5.8, 6.3]	—	—
Observed limit at 68% CL (linear)	[−1.0, 2.9]	[−1.8, 4.4]	—	—
Observed limit at 95% CL (linear)	[−2.9, 4.9]	[−4.8, 7.5]	—	—

9 Conclusion

Measurements of the production cross sections of a top-quark pair in association with a Z or W boson using 36.1 fb^{-1} of data collected by the ATLAS detector in $\sqrt{s} = 13 \text{ TeV}$ pp collisions at the LHC are presented. Final states with two same- or opposite-sign leptons, three leptons or four leptons are analyzed. The $t\bar{t}Z$ and $t\bar{t}W$ production cross sections are determined to be $\sigma_{t\bar{t}Z} = 0.95 \pm 0.08_{\text{stat.}} \pm 0.10_{\text{syst.}} \text{ pb} = 0.95 \pm 0.13 \text{ pb}$ and $\sigma_{t\bar{t}W} = 0.87 \pm 0.13_{\text{stat.}} \pm 0.14_{\text{syst.}} \text{ pb} = 0.87 \pm 0.19 \text{ pb}$. The measured values are consistent with the SM predictions. The measurements are used to derive confidence intervals for the Wilson coefficients of dimension-6 effective field theory operators involving the top quark and the Z boson.

Acknowledgments

We thank CERN for the very successful operation of the LHC, as well as the support staff from our institutions without whom ATLAS could not be operated efficiently.

We acknowledge the support of ANPCyT, Argentina; YerPhI, Armenia; ARC, Australia; BMWFW and FWF, Austria; ANAS, Azerbaijan; SSTC, Belarus; CNPq and FAPESP, Brazil; NSERC, NRC and CFI, Canada; CERN; CONICYT, Chile; CAS, MOST and NSFC, China; COLCIENCIAS, Colombia; MSMT CR, MPO CR and VSC CR, Czech Republic; DNRF and DNSRC, Denmark; IN2P3-CNRS,

CEA-DRF/IRFU, France; SRNSFG, Georgia; BMBF, HGF, and MPG, Germany; GSRT, Greece; RGC, Hong Kong SAR, China; ISF and Benoziyo Center, Israel; INFN, Italy; MEXT and JSPS, Japan; CNRST, Morocco; NWO, Netherlands; RCN, Norway; MNiSW and NCN, Poland; FCT, Portugal; MNE/IFA, Romania; MES of Russia and NRC KI, Russian Federation; JINR; MESTD, Serbia; MSSR, Slovakia; ARRS and MIZŠ, Slovenia; DST/NRF, South Africa; MINECO, Spain; SRC and Wallenberg Foundation, Sweden; SERI, SNSF and Cantons of Bern and Geneva, Switzerland; MOST, Taiwan; TAEK, Turkey; STFC, United Kingdom; DOE and NSF, United States of America. In addition, individual groups and members have received support from BCKDF, CANARIE, CRC and Compute Canada, Canada; COST, ERC, ERDF, Horizon 2020, and Marie Skłodowska-Curie Actions, European Union; Investissements d’Avenir Labex and Idex, ANR, France; DFG and AvH Foundation, Germany; Herakleitos, Thales and Aristeia programmes co-financed by EU-ESF and the Greek NSRF, Greece; BSF-NSF and GIF, Israel; CERCA Programme Generalitat de Catalunya, Spain; The Royal Society and Leverhulme Trust, United Kingdom.

The crucial computing support from all WLCG partners is acknowledged gratefully, in particular from CERN, the ATLAS Tier-1 facilities at TRIUMF (Canada), NDGF (Denmark, Norway, Sweden), CC-IN2P3 (France), KIT/GridKA (Germany), INFN-CNAF (Italy), NL-T1 (Netherlands), PIC (Spain), ASGC (Taiwan), RAL (UK) and BNL (USA), the Tier-2 facilities worldwide and large non-WLCG resource providers. Major contributors of computing resources are listed in Ref. [91].

References

- [1] ATLAS Collaboration, *Evidence for the associated production of the Higgs boson and a top quark pair with the ATLAS detector*, *Phys. Rev. D* **97** (2018) 072003, arXiv: [1712.08891 \[hep-ex\]](#).
- [2] CMS Collaboration, *Evidence for associated production of a Higgs boson with a top quark pair in final states with electrons, muons, and hadronically decaying τ leptons at $\sqrt{s} = 13$ TeV*, *JHEP* **08** (2018) 066, arXiv: [1803.05485 \[hep-ex\]](#).
- [3] CMS Collaboration, *Observation of $t\bar{t}H$ Production*, *Phys. Rev. Lett.* **120** (2018) 231801, arXiv: [1804.02610 \[hep-ex\]](#).
- [4] ATLAS Collaboration, *Observation of Higgs boson production in association with a top quark pair at the LHC with the ATLAS detector*, *Phys. Lett. B* **784** (2018) 173, arXiv: [1806.00425 \[hep-ex\]](#).
- [5] ATLAS Collaboration, *Observation of top-quark pair production in association with a photon and measurement of the $t\bar{t}\gamma$ production cross section in pp collisions at $\sqrt{s} = 7$ TeV using the ATLAS detector*, *Phys. Rev. D* **91** (2015) 072007, arXiv: [1502.00586 \[hep-ex\]](#).
- [6] ATLAS Collaboration, *Measurement of the $t\bar{t}\gamma$ production cross section in proton–proton collisions at $\sqrt{s} = 8$ TeV with the ATLAS detector*, *JHEP* **11** (2017) 086, arXiv: [1706.03046 \[hep-ex\]](#).
- [7] CMS Collaboration, *Measurement of the semileptonic $t\bar{t} + \gamma$ production cross section in pp collisions at $\sqrt{s} = 8$ TeV*, *JHEP* **10** (2017) 006, arXiv: [1706.08128 \[hep-ex\]](#).
- [8] ATLAS Collaboration, *Measurements of inclusive and differential fiducial cross-sections of $t\bar{t}\gamma$ production in leptonic final states at $\sqrt{s} = 13$ TeV in ATLAS*, (2018), arXiv: [1812.01697 \[hep-ex\]](#).
- [9] J. A. Dror, M. Farina, E. Salvioni, and J. Serra, *Strong tW scattering at the LHC*, *JHEP* **01** (2016) 071, arXiv: [1511.03674 \[hep-ph\]](#).
- [10] A. Buckley, C. Englert, J. Ferrando, D. J. Miller, L. Moore, M. Russell, and C. D. White, *Constraining top quark effective theory in the LHC Run II era*, *JHEP* **04** (2016) 015, arXiv: [1512.03360 \[hep-ph\]](#).
- [11] O. Bessidskaia Bylund, F. Maltoni, I. Tsinikos, E. Vryonidou, and C. Zhang, *Probing top quark neutral couplings in the Standard Model Effective Field Theory at NLO in QCD*, *JHEP* **05** (2016) 052, arXiv: [1601.08193 \[hep-ph\]](#).
- [12] S. Weinberg, *Phenomenological Lagrangians*, *Physica A* **96** (1979) 327.
- [13] W. Buchmüller and D. Wyler, *Effective Lagrangian analysis of new interactions and flavour conservation*, *Nucl. Phys. B* **268** (1986) 621.
- [14] C. N. Leung, S. T. Love, and S. Rao, *Low-energy manifestations of a new interactions scale: Operator analysis*, *Z. Phys. C* **31** (1986) 433.
- [15] ATLAS Collaboration, *Measurement of the $t\bar{t}W$ and $t\bar{t}Z$ production cross sections in pp collisions at $\sqrt{s} = 8$ TeV with the ATLAS detector*, *JHEP* **11** (2015) 172, arXiv: [1509.05276 \[hep-ex\]](#).

- [16] ATLAS Collaboration, *Measurement of the $t\bar{t}Z$ and $t\bar{t}W$ production cross sections in multilepton final states using 3.2 fb^{-1} of pp collisions at $\sqrt{s} = 13\text{ TeV}$ with the ATLAS detector*, *Eur. Phys. J. C* **77** (2017) 40, arXiv: [1609.01599 \[hep-ex\]](#).
- [17] CMS Collaboration, *Observation of top quark pairs produced in association with a vector boson in pp collisions at $\sqrt{s} = 8\text{ TeV}$* , *JHEP* **01** (2016) 096, arXiv: [1510.01131 \[hep-ex\]](#).
- [18] CMS Collaboration, *Measurement of the cross section for top quark pair production in association with a W or Z boson in proton–proton collisions at $\sqrt{s} = 13\text{ TeV}$* , *JHEP* **08** (2018) 011, arXiv: [1711.02547 \[hep-ex\]](#).
- [19] ATLAS Collaboration, *The ATLAS Experiment at the CERN Large Hadron Collider*, *JINST* **3** (2008) S08003.
- [20] ATLAS Collaboration, *Study of the mechanical stability of the ATLAS Insertable B-Layer*, ATL-INDET-PUB-2015-001, 2015, URL: <https://cds.cern.ch/record/2022587>.
- [21] B. Abbott et al., *Production and Integration of the ATLAS Insertable B-Layer*, *JINST* **13** (2018) T05008, arXiv: [1803.00844 \[physics.ins-det\]](#).
- [22] ATLAS Collaboration, *Performance of the ATLAS trigger system in 2015*, *Eur. Phys. J. C* **77** (2017) 317, arXiv: [1611.09661 \[hep-ex\]](#).
- [23] ATLAS Collaboration, *Luminosity determination in pp collisions at $\sqrt{s} = 8\text{ TeV}$ using the ATLAS detector at the LHC*, *Eur. Phys. J. C* **76** (2016) 653, arXiv: [1608.03953 \[hep-ex\]](#).
- [24] G. Avoni et al., *The new LUCID-2 detector for luminosity measurement and monitoring in ATLAS*, *JINST* **13** (2018) P07017.
- [25] D. J. Lange, *The EvtGen particle decay simulation package*, *Nucl. Instrum. Meth. A* **462** (2001) 152.
- [26] T. Gleisberg, S. Hoeche, F. Krauss, M. Schonherr, S. Schumann, F. Siegert, and J. Winter, *Event generation with SHERPA 1.1*, *JHEP* **02** (2009) 007, arXiv: [0811.4622 \[hep-ph\]](#).
- [27] ATLAS Collaboration, *The ATLAS Simulation Infrastructure*, *Eur. Phys. J. C* **70** (2010) 823, arXiv: [1005.4568 \[physics.ins-det\]](#).
- [28] S. Agostinelli et al., *Geant4—a simulation toolkit*, *Nucl. Instrum. Meth. A* **506** (2003) 250.
- [29] ATLAS Collaboration, *The simulation principle and performance of the ATLAS fast calorimeter simulation FastCaloSim*, ATL-PHYS-PUB-2010-013, 2010, URL: <https://cds.cern.ch/record/1300517>.
- [30] T. Sjöstrand, S. Ask, J. R. Christiansen, R. Corke, N. Desai, P. Ilten, S. Mrenna, S. Prestel, C. O. Rasmussen, and P. Z. Skands, *An introduction to PYTHIA 8.2*, *Comp. Phys. Comm.* **191** (2015) 159, arXiv: [1410.3012 \[hep-ph\]](#).
- [31] ATLAS Collaboration, *Further ATLAS tunes of Pythia 6 and Pythia 8*, ATL-PHYS-PUB-2011-014, 2011, URL: <https://cds.cern.ch/record/1400677>.
- [32] J. Alwall, R. Frederix, S. Frixione, V. Hirschi, F. Maltoni, O. Mattelaer, H. Shao, T. Stelzer, P. Torrielli, and M. Zaro, *The automated computation of tree-level and next-to-leading order differential cross sections, and their matching to parton shower simulations*, *JHEP* **07** (2014) 079, arXiv: [1405.0301 \[hep-ph\]](#).

- [33] S. Frixione, V. Hirschi, D. Pagani, H.-S. Shao, and M. Zaro, *Electroweak and QCD corrections to top-pair hadroproduction in association with heavy bosons*, JHEP **06** (2015) 184, arXiv: [1504.03446 \[hep-ph\]](#).
- [34] D. de Florian et al., *Handbook of LHC Higgs cross sections: 4. Deciphering the nature of the Higgs sector*, (2016), arXiv: [1610.07922 \[hep-ph\]](#).
- [35] R. D. Ball et al., *Parton distributions for the LHC run II*, JHEP **04** (2015) 040, arXiv: [1410.8849 \[hep-ph\]](#).
- [36] ATLAS Collaboration, *ATLAS Pythia 8 tunes to 7 TeV data*, ATL-PHYS-PUB-2014-021, 2014, URL: <https://cds.cern.ch/record/1966419>.
- [37] R. D. Ball et al., *Parton distributions with LHC data*, Nucl. Phys. B **867** (2013) 244, arXiv: [1207.1303 \[hep-ph\]](#).
- [38] T. Sjöstrand, S. Mrenna, and P. Z. Skands, *PYTHIA 6.4 physics and manual*, JHEP **05** (2006) 026, arXiv: [hep-ph/0603175](#).
- [39] J. Pumplin, D. R. Stump, J. Huston, H. L. Lai, P. M. Nadolsky, and W. K. Tung, *New generation of parton distributions with uncertainties from global QCD analysis*, JHEP **07** (2002) 012, arXiv: [hep-ph/0201195](#).
- [40] P. Z. Skands, *Tuning Monte Carlo generators: The Perugia tunes*, Phys. Rev. D **82** (2010) 074018, arXiv: [1005.3457 \[hep-ph\]](#).
- [41] T. Gleisberg and S. Höche, *Comix, a new matrix element generator*, JHEP **12** (2008) 039, arXiv: [0808.3674 \[hep-ph\]](#).
- [42] F. Cascioli, P. Maierhöfer, and S. Pozzorini, *Scattering Amplitudes with Open Loops*, Phys. Rev. Lett. **108** (2012) 111601, arXiv: [1111.5206 \[hep-ph\]](#).
- [43] S. Schumann and F. Krauss, *A parton shower algorithm based on Catani–Seymour dipole factorisation*, JHEP **03** (2008) 038, arXiv: [0709.1027 \[hep-ph\]](#).
- [44] S. Höche, F. Krauss, M. Schönherr, and F. Siegert, *QCD matrix elements + parton showers. The NLO case*, JHEP **04** (2013) 027, arXiv: [1207.5030 \[hep-ph\]](#).
- [45] R. Gavin, Y. Li, F. Petriello, and S. Quackenbush, *FEWZ 2.0: A code for hadronic Z production at next-to-next-to-leading order*, Comp. Phys. Comm. **182** (2011) 2388, arXiv: [1011.3540 \[hep-ph\]](#).
- [46] H.-L. Lai et al., *New parton distributions for collider physics*, Phys. Rev. D **82** (2010) 074024, arXiv: [1007.2241 \[hep-ph\]](#).
- [47] S. Frixione, G. Ridolfi, and P. Nason, *A positive-weight next-to-leading-order Monte Carlo for heavy flavour hadroproduction*, JHEP **09** (2007) 126, arXiv: [0707.3088 \[hep-ph\]](#).
- [48] P. Nason, *A new method for combining NLO QCD with shower Monte Carlo algorithms*, JHEP **11** (2004) 040, arXiv: [hep-ph/0409146](#).
- [49] S. Frixione, P. Nason, and C. Oleari, *Matching NLO QCD computations with parton shower simulations: the POWHEG method*, JHEP **11** (2007) 070, arXiv: [0709.2092 \[hep-ph\]](#).

- [50] S. Alioli, P. Nason, C. Oleari, and E. Re, *A general framework for implementing NLO calculations in shower Monte Carlo programs: the POWHEG BOX*, *JHEP* **06** (2010) 043, arXiv: [1002.2581 \[hep-ph\]](#).
- [51] M. Czakon and A. Mitov, *Top++: A program for the calculation of the top-pair cross-section at hadron colliders*, *Comp. Phys. Comm.* **185** (2014) 2930, arXiv: [1112.5675 \[hep-ph\]](#).
- [52] E. Re, *Single-top Wt-channel production matched with parton showers using the POWHEG method*, *Eur. Phys. J. C* **71** (2011) 1547, arXiv: [1009.2450 \[hep-ph\]](#).
- [53] M. Aliev, H. Lacker, U. Langenfeld, S. Moch, P. Uwer, and M. Wiedermann, *HATHOR — HAdronic Top and Heavy quarks crOSS section calculatoR*, *Comp. Phys. Comm.* **182** (2011) 1034, arXiv: [1007.1327 \[hep-ph\]](#).
- [54] P. Kant, O. M. Kind, T. Kintscher, T. Lohse, T. Martini, S. Mölbitz, P. Rieck, and P. Uwer, *HATHor for single top-quark production: Updated predictions and uncertainty estimates for single top-quark production in hadronic collisions*, *Comp. Phys. Comm.* **191** (2015) 74, arXiv: [1406.4403 \[hep-ph\]](#).
- [55] N. Kidonakis, *Top Quark Production*, DESY-PROC-2013-03, arXiv: [1311.0283 \[hep-ph\]](#).
- [56] V. Barger, W.-Y. Keung, and B. Yencho, *Triple-top signal of new physics at the LHC*, *Phys. Lett. B* **687** (2010) 70, arXiv: [1001.0221 \[hep-ph\]](#).
- [57] G. Bevilacqua and M. Worek, *Constraining BSM physics at the LHC: four top final states with NLO accuracy in perturbative QCD*, *JHEP* **07** (2012) 111, arXiv: [1206.3064 \[hep-ph\]](#).
- [58] ATLAS Collaboration, *Electron efficiency measurements with the ATLAS detector using 2012 LHC proton–proton collision data*, *Eur. Phys. J. C* **77** (2017) 195, arXiv: [1612.01456 \[hep-ex\]](#).
- [59] ATLAS Collaboration, *Muon reconstruction performance of the ATLAS detector in proton–proton collision data at $\sqrt{s} = 13$ TeV*, *Eur. Phys. J. C* **76** (2016) 292, arXiv: [1603.05598 \[hep-ex\]](#).
- [60] M. Cacciari, G. P. Salam, and G. Soyez, *The anti- k_t jet clustering algorithm*, *JHEP* **04** (2008) 063, arXiv: [0802.1189 \[hep-ph\]](#).
- [61] M. Cacciari and G. P. Salam, *Dispelling the N^3 myth for the k_t jet-finder*, *Phys. Lett. B* **641** (2006) 57, arXiv: [hep-ph/0512210](#).
- [62] ATLAS Collaboration, *Topological cell clustering in the ATLAS calorimeters and its performance in LHC Run 1*, *Eur. Phys. J. C* **77** (2017) 490, arXiv: [1603.02934 \[hep-ex\]](#).
- [63] M. Cacciari, G. P. Salam, and G. Soyez, *The catchment area of jets*, *JHEP* **04** (2008) 005, arXiv: [0802.1188 \[hep-ph\]](#).
- [64] ATLAS Collaboration, *Jet energy scale measurements and their systematic uncertainties in proton–proton collisions at $\sqrt{s} = 13$ TeV with the ATLAS detector*, *Phys. Rev. D* **96** (2017) 072002, arXiv: [1703.09665 \[hep-ex\]](#).
- [65] ATLAS Collaboration, *Performance of pile-up mitigation techniques for jets in pp collisions at $\sqrt{s} = 8$ TeV using the ATLAS detector*, *Eur. Phys. J. C* **76** (2016) 581, arXiv: [1510.03823 \[hep-ex\]](#).

- [66] ATLAS Collaboration, *Measurements of b-jet tagging efficiency with the ATLAS detector using $t\bar{t}$ events at $\sqrt{s} = 13$ TeV*, JHEP **08** (2018) 089, arXiv: [1805.01845 \[hep-ex\]](#).
- [67] ATLAS Collaboration, *Performance of algorithms that reconstruct missing transverse momentum in $\sqrt{s} = 8$ TeV proton–proton collisions in the ATLAS detector*, Eur. Phys. J. C **77** (2017) 241, arXiv: [1609.09324 \[hep-ex\]](#).
- [68] ATLAS Collaboration, *Performance of missing transverse momentum reconstruction with the ATLAS detector using proton–proton collisions at $\sqrt{s} = 13$ TeV*, Eur. Phys. J. C **78** (2018) 903, arXiv: [1802.08168 \[hep-ex\]](#).
- [69] ATLAS Collaboration, *Measurement of the top quark-pair production cross section with ATLAS in pp collisions at $\sqrt{s} = 7$ TeV*, Eur. Phys. J. C **71** (2011) 1577, arXiv: [1012.1792 \[hep-ex\]](#).
- [70] G. C. Fox and S. Wolfram, *Observables for the Analysis of Event Shapes in e^+e^- Annihilation and Other Processes*, Phys. Rev. Lett. **41** (1978) 1581.
- [71] ATLAS Collaboration, *Electron reconstruction and identification efficiency measurements with the ATLAS detector using the 2011 LHC proton–proton collision data*, Eur. Phys. J. C **74** (2014) 2941, arXiv: [1404.2240 \[hep-ex\]](#).
- [72] ATLAS Collaboration, *Electron efficiency measurements with the ATLAS detector using the 2012 LHC proton–proton collision data*, ATLAS-CONF-2014-032, 2014, URL: <https://cds.cern.ch/record/1706245>.
- [73] ATLAS Collaboration, *Electron identification measurements in ATLAS using $\sqrt{s} = 13$ TeV data with 50 ns bunch spacing*, ATL-PHYS-PUB-2015-041, 2015, URL: <https://cds.cern.ch/record/2048202>.
- [74] ATLAS Collaboration, *Measurement of b-tagging efficiency of c-jets in $t\bar{t}$ events using a likelihood approach with the ATLAS detector*, ATLAS-CONF-2018-001, 2018, URL: <https://cds.cern.ch/record/2306649>.
- [75] ATLAS Collaboration, *Calibration of light-flavour b-jet mistagging rates using ATLAS proton–proton collision data at $\sqrt{s} = 13$ TeV*, ATLAS-CONF-2018-006, 2018, URL: <https://cds.cern.ch/record/2314418>.
- [76] ATLAS Collaboration, *Calibration of b-tagging using dileptonic top pair events in a combinatorial likelihood approach with the ATLAS experiment*, ATLAS-CONF-2014-004, 2014, URL: <https://cds.cern.ch/record/1664335>.
- [77] ATLAS Collaboration, *Modelling of the $t\bar{t}H$ and $t\bar{t}V(V = W, Z)$ processes for $\sqrt{s} = 13$ TeV ATLAS analyses*, ATL-PHYS-PUB-2016-005, 2016, URL: <https://cds.cern.ch/record/2120826>.
- [78] ATLAS Collaboration, *Measurement of the production cross-section of a single top quark in association with a Z boson in proton–proton collisions at 13 TeV with the ATLAS detector*, Phys. Lett. B **780** (2018) 557, arXiv: [1710.03659 \[hep-ex\]](#).
- [79] CMS Collaboration, *Measurement of the associated production of a single top quark and a Z boson in pp collisions at $\sqrt{s} = 13$ TeV*, Phys. Lett. B **779** (2018) 358, arXiv: [1712.02825 \[hep-ex\]](#).
- [80] W. Verkerke and D. Kirkby, *The RooFit toolkit for data modeling*, arXiv: [physics/0306116](#).

- [81] W. Verkerke and D. Kirkby, *RooFit Users Manual v2.91*, URL: <http://roofit.sourceforge.net>.
- [82] G. Cowan, K. Cranmer, E. Gross, and O. Vitells, *Asymptotic formulae for likelihood-based tests of new physics*, *Eur. Phys. J. C* **71** (2011) 1554, arXiv: [1007.1727 \[physics.data-an\]](#), Erratum: *Eur. Phys. J. C* **73** (2013) 2501.
- [83] J. A. Aguilar-Saavedra, *A minimal set of top anomalous couplings*, *Nucl. Phys. B* **812** (2009) 181, arXiv: [0811.3842 \[hep-ph\]](#).
- [84] B. Grzadkowski, M. Iskrzyński, M. Misiak, and J. Rosiek, *Dimension-six terms in the Standard Model Lagrangian*, *JHEP* **10** (2010) 085, arXiv: [1008.4884 \[hep-ph\]](#).
- [85] J. A. Aguilar-Saavedra et al., *Interpreting top-quark LHC measurements in the standard-model effective field theory*, 2018, arXiv: [1802.07237 \[hep-ph\]](#).
- [86] N. D. Christensen and C. Duhr, *FeynRules — Feynman rules made easy*, *Comp. Phys. Comm.* **180** (2009) 1614, arXiv: [0806.4194 \[hep-ph\]](#).
- [87] C. Degrande, C. Duhr, B. Fuks, D. Grellscheid, O. Mattelaer, and T. Reiter, *UFO — The Universal FeynRules Output*, *Comp. Phys. Comm.* **183** (2012) 1201, arXiv: [1108.2040 \[hep-ph\]](#).
- [88] C. Zhang, N. Greiner, and S. Willenbrock, *Constraints on nonstandard top quark couplings*, *Phys. Rev. D* **86** (2012) 014024, arXiv: [1201.6670 \[hep-ph\]](#).
- [89] CMS Collaboration, *Measurement of the t-channel single-top-quark production cross section and of the $|V_{tb}|$ CKM matrix element in pp collisions at $\sqrt{s} = 8$ TeV*, *JHEP* **06** (2014) 090, arXiv: [1403.7366 \[hep-ex\]](#).
- [90] ATLAS Collaboration, *Measurement of the W boson polarisation in $t\bar{t}$ events from pp collisions at $\sqrt{s} = 8$ TeV in the lepton+jets channel with ATLAS*, *Eur. Phys. J. C* **77** (2017) 264, arXiv: [1612.02577 \[hep-ex\]](#).
- [91] ATLAS Collaboration, *ATLAS Computing Acknowledgements*, ATL-GEN-PUB-2016-002, URL: <https://cds.cern.ch/record/2202407>.

Appendix

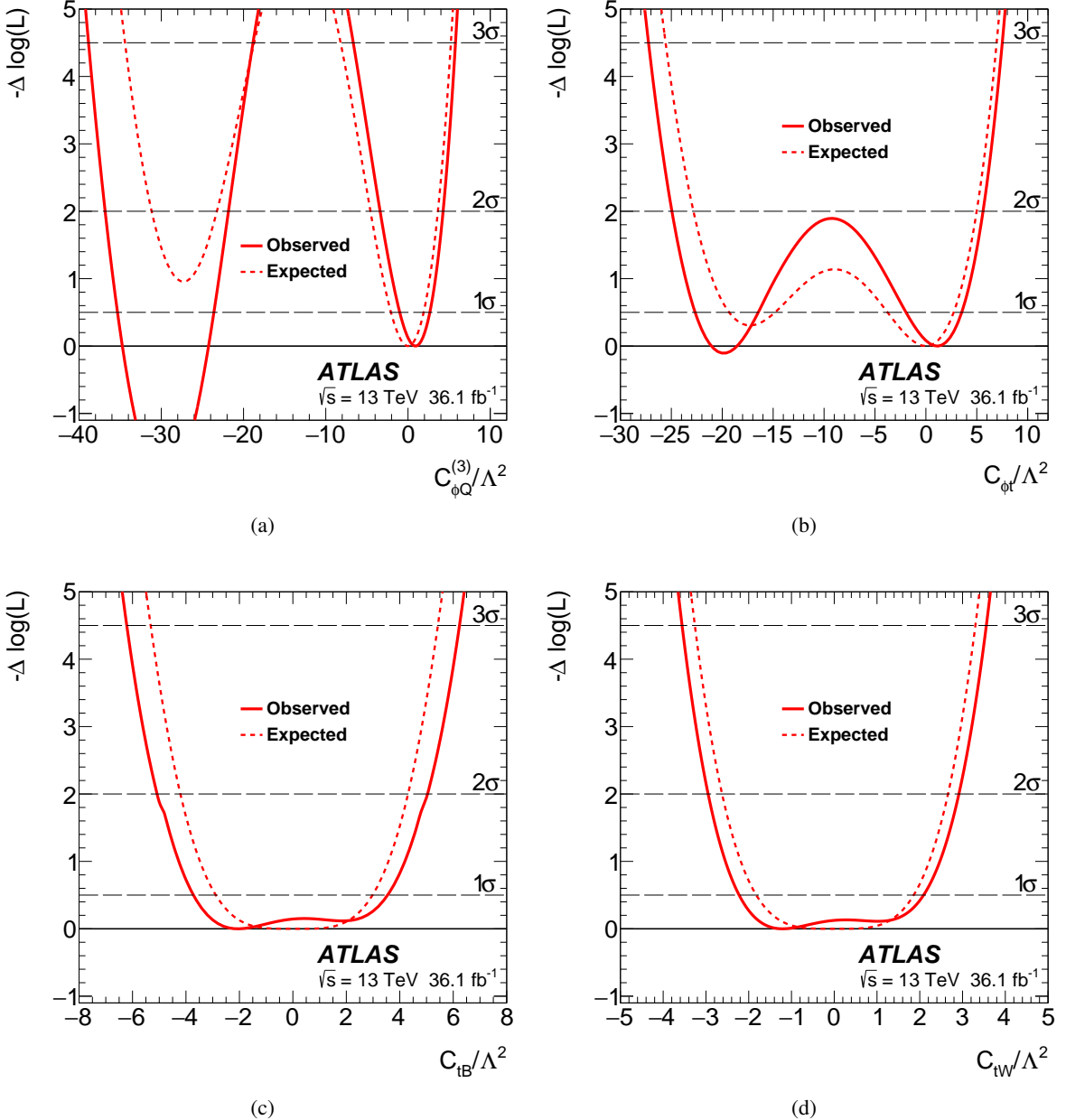


Figure 14: The value of the profile-likelihood test statistic as a function of c/Λ^2 , for (a) $C_{\phi Q}^{(3)}$, (b) $C_{\phi t}$, (c) C_{tB} , and (d) C_{tw} . In the $C_{\phi Q}^{(3)}$ and $C_{\phi t}$ distributions, another, deeper minimum exists for large negative values of C_i , which is excluded by indirect measurements. There, the vertical axis is chosen such that the value of the likelihood at the minimum near $C_i = 0$ is zero.

Table 11: The definitions and ranking of input variables for the BDT in the OS dilepton analysis. Jets and leptons are ordered in descending order of p_T . Only the first eight jets are considered when calculating the input variables.

Definition	Ranking		
	6j1b	5j2b	6j2b
p_T of the lepton pair	8	11	8
p_T of the fourth jet	6	12	6
p_T of the fifth jet	–	14	–
p_T of the sixth jet	9	–	11
ΔR_η between the two leptons	7	8	12
Number of jet pairs with mass within a window of 30 GeV around 85 GeV	4	6	4
Number of three-jet combinations (containing exactly one b -tagged jet) compatible with a top quark ($ m_{bjj} - m_t < 15$ GeV) and ($ m_{jj} - m_W < 15$ GeV)	–	–	17
Invariant mass of the two jets with the smallest ΔR_η	13	7	14
Invariant mass of the two untagged jets with the highest p_T	15	13	–
Invariant mass of the two jets with the highest value of the b -tagging discriminant	–	10	9
Scalar sum of p_T divided by the sum of energy of all jets	2	1	2
Average ΔR_η of all jet pairs	5	4	5
Maximum invariant mass of a lepton and the b -tagged jet with the smallest ΔR_η	14	–	13
First Fox–Wolfram moment built from jets and leptons	3	2	1
Sum of jet p_T , using up to six jets	12	5	10
η of dilepton system	1	3	3
Sum of the two closest two-jet invariant masses from jjj_1 and jjj_2 divided by two	10	–	15
ΔR_η between two jets with the highest value of the b -tagging discriminant in the event	–	9	7
p_T of the b -tagged jet with the highest p_T	11	–	16

The ATLAS Collaboration

M. Aaboud^{34d}, G. Aad⁹⁹, B. Abbott¹²⁵, D.C. Abbott¹⁰⁰, O. Abdinov^{13,*}, B. Abeloos¹²⁹,
D.K. Abhayasinghe⁹¹, S.H. Abidi¹⁶⁴, O.S. AbouZeid³⁹, N.L. Abraham¹⁵³, H. Abramowicz¹⁵⁸,
H. Abreu¹⁵⁷, Y. Abulaiti⁶, B.S. Acharya^{64a,64b,p}, S. Adachi¹⁶⁰, L. Adam⁹⁷, L. Adamczyk^{81a}, L. Adamek¹⁶⁴,
J. Adelman¹¹⁹, M. Adlersberger¹¹², A. Adiguzel^{12c,ai}, T. Adye¹⁴¹, A.A. Affolder¹⁴³, Y. Afik¹⁵⁷,
C. Agheorghiesei^{27c}, J.A. Aguilar-Saavedra^{137f,137a,ah}, F. Ahmadov^{77,af}, G. Aielli^{71a,71b}, S. Akatsuka⁸³,
T.P.A. Åkesson⁹⁴, E. Akilli⁵², A.V. Akimov¹⁰⁸, G.L. Alberghi^{23b,23a}, J. Albert¹⁷³, P. Albicocco⁴⁹,
M.J. Alconada Verzini⁸⁶, S. Alderweireldt¹¹⁷, M. Aleksi³⁵, I.N. Aleksandrov⁷⁷, C. Alexa^{27b},
D. Alexandre¹⁹, T. Alexopoulos¹⁰, M. Alhroob¹²⁵, B. Ali¹³⁹, G. Alimonti^{66a}, J. Alison³⁶, S.P. Alkire¹⁴⁵,
C. Allaire¹²⁹, B.M.M. Allbrooke¹⁵³, B.W. Allen¹²⁸, P.P. Allport²¹, A. Aloisio^{67a,67b}, A. Alonso³⁹,
F. Alonso⁸⁶, C. Alpigiani¹⁴⁵, A.A. Alshehri⁵⁵, M.I. Alstaty⁹⁹, B. Alvarez Gonzalez³⁵,
D. Álvarez Piqueras¹⁷¹, M.G. Alviggi^{67a,67b}, B.T. Amadio¹⁸, Y. Amaral Coutinho^{78b}, A. Ambler¹⁰¹,
L. Ambroz¹³², C. Amelung²⁶, D. Amidei¹⁰³, S.P. Amor Dos Santos^{137a,137c}, S. Amoroso⁴⁴,
C.S. Amrouche⁵², F. An⁷⁶, C. Anastopoulos¹⁴⁶, L.S. Ancu⁵², N. Andari¹⁴², T. Andeen¹¹, C.F. Anders^{59b},
J.K. Anders²⁰, K.J. Anderson³⁶, A. Andreazza^{66a,66b}, V. Andrei^{59a}, C.R. Anelli¹⁷³, S. Angelidakis³⁷,
I. Angelozzi¹¹⁸, A. Angerami³⁸, A.V. Anisenkov^{120b,120a}, A. Annovi^{69a}, C. Antel^{59a}, M.T. Anthony¹⁴⁶,
M. Antonelli⁴⁹, D.J.A. Antrim¹⁶⁸, F. Anulli^{70a}, M. Aoki⁷⁹, J.A. Aparisi Pozo¹⁷¹, L. Aperio Bella³⁵,
G. Arabidze¹⁰⁴, J.P. Araque^{137a}, V. Araujo Ferraz^{78b}, R. Araujo Pereira^{78b}, A.T.H. Arce⁴⁷, R.E. Ardell⁹¹,
F.A. Arduh⁸⁶, J.-F. Arguin¹⁰⁷, S. Argyropoulos⁷⁵, J.-H. Arling⁴⁴, A.J. Armbruster³⁵, L.J. Armitage⁹⁰,
A. Armstrong¹⁶⁸, O. Arnaez¹⁶⁴, H. Arnold¹¹⁸, M. Arratia³¹, O. Arslan²⁴, A. Artamonov^{109,*}, G. Artoni¹³²,
S. Artz⁹⁷, S. Asai¹⁶⁰, N. Asbah⁵⁷, E.M. Asimakopoulou¹⁶⁹, L. Asquith¹⁵³, K. Assamagan²⁹, R. Astalos^{28a},
R.J. Atkin^{32a}, M. Atkinson¹⁷⁰, N.B. Atlay¹⁴⁸, K. Augsten¹³⁹, G. Avolio³⁵, R. Avramidou^{58a},
M.K. Ayoub^{15a}, A.M. Azoulay^{165b}, G. Azuelos^{107,aw}, A.E. Baas^{59a}, M.J. Baca²¹, H. Bachacou¹⁴²,
K. Bachas^{65a,65b}, M. Backes¹³², P. Bagnaia^{70a,70b}, M. Bahmani⁸², H. Bahrasemani¹⁴⁹, A.J. Bailey¹⁷¹,
V.R. Bailey¹⁷⁰, J.T. Baines¹⁴¹, M. Bajic³⁹, C. Bakalis¹⁰, O.K. Baker¹⁸⁰, P.J. Bakker¹¹⁸, D. Bakshi Gupta⁸,
S. Balaji¹⁵⁴, E.M. Baldin^{120b,120a}, P. Balek¹⁷⁷, F. Balli¹⁴², W.K. Balunas¹³⁴, J. Balz⁹⁷, E. Banas⁸²,
A. Bandyopadhyay²⁴, S. Banerjee^{178,l}, A.A.E. Bannoura¹⁷⁹, L. Barak¹⁵⁸, W.M. Barbe³⁷, E.L. Barberio¹⁰²,
D. Barberis^{53b,53a}, M. Barbero⁹⁹, T. Barillari¹¹³, M.-S. Barisits³⁵, J. Barkeloo¹²⁸, T. Barklow¹⁵⁰,
R. Barnea¹⁵⁷, S.L. Barnes^{58c}, B.M. Barnett¹⁴¹, R.M. Barnett¹⁸, Z. Barnovska-Blenessy^{58a},
A. Baroncelli^{72a}, G. Barone²⁹, A.J. Barr¹³², L. Barranco Navarro¹⁷¹, F. Barreiro⁹⁶,
J. Barreiro Guimarães da Costa^{15a}, R. Bartoldus¹⁵⁰, A.E. Barton⁸⁷, P. Bartos^{28a}, A. Basalaev¹³⁵,
A. Bassalat¹²⁹, R.L. Bates⁵⁵, S.J. Batista¹⁶⁴, S. Batlamous^{34e}, J.R. Batley³¹, M. Battaglia¹⁴³,
M. Bauce^{70a,70b}, F. Bauer¹⁴², K.T. Bauer¹⁶⁸, H.S. Bawa¹⁵⁰, J.B. Beacham¹²³, T. Beau¹³³,
P.H. Beauchemin¹⁶⁷, P. Bechtle²⁴, H.C. Beck⁵¹, H.P. Beck^{20,s}, K. Becker⁵⁰, M. Becker⁹⁷, C. Becot⁴⁴,
A. Beddall^{12d}, A.J. Beddall^{12a}, V.A. Bednyakov⁷⁷, M. Bedognetti¹¹⁸, C.P. Bee¹⁵², T.A. Beermann⁷⁴,
M. Begalli^{78b}, M. Begel²⁹, A. Behera¹⁵², J.K. Behr⁴⁴, F. Beisiegel²⁴, A.S. Bell⁹², G. Bella¹⁵⁸,
L. Bellagamba^{23b}, A. Bellerive³³, M. Bellomo¹⁵⁷, P. Bellos⁹, K. Belotskiy¹¹⁰, N.L. Belyaev¹¹⁰,
O. Benary^{158,*}, D. Benchekroun^{34a}, M. Bender¹¹², N. Benekos¹⁰, Y. Benhammou¹⁵⁸,
E. Benhar Noccioli¹⁸⁰, J. Benitez⁷⁵, D.P. Benjamin⁶, M. Benoit⁵², J.R. Bensinger²⁶, S. Bentvelsen¹¹⁸,
L. Beresford¹³², M. Beretta⁴⁹, D. Berge⁴⁴, E. Bergeaas Kuutmann¹⁶⁹, N. Berger⁵, B. Bergmann¹³⁹,
L.J. Bergsten²⁶, J. Beringer¹⁸, S. Berlendis⁷, N.R. Bernard¹⁰⁰, G. Bernardi¹³³, C. Bernius¹⁵⁰,
F.U. Bernlochner²⁴, T. Berry⁹¹, P. Berta⁹⁷, C. Bertella^{15a}, G. Bertoli^{43a,43b}, I.A. Bertram⁸⁷, G.J. Besjes³⁹,
O. Bessidskaia Bylund¹⁷⁹, M. Bessner⁴⁴, N. Besson¹⁴², A. Bethani⁹⁸, S. Bethke¹¹³, A. Betti²⁴,
A.J. Bevan⁹⁰, J. Beyer¹¹³, R. Bi¹³⁶, R.M. Bianchi¹³⁶, O. Biebel¹¹², D. Biedermann¹⁹, R. Bielski³⁵,
K. Bierwagen⁹⁷, N.V. Biesuz^{69a,69b}, M. Biglietti^{72a}, T.R.V. Billoud¹⁰⁷, M. Bindi⁵¹, A. Bingul^{12d},

C. Bini^{70a,70b}, S. Biondi^{23b,23a}, M. Birman¹⁷⁷, T. Bisanz⁵¹, J.P. Biswal¹⁵⁸, C. Bitrich⁴⁶, D.M. Bjergaard⁴⁷, J.E. Black¹⁵⁰, K.M. Black²⁵, T. Blazek^{28a}, I. Bloch⁴⁴, C. Blocker²⁶, A. Blue⁵⁵, U. Blumenschein⁹⁰, Dr. Blunier^{144a}, G.J. Bobbink¹¹⁸, V.S. Bobrovnikov^{120b,120a}, S.S. Bocchetta⁹⁴, A. Bocci⁴⁷, D. Boerner¹⁷⁹, D. Bogavac¹¹², A.G. Bogdanchikov^{120b,120a}, C. Bohm^{43a}, V. Boisvert⁹¹, P. Bokan^{51,169}, T. Bold^{81a}, A.S. Boldyrev¹¹¹, A.E. Bolz^{59b}, M. Bomben¹³³, M. Bona⁹⁰, J.S. Bonilla¹²⁸, M. Boonekamp¹⁴², H.M. Borecka-Bielska⁸⁸, A. Borisov¹²¹, G. Borissov⁸⁷, J. Bortfeldt³⁵, D. Bortoletto¹³², V. Bortolotto^{71a,71b}, D. Boscherini^{23b}, M. Bosman¹⁴, J.D. Bossio Sola³⁰, K. Bouaouda^{34a}, J. Boudreau¹³⁶, E.V. Bouhova-Thacker⁸⁷, D. Boumediene³⁷, C. Bourdarios¹²⁹, S.K. Boutle⁵⁵, A. Boveia¹²³, J. Boyd³⁵, D. Boye^{32b,aq}, I.R. Boyko⁷⁷, A.J. Bozson⁹¹, J. Bracinik²¹, N. Brahimi⁹⁹, A. Brandt⁸, G. Brandt¹⁷⁹, O. Brandt^{59a}, F. Braren⁴⁴, U. Bratzler¹⁶¹, B. Brau¹⁰⁰, J.E. Brau¹²⁸, W.D. Breaden Madden⁵⁵, K. Brendlinger⁴⁴, L. Brenner⁴⁴, R. Brenner¹⁶⁹, S. Bressler¹⁷⁷, B. Brickwedde⁹⁷, D.L. Briglin²¹, D. Britton⁵⁵, D. Britzger¹¹³, I. Brock²⁴, R. Brock¹⁰⁴, G. Brooijmans³⁸, T. Brooks⁹¹, W.K. Brooks^{144b}, E. Brost¹¹⁹, J.H. Broughton²¹, P.A. Bruckman de Renstrom⁸², D. Bruncko^{28b}, A. Bruni^{23b}, G. Bruni^{23b}, L.S. Bruni¹¹⁸, S. Bruno^{71a,71b}, B.H. Brunt³¹, M. Bruschi^{23b}, N. Bruscino¹³⁶, P. Bryant³⁶, L. Bryngemark⁹⁴, T. Buanes¹⁷, Q. Buat³⁵, P. Buchholz¹⁴⁸, A.G. Buckley⁵⁵, I.A. Budagov⁷⁷, M.K. Bugge¹³¹, F. Bührer⁵⁰, O. Bulekov¹¹⁰, D. Bullock⁸, T.J. Burch¹¹⁹, S. Burdin⁸⁸, C.D. Burgard¹¹⁸, A.M. Burger⁵, B. Burghgrave⁸, K. Burk⁸², S. Burke¹⁴¹, I. Burmeister⁴⁵, J.T.P. Burr¹³², V. Büscher⁹⁷, E. Buschmann⁵¹, P. Bussey⁵⁵, J.M. Butler²⁵, C.M. Buttar⁵⁵, J.M. Butterworth⁹², P. Butti³⁵, W. Buttlinger³⁵, A. Buzatu¹⁵⁵, A.R. Buzykaev^{120b,120a}, G. Cabras^{23b,23a}, S. Cabrera Urbán¹⁷¹, D. Caforio¹³⁹, H. Cai¹⁷⁰, V.M.M. Cairo², O. Cakir^{4a}, N. Calace³⁵, P. Calafiura¹⁸, A. Calandri⁹⁹, G. Calderini¹³³, P. Calfayan⁶³, G. Callea⁵⁵, L.P. Caloba^{78b}, S. Calvente Lopez⁹⁶, D. Calvet³⁷, S. Calvet³⁷, T.P. Calvet¹⁵², M. Calvetti^{69a,69b}, R. Camacho Toro¹³³, S. Camarda³⁵, D. Camarero Munoz⁹⁶, P. Camarri^{71a,71b}, D. Cameron¹³¹, R. Caminal Armadans¹⁰⁰, C. Camincher³⁵, S. Campana³⁵, M. Campanelli⁹², A. Camplani³⁹, A. Campoverde¹⁴⁸, V. Canale^{67a,67b}, M. Cano Bret^{58c}, J. Cantero¹²⁶, T. Cao¹⁵⁸, Y. Cao¹⁷⁰, M.D.M. Capeans Garrido³⁵, I. Caprini^{27b}, M. Caprini^{27b}, M. Capua^{40b,40a}, R.M. Carbone³⁸, R. Cardarelli^{71a}, F.C. Cardillo¹⁴⁶, I. Carli¹⁴⁰, T. Carli³⁵, G. Carlino^{67a}, B.T. Carlson¹³⁶, L. Carminati^{66a,66b}, R.M.D. Carney^{43a,43b}, S. Caron¹¹⁷, E. Carquin^{144b}, S. Carrá^{66a,66b}, J.W.S. Carter¹⁶⁴, D. Casadei^{32b}, M.P. Casado^{14,g}, A.F. Casha¹⁶⁴, D.W. Casper¹⁶⁸, R. Castelijn¹¹⁸, F.L. Castillo¹⁷¹, V. Castillo Gimenez¹⁷¹, N.F. Castro^{137a,137e}, A. Catinaccio³⁵, J.R. Catmore¹³¹, A. Cattai³⁵, J. Caudron²⁴, V. Cavalieri²⁹, E. Cavallaro¹⁴, D. Cavalli^{66a}, M. Cavalli-Sforza¹⁴, V. Cavasinni^{69a,69b}, E. Celebi^{12b}, F. Ceradini^{72a,72b}, L. Cerdá Alberich¹⁷¹, A.S. Cerqueira^{78a}, A. Cerri¹⁵³, L. Cerrito^{71a,71b}, F. Cerutti¹⁸, A. Cervelli^{23b,23a}, S.A. Cetin^{12b}, A. Chafaq^{34a}, D. Chakraborty¹¹⁹, S.K. Chan⁵⁷, W.S. Chan¹¹⁸, W.Y. Chan⁸⁸, J.D. Chapman³¹, B. Chargeishvili^{156b}, D.G. Charlton²¹, C.C. Chau³³, C.A. Chavez Barajas¹⁵³, S. Che¹²³, A. Chegwidden¹⁰⁴, S. Chekanov⁶, S.V. Chekulaev^{165a}, G.A. Chelkov^{77,av}, M.A. Chelstowska³⁵, B. Chen⁷⁶, C. Chen^{58a}, C.H. Chen⁷⁶, H. Chen²⁹, J. Chen^{58a}, J. Chen³⁸, S. Chen¹³⁴, S.J. Chen^{15c}, X. Chen^{15b,au}, Y. Chen⁸⁰, Y-H. Chen⁴⁴, H.C. Cheng^{61a}, H.J. Cheng^{15d}, A. Cheplakov⁷⁷, E. Cheremushkina¹²¹, R. Cherkaoui El Moursli^{34e}, E. Cheu⁷, K. Cheung⁶², T.J.A. Chevaléria¹⁴², L. Chevalier¹⁴², V. Chiarella⁴⁹, G. Chiarelli^{69a}, G. Chiodini^{65a}, A.S. Chisholm^{35,21}, A. Chitan^{27b}, I. Chiu¹⁶⁰, Y.H. Chiu¹⁷³, M.V. Chizhov⁷⁷, K. Choi⁶³, A.R. Chomont¹²⁹, S. Chouridou¹⁵⁹, Y.S. Chow¹¹⁸, V. Christodoulou⁹², M.C. Chu^{61a}, J. Chudoba¹³⁸, A.J. Chuinard¹⁰¹, J.J. Chwastowski⁸², L. Chytka¹²⁷, D. Cinca⁴⁵, V. Cindro⁸⁹, I.A. Cioară²⁴, A. Ciocio¹⁸, F. Cirotto^{67a,67b}, Z.H. Citron¹⁷⁷, M. Citterio^{66a}, A. Clark⁵², M.R. Clark³⁸, P.J. Clark⁴⁸, C. Clement^{43a,43b}, Y. Coadou⁹⁹, M. Cobal^{64a,64c}, A. Coccato^{53b}, J. Cochran⁷⁶, H. Cohen¹⁵⁸, A.E.C. Coimbra¹⁷⁷, L. Colasurdo¹¹⁷, B. Cole³⁸, A.P. Colijn¹¹⁸, J. Collot⁵⁶, P. Conde Muñoz^{137a,i}, E. Coniavitis⁵⁰, S.H. Connell^{32b}, I.A. Connelly⁹⁸, S. Constantinescu^{27b}, F. Conventi^{67a,ax}, A.M. Cooper-Sarkar¹³², F. Cormier¹⁷², K.J.R. Cormier¹⁶⁴, L.D. Corpe⁹², M. Corradi^{70a,70b}, E.E. Corrigan⁹⁴, F. Corriveau^{101,ad}, A. Cortes-Gonzalez³⁵, M.J. Costa¹⁷¹, F. Costanza⁵, D. Costanzo¹⁴⁶, G. Cottin³¹, G. Cowan⁹¹, J.W. Cowley³¹, B.E. Cox⁹⁸, J. Crane⁹⁸, K. Cranmer¹²², S.J. Crawley⁵⁵,

R.A. Creager¹³⁴, G. Cree³³, S. Crépé-Renaudin⁵⁶, F. Crescioli¹³³, M. Cristinziani²⁴, V. Croft¹²²,
 G. Crosetti^{40b,40a}, A. Cueto⁹⁶, T. Cuhadar Donszelmann¹⁴⁶, A.R. Cukierman¹⁵⁰, S. Czekierda⁸²,
 P. Czodrowski³⁵, M.J. Da Cunha Sargedas De Sousa^{58b}, C. Da Via⁹⁸, W. Dabrowski^{81a}, T. Dado^{28a,y},
 S. Dahbi^{34e}, T. Dai¹⁰³, F. Dallaire¹⁰⁷, C. Dallapiccola¹⁰⁰, M. Dam³⁹, G. D'amen^{23b,23a}, J. Damp⁹⁷,
 J.R. Dandoy¹³⁴, M.F. Daneri³⁰, N.P. Dang^{178,l}, N.D Dann⁹⁸, M. Danninger¹⁷², V. Dao³⁵, G. Darbo^{53b},
 S. Darmora⁸, O. Dartsi⁵, A. Dattagupta¹²⁸, T. Daubney⁴⁴, S. D'Auria^{66a,66b}, W. Davey²⁴, C. David⁴⁴,
 T. Davidek¹⁴⁰, D.R. Davis⁴⁷, E. Dawe¹⁰², I. Dawson¹⁴⁶, K. De⁸, R. De Asmundis^{67a}, A. De Benedetti¹²⁵,
 M. De Beurs¹¹⁸, S. De Castro^{23b,23a}, S. De Cecco^{70a,70b}, N. De Groot¹¹⁷, P. de Jong¹¹⁸, H. De la Torre¹⁰⁴,
 F. De Lorenzi⁷⁶, A. De Maria^{69a,69b}, D. De Pedis^{70a}, A. De Salvo^{70a}, U. De Sanctis^{71a,71b},
 M. De Santis^{71a,71b}, A. De Santo¹⁵³, K. De Vasconcelos Corga⁹⁹, J.B. De Vivie De Regie¹²⁹,
 C. Debenedetti¹⁴³, D.V. Dedovich⁷⁷, N. Dehghanian³, M. Del Gaudio^{40b,40a}, J. Del Peso⁹⁶,
 Y. Delabat Diaz⁴⁴, D. Delgove¹²⁹, F. Deliot¹⁴², C.M. Delitzsch⁷, M. Della Pietra^{67a,67b}, D. Della Volpe⁵²,
 A. Dell'Acqua³⁵, L. Dell'Asta²⁵, M. Delmastro⁵, C. Delporte¹²⁹, P.A. Delsart⁵⁶, D.A. DeMarco¹⁶⁴,
 S. Demers¹⁸⁰, M. Demichev⁷⁷, S.P. Denisov¹²¹, D. Denysiuk¹¹⁸, L. D'Eramo¹³³, D. Derendarz⁸²,
 J.E. Derkaoui^{34d}, F. Derue¹³³, P. Dervan⁸⁸, K. Desch²⁴, C. Deterre⁴⁴, K. Dette¹⁶⁴, M.R. Devesa³⁰,
 P.O. Deviveiros³⁵, A. Dewhurst¹⁴¹, S. Dhaliwal²⁶, F.A. Di Bello⁵², A. Di Ciaccio^{71a,71b}, L. Di Ciaccio⁵,
 W.K. Di Clemente¹³⁴, C. Di Donato^{67a,67b}, A. Di Girolamo³⁵, G. Di Gregorio^{69a,69b}, B. Di Micco^{72a,72b},
 R. Di Nardo¹⁰⁰, K.F. Di Petrillo⁵⁷, R. Di Sipio¹⁶⁴, D. Di Valentino³³, C. Diaconu⁹⁹, M. Diamond¹⁶⁴,
 F.A. Dias³⁹, T. Dias Do Vale^{137a}, M.A. Diaz^{144a}, J. Dickinson¹⁸, E.B. Diehl¹⁰³, J. Dietrich¹⁹,
 S. Díez Cornell⁴⁴, A. Dimitrievska¹⁸, J. Dingfelder²⁴, F. Dittus³⁵, F. Djama⁹⁹, T. Djobava^{156b},
 J.I. Djuvsland¹⁷, M.A.B. Do Vale^{78c}, M. Dobre^{27b}, D. Dodsworth²⁶, C. Doglioni⁹⁴, J. Dolejsi¹⁴⁰,
 Z. Dolezal¹⁴⁰, M. Donadelli^{78d}, J. Donini³⁷, A. D'onofrio⁹⁰, M. D'Onofrio⁸⁸, J. Dopke¹⁴¹, A. Doria^{67a},
 M.T. Dova⁸⁶, A.T. Doyle⁵⁵, E. Drechsler¹⁴⁹, E. Dreyer¹⁴⁹, T. Dreyer⁵¹, Y. Du^{58b}, F. Dubinin¹⁰⁸,
 M. Dubovsky^{28a}, A. Dubreuil⁵², E. Duchovni¹⁷⁷, G. Duckeck¹¹², A. Ducourthial¹³³, O.A. Ducu^{107,x},
 D. Duda¹¹³, A. Dudarev³⁵, A.C. Dudder⁹⁷, E.M. Duffield¹⁸, L. Duflot¹²⁹, M. Dührssen³⁵, C. Dülsen¹⁷⁹,
 M. Dumancic¹⁷⁷, A.E. Dumitriu^{27b,e}, A.K. Duncan⁵⁵, M. Dunford^{59a}, A. Duperrin⁹⁹, H. Duran Yildiz^{4a},
 M. Düren⁵⁴, A. Durglishvili^{156b}, D. Duschinger⁴⁶, B. Dutta⁴⁴, D. Duvnjak¹, G. Dyckes¹³⁴, M. Dyndal⁴⁴,
 S. Dysch⁹⁸, B.S. Dziedzic⁸², K.M. Ecker¹¹³, R.C. Edgar¹⁰³, T. Eifert³⁵, G. Eigen¹⁷, K. Einsweiler¹⁸,
 T. Ekelof¹⁶⁹, M. El Kacimi^{34c}, R. El Kosseifi⁹⁹, V. Ellajosyula⁹⁹, M. Ellert¹⁶⁹, F. Ellinghaus¹⁷⁹,
 A.A. Elliot⁹⁰, N. Ellis³⁵, J. Elmsheuser²⁹, M. Elsing³⁵, D. Emeliyanov¹⁴¹, A. Emerman³⁸, Y. Enari¹⁶⁰,
 J.S. Ennis¹⁷⁵, M.B. Epland⁴⁷, J. Erdmann⁴⁵, A. Ereditato²⁰, S. Errede¹⁷⁰, M. Escalier¹²⁹, C. Escobar¹⁷¹,
 O. Estrada Pastor¹⁷¹, A.I. Etienne¹⁴², E. Etzion¹⁵⁸, H. Evans⁶³, A. Ezhilov¹³⁵, M. Ezzi^{34e}, F. Fabbri⁵⁵,
 L. Fabbri^{23b,23a}, V. Fabiani¹¹⁷, G. Facini⁹², R.M. Faisca Rodrigues Pereira^{137a}, R.M. Fakhrutdinov¹²¹,
 S. Falciano^{70a}, P.J. Falke⁵, S. Falke⁵, J. Faltova¹⁴⁰, Y. Fang^{15a}, M. Fanti^{66a,66b}, A. Farbin⁸, A. Farilla^{72a},
 E.M. Farina^{68a,68b}, T. Farooque¹⁰⁴, S. Farrell¹⁸, S.M. Farrington¹⁷⁵, P. Farthouat³⁵, F. Fassi^{34e},
 P. Fassnacht³⁵, D. Fassouliotis⁹, M. Fucci Giannelli⁴⁸, W.J. Fawcett³¹, L. Fayard¹²⁹, O.L. Fedin^{135,q},
 W. Fedorko¹⁷², M. Feickert⁴¹, S. Feigl¹³¹, L. Feligioni⁹⁹, C. Feng^{58b}, E.J. Feng³⁵, M. Feng⁴⁷,
 M.J. Fenton⁵⁵, A.B. Fenyuk¹²¹, J. Ferrando⁴⁴, A. Ferrari¹⁶⁹, P. Ferrari¹¹⁸, R. Ferrari^{68a},
 D.E. Ferreira de Lima^{59b}, A. Ferrer¹⁷¹, D. Ferrere⁵², C. Ferretti¹⁰³, F. Fiedler⁹⁷, A. Filipčič⁸⁹,
 F. Filthaut¹¹⁷, K.D. Finelli²⁵, M.C.N. Fiolhais^{137a,137c,a}, L. Fiorini¹⁷¹, C. Fischer¹⁴, W.C. Fisher¹⁰⁴,
 N. Flaschel⁴⁴, I. Fleck¹⁴⁸, P. Fleischmann¹⁰³, R.R.M. Fletcher¹³⁴, T. Flick¹⁷⁹, B.M. Flierl¹¹²,
 L.M. Flores¹³⁴, L.R. Flores Castillo^{61a}, F.M. Follega^{73a,73b}, N. Fomin¹⁷, G.T. Forcolin^{73a,73b},
 A. Formica¹⁴², F.A. Förster¹⁴, A.C. Forti⁹⁸, A.G. Foster²¹, D. Fournier¹²⁹, H. Fox⁸⁷, S. Fracchia¹⁴⁶,
 P. Francavilla^{69a,69b}, M. Franchini^{23b,23a}, S. Franchino^{59a}, D. Francis³⁵, L. Franconi¹⁴³, M. Franklin⁵⁷,
 M. Frate¹⁶⁸, A.N. Fray⁹⁰, D. Freeborn⁹², B. Freund¹⁰⁷, W.S. Freund^{78b}, E.M. Freundlich⁴⁵,
 D.C. Frizzell¹²⁵, D. Froidevaux³⁵, J.A. Frost¹³², C. Fukunaga¹⁶¹, E. Fullana Torregrosa¹⁷¹,
 E. Fumagalli^{53b,53a}, T. Fusayasu¹¹⁴, J. Fuster¹⁷¹, O. Gabizon¹⁵⁷, A. Gabrielli^{23b,23a}, A. Gabrielli¹⁸,

G.P. Gach^{81a}, S. Gadatsch⁵², P. Gadow¹¹³, G. Gagliardi^{53b,53a}, L.G. Gagnon¹⁰⁷, C. Galea^{27b},
 B. Galhardo^{137a,137c}, E.J. Gallas¹³², B.J. Gallop¹⁴¹, P. Gallus¹³⁹, G. Galster³⁹, R. Gamboa Goni⁹⁰,
 K.K. Gan¹²³, S. Ganguly¹⁷⁷, J. Gao^{58a}, Y. Gao⁸⁸, Y.S. Gao^{150,n}, C. García¹⁷¹, J.E. García Navarro¹⁷¹,
 J.A. García Pascual^{15a}, C. Garcia-Argos⁵⁰, M. Garcia-Sciveres¹⁸, R.W. Gardner³⁶, N. Garelli¹⁵⁰,
 S. Gargiulo⁵⁰, V. Garonne¹³¹, K. Gasnikova⁴⁴, A. Gaudiello^{53b,53a}, G. Gaudio^{68a}, I.L. Gavrilenko¹⁰⁸,
 A. Gavriluk¹⁰⁹, C. Gay¹⁷², G. Gaycken²⁴, E.N. Gazis¹⁰, C.N.P. Gee¹⁴¹, J. Geisen⁵¹, M. Geisen⁹⁷,
 M.P. Geisler^{59a}, C. Gemme^{53b}, M.H. Genest⁵⁶, C. Geng¹⁰³, S. Gentile^{70a,70b}, S. George⁹¹, D. Gerbaudo¹⁴,
 G. Gessner⁴⁵, S. Ghasemi¹⁴⁸, M. Ghasemi Bostanabad¹⁷³, M. Ghneimat²⁴, B. Giacobbe^{23b},
 S. Giagu^{70a,70b}, N. Giangiacomi^{23b,23a}, P. Giannetti^{69a}, A. Giannini^{67a,67b}, S.M. Gibson⁹¹, M. Gignac¹⁴³,
 D. Gillberg³³, G. Gilles¹⁷⁹, D.M. Gingrich^{3,aw}, M.P. Giordani^{64a,64c}, F.M. Giorgi^{23b}, P.F. Giraud¹⁴²,
 P. Giromini⁵⁷, G. Giugliarelli^{64a,64c}, D. Giugni^{66a}, F. Giuli¹³², M. Giulini^{59b}, S. Gkaitatzis¹⁵⁹, I. Gkialas^{9,k},
 E.L. Gkougkousis¹⁴, P. Gkountoumis¹⁰, L.K. Gladilin¹¹¹, C. Glasman⁹⁶, J. Glatzer¹⁴, P.C.F. Glaysher⁴⁴,
 A. Glazov⁴⁴, M. Goblirsch-Kolb²⁶, J. Godlewski⁸², S. Goldfarb¹⁰², T. Golling⁵², D. Golubkov¹²¹,
 A. Gomes^{137a,137b}, R. Goncalves Gama⁵¹, R. Gonçalo^{137a}, G. Gonella⁵⁰, L. Gonella²¹, A. Gongadze⁷⁷,
 F. Gonnella²¹, J.L. Gonski⁵⁷, S. González de la Hoz¹⁷¹, S. Gonzalez-Sevilla⁵², L. Goossens³⁵,
 P.A. Gorbounov¹⁰⁹, H.A. Gordon²⁹, B. Gorini³⁵, E. Gorini^{65a,65b}, A. Gorišek⁸⁹, A.T. Goshaw⁴⁷,
 C. Gössling⁴⁵, M.I. Gostkin⁷⁷, C.A. Gottardo²⁴, C.R. Goudet¹²⁹, D. Goujdami^{34c}, A.G. Goussiou¹⁴⁵,
 N. Govender^{32b,c}, C. Goy⁵, E. Gozani¹⁵⁷, I. Grabowska-Bold^{81a}, P.O.J. Gradin¹⁶⁹, E.C. Graham⁸⁸,
 J. Gramling¹⁶⁸, E. Gramstad¹³¹, S. Grancagnolo¹⁹, V. Gratchev¹³⁵, P.M. Gravila^{27f}, F.G. Gravili^{65a,65b},
 C. Gray⁵⁵, H.M. Gray¹⁸, Z.D. Greenwood^{93,al}, C. Grefe²⁴, K. Gregersen⁹⁴, I.M. Gregor⁴⁴, P. Grenier¹⁵⁰,
 K. Grevtsov⁴⁴, N.A. Grieser¹²⁵, J. Griffiths⁸, A.A. Grillo¹⁴³, K. Grimm^{150,b}, S. Grinstein^{14,z}, Ph. Gris³⁷,
 J.-F. Grivaz¹²⁹, S. Groh⁹⁷, E. Gross¹⁷⁷, J. Grosse-Knetter⁵¹, G.C. Grossi⁹³, Z.J. Grout⁹², C. Grud¹⁰³,
 A. Grummer¹¹⁶, L. Guan¹⁰³, W. Guan¹⁷⁸, J. Guenther³⁵, A. Guerguichon¹²⁹, F. Guescini^{165a}, D. Guest¹⁶⁸,
 R. Gugel⁵⁰, B. Gui¹²³, T. Guillemin⁵, S. Guindon³⁵, U. Gul⁵⁵, J. Guo^{58c}, W. Guo¹⁰³, Y. Guo^{58a,t}, Z. Guo⁹⁹,
 R. Gupta⁴⁴, S. Gurbuz^{12c}, G. Gustavino¹²⁵, P. Gutierrez¹²⁵, C. Gutschow⁹², C. Guyot¹⁴², M.P. Guzik^{81a},
 C. Gwenlan¹³², C.B. Gwilliam⁸⁸, A. Haas¹²², C. Haber¹⁸, H.K. Hadavand⁸, N. Haddad^{34e}, A. Hadef^{58a},
 S. Hageböck²⁴, M. Hagihara¹⁶⁶, M. Haleem¹⁷⁴, J. Haley¹²⁶, G. Halladjian¹⁰⁴, G.D. Hallewell⁹⁹,
 K. Hamacher¹⁷⁹, P. Hamal¹²⁷, K. Hamano¹⁷³, A. Hamilton^{32a}, G.N. Hamity¹⁴⁶, K. Han^{58a,ak}, L. Han^{58a},
 S. Han^{15d}, K. Hanagaki^{79,v}, M. Hance¹⁴³, D.M. Handl¹¹², B. Haney¹³⁴, R. Hankache¹³³, P. Hanke^{59a},
 E. Hansen⁹⁴, J.B. Hansen³⁹, J.D. Hansen³⁹, M.C. Hansen²⁴, P.H. Hansen³⁹, K. Hara¹⁶⁶, A.S. Hard¹⁷⁸,
 T. Harenberg¹⁷⁹, S. Harkusha¹⁰⁵, P.F. Harrison¹⁷⁵, N.M. Hartmann¹¹², Y. Hasegawa¹⁴⁷, A. Hasib⁴⁸,
 S. Hassani¹⁴², S. Haug²⁰, R. Hauser¹⁰⁴, L. Hauswald⁴⁶, L.B. Havener³⁸, M. Havranek¹³⁹, C.M. Hawkes²¹,
 R.J. Hawkings³⁵, D. Hayden¹⁰⁴, C. Hayes¹⁵², C.P. Hays¹³², J.M. Hays⁹⁰, H.S. Hayward⁸⁸,
 S.J. Haywood¹⁴¹, F. He^{58a}, M.P. Heath⁴⁸, V. Hedberg⁹⁴, L. Heelan⁸, S. Heer²⁴, K.K. Heidegger⁵⁰,
 J. Heilman³³, S. Heim⁴⁴, T. Heim¹⁸, B. Heinemann^{44,ar}, J.J. Heinrich¹¹², L. Heinrich¹²², C. Heinz⁵⁴,
 J. Hejbal¹³⁸, L. Helary³⁵, A. Held¹⁷², S. Hellesund¹³¹, C.M. Helling¹⁴³, S. Hellman^{43a,43b}, C. Helsens³⁵,
 R.C.W. Henderson⁸⁷, Y. Heng¹⁷⁸, S. Henkelmann¹⁷², A.M. Henriques Correia³⁵, G.H. Herbert¹⁹,
 H. Herde²⁶, V. Herget¹⁷⁴, Y. Hernández Jiménez^{32c}, H. Herr⁹⁷, M.G. Herrmann¹¹², T. Herrmann⁴⁶,
 G. Herten⁵⁰, R. Hertenberger¹¹², L. Hervas³⁵, T.C. Herwig¹³⁴, G.G. Hesketh⁹², N.P. Hessey^{165a},
 A. Higashida¹⁶⁰, S. Higashino⁷⁹, E. Higón-Rodriguez¹⁷¹, K. Hildebrand³⁶, E. Hill¹⁷³, J.C. Hill³¹,
 K.K. Hill²⁹, K.H. Hiller⁴⁴, S.J. Hillier²¹, M. Hils⁴⁶, I. Hinchliffe¹⁸, F. Hinterkeuser²⁴, M. Hirose¹³⁰,
 D. Hirschbuehl¹⁷⁹, B. Hiti⁸⁹, O. Hladík¹³⁸, D.R. Hlálučka^{32c}, X. Hoad⁴⁸, J. Hobbs¹⁵², N. Hod^{165a},
 M.C. Hodgkinson¹⁴⁶, A. Hoecker³⁵, M.R. Hoeferkamp¹¹⁶, F. Hoenig¹¹², D. Hohn⁵⁰, D. Hohov¹²⁹,
 T.R. Holmes³⁶, M. Holzbock¹¹², M. Homann⁴⁵, B.H. Hommels³¹, S. Honda¹⁶⁶, T. Honda⁷⁹, T.M. Hong¹³⁶,
 A. Hönl¹¹³, B.H. Hooberman¹⁷⁰, W.H. Hopkins¹²⁸, Y. Horii¹¹⁵, P. Horn⁴⁶, A.J. Horton¹⁴⁹, L.A. Horyn³⁶,
 J-Y. Hostachy⁵⁶, A. Hostiuc¹⁴⁵, S. Hou¹⁵⁵, A. Hoummada^{34a}, J. Howarth⁹⁸, J. Hoya⁸⁶, M. Hrabovsky¹²⁷,
 J. Hrdinka³⁵, I. Hristova¹⁹, J. Hrivnac¹²⁹, A. Hrynevich¹⁰⁶, T. Hrynev'ova⁵, P.J. Hsu⁶², S.-C. Hsu¹⁴⁵, Q. Hu²⁹,

S. Hu^{58c}, Y. Huang^{15a}, Z. Hubacek¹³⁹, F. Hubaut⁹⁹, M. Huebner²⁴, F. Huegging²⁴, T.B. Huffman¹³², M. Huhtinen³⁵, R.F.H. Hunter³³, P. Huo¹⁵², A.M. Hupe³³, N. Huseynov^{77,af}, J. Huston¹⁰⁴, J. Huth⁵⁷, R. Hyneman¹⁰³, G. Iacobucci⁵², G. Iakovidis²⁹, I. Ibragimov¹⁴⁸, L. Iconomidou-Fayard¹²⁹, Z. Idrissi^{34e}, P. Iengo³⁵, R. Ignazzi³⁹, O. Igonkina^{118,ab}, R. Iguchi¹⁶⁰, T. Iizawa⁵², Y. Ikegami⁷⁹, M. Ikeno⁷⁹, D. Iliadis¹⁵⁹, N. Ilic¹¹⁷, F. Iltzsche⁴⁶, G. Introzzi^{68a,68b}, M. Iodice^{72a}, K. Iordanidou³⁸, V. Ippolito^{70a,70b}, M.F. Isacson¹⁶⁹, N. Ishijima¹³⁰, M. Ishino¹⁶⁰, M. Ishitsuka¹⁶², W. Islam¹²⁶, C. Issever¹³², S. Istin¹⁵⁷, F. Ito¹⁶⁶, J.M. Iturbe Ponce^{61a}, R. Iuppa^{73a,73b}, A. Ivina¹⁷⁷, H. Iwasaki⁷⁹, J.M. Izen⁴², V. Izzo^{67a}, P. Jacka¹³⁸, P. Jackson¹, R.M. Jacobs²⁴, V. Jain², G. Jäkel¹⁷⁹, K.B. Jakobi⁹⁷, K. Jakobs⁵⁰, S. Jakobsen⁷⁴, T. Jakoubek¹³⁸, D.O. Jamin¹²⁶, R. Jansky⁵², J. Janssen²⁴, M. Janus⁵¹, P.A. Janus^{81a}, G. Jarlskog⁹⁴, N. Javadov^{77,af}, T. Javůrek³⁵, M. Javurkova⁵⁰, F. Jeanneau¹⁴², L. Jeanty¹⁸, J. Jejelava^{156a,ag}, A. Jelinskas¹⁷⁵, P. Jenni^{50,d}, J. Jeong⁴⁴, N. Jeong⁴⁴, S. Jézéquel⁵, H. Ji¹⁷⁸, J. Jia¹⁵², H. Jiang⁷⁶, Y. Jiang^{58a}, Z. Jiang^{150,r}, S. Jiggins⁵⁰, F.A. Jimenez Morales³⁷, J. Jimenez Pena¹⁷¹, S. Jin^{15c}, A. Jinaru^{27b}, O. Jinnouchi¹⁶², H. Jivan^{32c}, P. Johansson¹⁴⁶, K.A. Johns⁷, C.A. Johnson⁶³, K. Jon-And^{43a,43b}, R.W.L. Jones⁸⁷, S.D. Jones¹⁵³, S. Jones⁷, T.J. Jones⁸⁸, J. Jongmanns^{59a}, P.M. Jorge^{137a,137b}, J. Jovicevic^{165a}, X. Ju¹⁸, J.J. Junggeburth¹¹³, A. Juste Rozas^{14,z}, A. Kaczmarska⁸², M. Kado¹²⁹, H. Kagan¹²³, M. Kagan¹⁵⁰, T. Kaji¹⁷⁶, E. Kajomovitz¹⁵⁷, C.W. Kalderon⁹⁴, A. Kaluza⁹⁷, S. Kama⁴¹, A. Kamenshchikov¹²¹, L. Kanjur⁸⁹, Y. Kano¹⁶⁰, V.A. Kantserov¹¹⁰, J. Kanzaki⁷⁹, L.S. Kaplan¹⁷⁸, D. Kar^{32c}, M.J. Kareem^{165b}, E. Karentzos¹⁰, S.N. Karpov⁷⁷, Z.M. Karpova⁷⁷, V. Kartvelishvili⁸⁷, A.N. Karyukhin¹²¹, L. Kashif¹⁷⁸, R.D. Kass¹²³, A. Kastanas^{43a,43b}, Y. Kataoka¹⁶⁰, C. Kato^{58d,58c}, J. Katzy⁴⁴, K. Kawade⁸⁰, K. Kawagoe⁸⁵, T. Kawaguchi¹¹⁵, T. Kawamoto¹⁶⁰, G. Kawamura⁵¹, E.F. Kay⁸⁸, V.F. Kazanin^{120b,120a}, R. Keeler¹⁷³, R. Kehoe⁴¹, J.S. Keller³³, E. Kellermann⁹⁴, J.J. Kempster²¹, J. Kendrick²¹, O. Kepka¹³⁸, S. Kersten¹⁷⁹, B.P. Kerševan⁸⁹, S. Ketabchi Haghigat¹⁶⁴, R.A. Keyes¹⁰¹, M. Khader¹⁷⁰, F. Khalil-Zada¹³, A. Khanov¹²⁶, A.G. Kharlamov^{120b,120a}, T. Kharlamova^{120b,120a}, E.E. Khoda¹⁷², A. Khodinov¹⁶³, T.J. Khoo⁵², E. Khramov⁷⁷, J. Khubua^{156b}, S. Kido⁸⁰, M. Kiehn⁵², C.R. Kilby⁹¹, Y.K. Kim³⁶, N. Kimura^{64a,64c}, O.M. Kind¹⁹, B.T. King⁸⁸, D. Kirchmeier⁴⁶, J. Kirk¹⁴¹, A.E. Kiryunin¹¹³, T. Kishimoto¹⁶⁰, D. Kisielewska^{81a}, V. Kitali⁴⁴, O. Kivernyk⁵, E. Kladiva^{28b,*}, T. Klapdor-Kleingrothaus⁵⁰, M.H. Klein¹⁰³, M. Klein⁸⁸, U. Klein⁸⁸, K. Kleinknecht⁹⁷, P. Klimek¹¹⁹, A. Klimentov²⁹, T. Klingl²⁴, T. Klioutchnikova³⁵, F.F. Klitzner¹¹², P. Kluit¹¹⁸, S. Kluth¹¹³, E. Kneringer⁷⁴, E.B.F.G. Knoops⁹⁹, A. Knue⁵⁰, A. Kobayashi¹⁶⁰, D. Kobayashi⁸⁵, T. Kobayashi¹⁶⁰, M. Kobel⁴⁶, M. Kocian¹⁵⁰, P. Kodys¹⁴⁰, P.T. Koenig²⁴, T. Koffas³³, E. Koffeman¹¹⁸, N.M. Köhler¹¹³, T. Koi¹⁵⁰, M. Kolb^{59b}, I. Koletsou⁵, T. Kondo⁷⁹, N. Kondrashova^{58c}, K. Köneke⁵⁰, A.C. König¹¹⁷, T. Kono⁷⁹, R. Konoplich^{122,an}, V. Konstantinides⁹², N. Konstantinidis⁹², B. Konya⁹⁴, R. Kopeliansky⁶³, S. Koperny^{81a}, K. Korcyl⁸², K. Kordas¹⁵⁹, G. Koren¹⁵⁸, A. Korn⁹², I. Korolkov¹⁴, E.V. Korolkova¹⁴⁶, N. Korotkova¹¹¹, O. Kortner¹¹³, S. Kortner¹¹³, T. Kosek¹⁴⁰, V.V. Kostyukhin²⁴, A. Kotwal⁴⁷, A. Koumouris¹⁰, A. Kourkoumeli-Charalampidi^{68a,68b}, C. Kourkoumelis⁹, E. Kourlitis¹⁴⁶, V. Kouskoura²⁹, A.B. Kowalewska⁸², R. Kowalewski¹⁷³, T.Z. Kowalski^{81a}, C. Kozakai¹⁶⁰, W. Kozanecki¹⁴², A.S. Kozhin¹²¹, V.A. Kramarenko¹¹¹, G. Kramberger⁸⁹, D. Krasnopevtsev^{58a}, M.W. Krasny¹³³, A. Krasznahorkay³⁵, D. Krauss¹¹³, J.A. Kremer^{81a}, J. Kretzschmar⁸⁸, P. Krieger¹⁶⁴, K. Krizka¹⁸, K. Kroeninger⁴⁵, H. Kroha¹¹³, J. Kroll¹³⁸, J. Kroll¹³⁴, J. Krstic¹⁶, U. Kruchonak⁷⁷, H. Krüger²⁴, N. Krumnack⁷⁶, M.C. Kruse⁴⁷, T. Kubota¹⁰², S. Kuday^{4b}, J.T. Kuechler¹⁷⁹, S. Kuehn³⁵, A. Kugel^{59a}, T. Kuhl⁴⁴, V. Kukhtin⁷⁷, R. Kukla⁹⁹, Y. Kulchitsky^{105,aj}, S. Kuleshov^{144b}, Y.P. Kulinich¹⁷⁰, M. Kuna⁵⁶, T. Kunigo⁸³, A. Kupco¹³⁸, T. Kupfer⁴⁵, O. Kuprash¹⁵⁸, H. Kurashige⁸⁰, L.L. Kurchaninov^{165a}, Y.A. Kurochkin¹⁰⁵, A. Kurova¹¹⁰, M.G. Kurth^{15d}, E.S. Kuwertz³⁵, M. Kuze¹⁶², J. Kvita¹²⁷, T. Kwan¹⁰¹, A. La Rosa¹¹³, J.L. La Rosa Navarro^{78d}, L. La Rotonda^{40b,40a}, F. La Ruffa^{40b,40a}, C. Lacasta¹⁷¹, F. Lacava^{70a,70b}, J. Lacey⁴⁴, D.P.J. Lack⁹⁸, H. Lacker¹⁹, D. Lacour¹³³, E. Ladygin⁷⁷, R. Lafaye⁵, B. Laforge¹³³, T. Lagouri^{32c}, S. Lai⁵¹, S. Lammers⁶³, W. Lampl⁷, E. Lançon²⁹, U. Landgraf⁵⁰, M.P.J. Landon⁹⁰, M.C. Lanfermann⁵², V.S. Lang⁴⁴, J.C. Lange⁵¹, R.J. Langenberg³⁵, A.J. Lankford¹⁶⁸, F. Lanni²⁹, K. Lantzsch²⁴, A. Lanza^{68a}, A. Lapertosa^{53b,53a}, S. Laplace¹³³, J.F. Laporte¹⁴², T. Lari^{66a},

F. Lasagni Manghi^{23b,23a}, M. Lassnig³⁵, T.S. Lau^{61a}, A. Laudrain¹²⁹, M. Lavorgna^{67a,67b},
 M. Lazzaroni^{66a,66b}, B. Le¹⁰², O. Le Dertz¹³³, E. Le Guirrie⁹⁹, E.P. Le Quilleuc¹⁴², M. LeBlanc⁷,
 T. LeCompte⁶, F. Ledroit-Guillon⁵⁶, C.A. Lee²⁹, G.R. Lee^{144a}, L. Lee⁵⁷, S.C. Lee¹⁵⁵, B. Lefebvre¹⁰¹,
 M. Lefebvre¹⁷³, F. Legger¹¹², C. Leggett¹⁸, K. Lehmann¹⁴⁹, N. Lehmann¹⁷⁹, G. Lehmann Miotto³⁵,
 W.A. Leight⁴⁴, A. Leisos^{159,w}, M.A.L. Leite^{78d}, R. Leitner¹⁴⁰, D. Lellouch¹⁷⁷, K.J.C. Leney⁹², T. Lenz²⁴,
 B. Lenzi³⁵, R. Leone⁷, S. Leone^{69a}, C. Leonidopoulos⁴⁸, G. Lerner¹⁵³, C. Leroy¹⁰⁷, R. Les¹⁶⁴,
 A.A.J. Lesage¹⁴², C.G. Lester³¹, M. Levchenko¹³⁵, J. Levêque⁵, D. Levin¹⁰³, L.J. Levinson¹⁷⁷, D. Lewis⁹⁰,
 B. Li^{15b}, B. Li¹⁰³, C-Q. Li^{58a,am}, H. Li^{58a}, H. Li^{58b}, K. Li¹⁵⁰, L. Li^{58c}, M. Li^{15a}, Q. Li^{15d}, Q.Y. Li^{58a},
 S. Li^{58d,58c}, X. Li^{58c}, Y. Li¹⁴⁸, Z. Liang^{15a}, B. Liberti^{71a}, A. Liblong¹⁶⁴, K. Lie^{61c}, S. Liem¹¹⁸,
 A. Limosani¹⁵⁴, C.Y. Lin³¹, K. Lin¹⁰⁴, T.H. Lin⁹⁷, R.A. Linck⁶³, J.H. Lindon²¹, B.E. Lindquist¹⁵²,
 A.L. Lioni⁵², E. Lipeles¹³⁴, A. Lipniacka¹⁷, M. Lisovyi^{59b}, T.M. Liss^{170,at}, A. Lister¹⁷², A.M. Litke¹⁴³,
 J.D. Little⁸, B. Liu⁷⁶, B.L. Liu⁶, H.B. Liu²⁹, H. Liu¹⁰³, J.B. Liu^{58a}, J.K.K. Liu¹³², K. Liu¹³³, M. Liu^{58a},
 P. Liu¹⁸, Y. Liu^{15a}, Y.L. Liu^{58a}, Y.W. Liu^{58a}, M. Livan^{68a,68b}, A. Lleres⁵⁶, J. Llorente Merino^{15a},
 S.L. Lloyd⁹⁰, C.Y. Lo^{61b}, F. Lo Sterzo⁴¹, E.M. Lobodzinska⁴⁴, P. Loch⁷, T. Lohse¹⁹, K. Lohwasser¹⁴⁶,
 M. Lokajicek¹³⁸, J.D. Long¹⁷⁰, R.E. Long⁸⁷, L. Longo^{65a,65b}, K.A.Looper¹²³, J.A. Lopez^{144b},
 I. Lopez Paz⁹⁸, A. Lopez Solis¹⁴⁶, J. Lorenz¹¹², N. Lorenzo Martinez⁵, M. Losada²², P.J. Lösel¹¹²,
 A. Lösle⁵⁰, X. Lou⁴⁴, X. Lou^{15a}, A. Lounis¹²⁹, J. Love⁶, P.A. Love⁸⁷, J.J. Lozano Bahilo¹⁷¹, H. Lu^{61a},
 M. Lu^{58a}, Y.J. Lu⁶², H.J. Lubatti¹⁴⁵, C. Luci^{70a,70b}, A. Lucotte⁵⁶, C. Luedtke⁵⁰, F. Luehring⁶³, I. Luise¹³³,
 L. Luminari^{70a}, B. Lund-Jensen¹⁵¹, M.S. Lutz¹⁰⁰, P.M. Luzi¹³³, D. Lynn²⁹, R. Lysak¹³⁸, E. Lytken⁹⁴,
 F. Lyu^{15a}, V. Lyubushkin⁷⁷, T. Lyubushkina⁷⁷, H. Ma²⁹, L.L. Ma^{58b}, Y. Ma^{58b}, G. Maccarrone⁴⁹,
 A. Macchioli¹¹³, C.M. Macdonald¹⁴⁶, J. Machado Miguens^{134,137b}, D. Madaffari¹⁷¹, R. Madar³⁷,
 W.F. Mader⁴⁶, N. Madysa⁴⁶, J. Maeda⁸⁰, K. Maekawa¹⁶⁰, S. Maeland¹⁷, T. Maeno²⁹, M. Maerker⁴⁶,
 A.S. Maevskiy¹¹¹, V. Magerl⁵⁰, D.J. Mahon³⁸, C. Maidantchik^{78b}, T. Maier¹¹², A. Maio^{137a,137b,137d},
 O. Majersky^{28a}, S. Majewski¹²⁸, Y. Makida⁷⁹, N. Makovec¹²⁹, B. Malaescu¹³³, Pa. Malecki⁸²,
 V.P. Maleev¹³⁵, F. Malek⁵⁶, U. Mallik⁷⁵, D. Malon⁶, C. Malone³¹, S. Maltezos¹⁰, S. Malyukov³⁵,
 J. Mamuzic¹⁷¹, G. Mancini⁴⁹, I. Mandić⁸⁹, J. Maneira^{137a}, L. Manhaes de Andrade Filho^{78a},
 J. Manjarres Ramos⁴⁶, K.H. Mankinen⁹⁴, A. Mann¹¹², A. Manousos⁷⁴, B. Mansoulie¹⁴²,
 S. Manzoni^{66a,66b}, A. Marantis¹⁵⁹, G. Marceca³⁰, L. March⁵², L. Marchese¹³², G. Marchiori¹³³,
 M. Marcisovsky¹³⁸, C. Marcon⁹⁴, C.A. Marin Tobon³⁵, M. Marjanovic³⁷, F. Marroquin^{78b}, Z. Marshall¹⁸,
 M.U.F Martensson¹⁶⁹, S. Marti-Garcia¹⁷¹, C.B. Martin¹²³, T.A. Martin¹⁷⁵, V.J. Martin⁴⁸,
 B. Martin dit Latour¹⁷, M. Martinez^{14,z}, V.I. Martinez Outschoorn¹⁰⁰, S. Martin-Haugh¹⁴¹,
 V.S. Martoiu^{27b}, A.C. Martyniuk⁹², A. Marzin³⁵, L. Masetti⁹⁷, T. Mashimo¹⁶⁰, R. Mashinistov¹⁰⁸,
 J. Masik⁹⁸, A.L. Maslennikov^{120b,120a}, L.H. Mason¹⁰², L. Massa^{71a,71b}, P. Massarotti^{67a,67b},
 P. Mastrandrea¹⁵², A. Mastroberardino^{40b,40a}, T. Masubuchi¹⁶⁰, P. Mättig²⁴, J. Maurer^{27b}, B. Maček⁸⁹,
 S.J. Maxfield⁸⁸, D.A. Maximov^{120b,120a}, R. Mazini¹⁵⁵, I. Maznas¹⁵⁹, S.M. Mazza¹⁴³, S.P. Mc Kee¹⁰³,
 A. McCarn⁴¹, T.G. McCarthy¹¹³, L.I. McClymont⁹², W.P. McCormack¹⁸, E.F. McDonald¹⁰²,
 J.A. McFayden³⁵, G. Mchedlidze⁵¹, M.A. McKay⁴¹, K.D. McLean¹⁷³, S.J. McMahon¹⁴¹,
 P.C. McNamara¹⁰², C.J. McNicol¹⁷⁵, R.A. McPherson^{173,ad}, J.E. Mdhluli^{32c}, Z.A. Meadows¹⁰⁰,
 S. Meehan¹⁴⁵, T.M. Megy⁵⁰, S. Mehlhase¹¹², A. Mehta⁸⁸, T. Meideck⁵⁶, B. Meirose⁴², D. Melini^{171,h},
 B.R. Mellado Garcia^{32c}, J.D. Mellenthin⁵¹, M. Melo^{28a}, F. Meloni⁴⁴, A. Melzer²⁴, S.B. Menary⁹⁸,
 E.D. Mendes Gouveia^{137a}, L. Meng⁸⁸, X.T. Meng¹⁰³, S. Menke¹¹³, E. Meoni^{40b,40a}, S. Mergelmeyer¹⁹,
 S.A.M. Merkt¹³⁶, C. Merlassino²⁰, P. Mermod⁵², L. Merola^{67a,67b}, C. Meroni^{66a}, F.S. Merritt³⁶,
 A. Messina^{70a,70b}, J. Metcalfe⁶, A.S. Mete¹⁶⁸, C. Meyer⁶³, J. Meyer¹⁵⁷, J-P. Meyer¹⁴²,
 H. Meyer Zu Theenhausen^{59a}, F. Miano¹⁵³, R.P. Middleton¹⁴¹, L. Mijović⁴⁸, G. Mikenberg¹⁷⁷,
 M. Mikestikova¹³⁸, M. Mikuz⁸⁹, M. Milesi¹⁰², A. Milic¹⁶⁴, D.A. Millar⁹⁰, D.W. Miller³⁶, A. Milov¹⁷⁷,
 D.A. Milstead^{43a,43b}, R.A. Mina^{150,r}, A.A. Minaenko¹²¹, M. Miñano Moya¹⁷¹, I.A. Minashvili^{156b},
 A.I. Mincer¹²², B. Mindur^{81a}, M. Mineev⁷⁷, Y. Minegishi¹⁶⁰, Y. Ming¹⁷⁸, L.M. Mir¹⁴, A. Mirto^{65a,65b},

K.P. Mistry¹³⁴, T. Mitani¹⁷⁶, J. Mitrevski¹¹², V.A. Mitsou¹⁷¹, M. Mittal^{58c}, A. Miucci²⁰, P.S. Miyagawa¹⁴⁶, A. Mizukami⁷⁹, J.U. Mjörnmark⁹⁴, T. Mkrtchyan¹⁸¹, M. Mlynarikova¹⁴⁰, T. Moa^{43a,43b}, K. Mochizuki¹⁰⁷, P. Mogg⁵⁰, S. Mohapatra³⁸, S. Molander^{43a,43b}, R. Moles-Valls²⁴, M.C. Mondragon¹⁰⁴, K. Mönig⁴⁴, J. Monk³⁹, E. Monnier⁹⁹, A. Montalbano¹⁴⁹, J. Montejo Berlingen³⁵, F. Monticelli⁸⁶, S. Monzani^{66a}, N. Morange¹²⁹, D. Moreno²², M. Moreno Llácer³⁵, P. Morettini^{53b}, M. Morgenstern¹¹⁸, S. Morgenstern⁴⁶, D. Mori¹⁴⁹, M. Mori⁵⁷, M. Morinaga¹⁷⁶, V. Morisbak¹³¹, A.K. Morley³⁵, G. Mornacchi³⁵, A.P. Morris⁹², J.D. Morris⁹⁰, L. Morvaj¹⁵², P. Moschovakos¹⁰, M. Mosidze^{156b}, H.J. Moss¹⁴⁶, J. Moss^{150,o}, K. Motohashi¹⁶², R. Mount¹⁵⁰, E. Mountricha³⁵, E.J.W. Moyse¹⁰⁰, S. Muanza⁹⁹, F. Mueller¹¹³, J. Mueller¹³⁶, R.S.P. Mueller¹¹², D. Muenstermann⁸⁷, G.A. Mullier⁹⁴, F.J. Munoz Sanchez⁹⁸, P. Murin^{28b}, W.J. Murray^{175,141}, A. Murrone^{66a,66b}, M. Muškinja⁸⁹, C. Mwewa^{32a}, A.G. Myagkov^{121,ao}, J. Myers¹²⁸, M. Myska¹³⁹, B.P. Nachman¹⁸, O. Nackenhorst⁴⁵, K. Nagai¹³², K. Nagano⁷⁹, Y. Nagasaka⁶⁰, M. Nagel⁵⁰, E. Nagy⁹⁹, A.M. Nairz³⁵, Y. Nakahama¹¹⁵, K. Nakamura⁷⁹, T. Nakamura¹⁶⁰, I. Nakano¹²⁴, H. Nanjo¹³⁰, F. Napolitano^{59a}, R.F. Naranjo Garcia⁴⁴, R. Narayan¹¹, D.I. Narrias Villar^{59a}, I. Naryshkin¹³⁵, T. Naumann⁴⁴, G. Navarro²², R. Nayyar⁷, H.A. Neal^{103,*}, P.Y. Nechaeva¹⁰⁸, T.J. Neep¹⁴², A. Negri^{68a,68b}, M. Negrini^{23b}, S. Nektarijevic¹¹⁷, C. Nellist⁵¹, M.E. Nelson¹³², S. Nemecek¹³⁸, P. Nemethy¹²², M. Nessi^{35,f}, M.S. Neubauer¹⁷⁰, M. Neumann¹⁷⁹, P.R. Newman²¹, T.Y. Ng^{61c}, Y.S. Ng¹⁹, Y.W.Y. Ng¹⁶⁸, H.D.N. Nguyen⁹⁹, T. Nguyen Manh¹⁰⁷, E. Nibigira³⁷, R.B. Nickerson¹³², R. Nicolaïdou¹⁴², D.S. Nielsen³⁹, J. Nielsen¹⁴³, N. Nikiforou¹¹, V. Nikolaenko^{121,ao}, I. Nikolic-Audit¹³³, K. Nikolopoulos²¹, P. Nilsson²⁹, H.R. Nindhito⁵², Y. Ninomiya⁷⁹, A. Nisati^{70a}, N. Nishu^{58c}, R. Nisius¹¹³, I. Nitsche⁴⁵, T. Nitta¹⁷⁶, T. Nobe¹⁶⁰, Y. Noguchi⁸³, M. Nomachi¹³⁰, I. Nomidis¹³³, M.A. Nomura²⁹, T. Nooney⁹⁰, M. Nordberg³⁵, N. Norjoharuddeen¹³², T. Novak⁸⁹, O. Novgorodova⁴⁶, R. Novotny¹³⁹, L. Nozka¹²⁷, K. Ntekas¹⁶⁸, E. Nurse⁹², F. Nuti¹⁰², F.G. Oakham^{33,aw}, H. Oberlack¹¹³, J. Ocariz¹³³, A. Ochi⁸⁰, I. Ochoa³⁸, J.P. Ochoa-Ricoux^{144a}, K. O'Connor²⁶, S. Oda⁸⁵, S. Odaka⁷⁹, S. Oerdekk⁵¹, A. Oh⁹⁸, S.H. Oh⁴⁷, C.C. Ohm¹⁵¹, H. Oide^{53b,53a}, M.L. Ojeda¹⁶⁴, H. Okawa¹⁶⁶, Y. Okazaki⁸³, Y. Okumura¹⁶⁰, T. Okuyama⁷⁹, A. Olariu^{27b}, L.F. Oleiro Seabra^{137a}, S.A. Olivares Pino^{144a}, D. Oliveira Damazio²⁹, J.L. Oliver¹, M.J.R. Olsson³⁶, A. Olszewski⁸², J. Olszowska⁸², D.C. O'Neil¹⁴⁹, A. Onofre^{137a,137e}, K. Onogi¹¹⁵, P.U.E. Onyisi¹¹, H. Oppen¹³¹, M.J. Oreglia³⁶, G.E. Orellana⁸⁶, Y. Oren¹⁵⁸, D. Orestano^{72a,72b}, E.C. Orgill⁹⁸, N. Orlando^{61b}, A.A. O'Rourke⁴⁴, R.S. Orr¹⁶⁴, B. Osculati^{53b,53a,*}, V. O'Shea⁵⁵, R. Ospanov^{58a}, G. Otero y Garzon³⁰, H. Otono⁸⁵, M. Ouchrif^{34d}, F. Ould-Saada¹³¹, A. Ouraou¹⁴², Q. Ouyang^{15a}, M. Owen⁵⁵, R.E. Owen²¹, V.E. Ozcan^{12c}, N. Ozturk⁸, J. Pacalt¹²⁷, H.A. Pacey³¹, K. Pachal¹⁴⁹, A. Pacheco Pages¹⁴, L. Pacheco Rodriguez¹⁴², C. Padilla Aranda¹⁴, S. Pagan Griso¹⁸, M. Paganini¹⁸⁰, G. Palacino⁶³, S. Palazzo⁴⁸, S. Palestini³⁵, M. Palka^{81b}, D. Pallin³⁷, I. Panagoulias¹⁰, C.E. Pandini³⁵, J.G. Panduro Vazquez⁹¹, P. Pani³⁵, G. Panizzo^{64a,64c}, L. Paolozzi⁵², T.D. Papadopoulou¹⁰, K. Papageorgiou^{9,k}, A. Paramonov⁶, D. Paredes Hernandez^{61b}, S.R. Paredes Saenz¹³², B. Parida¹⁶³, T.H. Park³³, A.J. Parker⁸⁷, K.A. Parker⁴⁴, M.A. Parker³¹, F. Parodi^{53b,53a}, J.A. Parsons³⁸, U. Parzefall⁵⁰, V.R. Pascuzzi¹⁶⁴, J.M.P. Pasner¹⁴³, E. Pasqualucci^{70a}, S. Passaggio^{53b}, F. Pastore⁹¹, P. Pasuwan^{43a,43b}, S. Pataria⁹⁷, J.R. Pater⁹⁸, A. Pathak^{178,1}, T. Pauly³⁵, B. Pearson¹¹³, M. Pedersen¹³¹, L. Pedraza Diaz¹¹⁷, R. Pedro^{137a,137b}, S.V. Peleganchuk^{120b,120a}, O. Penc¹³⁸, C. Peng^{15d}, H. Peng^{58a}, B.S. Peralva^{78a}, M.M. Perego¹²⁹, A.P. Pereira Peixoto^{137a}, D.V. Perepelitsa²⁹, F. Peri¹⁹, L. Perini^{66a,66b}, H. Pernegger³⁵, S. Perrella^{67a,67b}, V.D. Peshekhonov^{77,*}, K. Peters⁴⁴, R.F.Y. Peters⁹⁸, B.A. Petersen³⁵, T.C. Petersen³⁹, E. Petit⁵⁶, A. Petridis¹, C. Petridou¹⁵⁹, P. Petroff¹²⁹, M. Petrov¹³², F. Petrucci^{72a,72b}, M. Pettee¹⁸⁰, N.E. Pettersson¹⁰⁰, A. Peyaud¹⁴², R. Pezoa^{144b}, T. Pham¹⁰², F.H. Phillips¹⁰⁴, P.W. Phillips¹⁴¹, M.W. Phipps¹⁷⁰, G. Piacquadio¹⁵², E. Pianori¹⁸, A. Picazio¹⁰⁰, R.H. Pickles⁹⁸, R. Piegaia³⁰, J.E. Pilcher³⁶, A.D. Pilkington⁹⁸, M. Pinamonti^{71a,71b}, J.L. Pinfold³, M. Pitt¹⁷⁷, L. Pizzimento^{71a,71b}, M.-A. Pleier²⁹, V. Pleskot¹⁴⁰, E. Plotnikova⁷⁷, D. Pluth⁷⁶, P. Podberezko^{120b,120a}, R. Poettgen⁹⁴, R. Poggi⁵², L. Poggiali¹²⁹, I. Pogrebnyak¹⁰⁴, D. Pohl²⁴, I. Pokharel⁵¹, G. Polesello^{68a}, A. Poley¹⁸, A. Policicchio^{70a,70b}, R. Polifka³⁵, A. Polini^{23b}, C.S. Pollard⁴⁴, V. Polychronakos²⁹, D. Ponomarenko¹¹⁰, L. Pontecorvo³⁵, G.A. Popeneciu^{27d},

D.M. Portillo Quintero¹³³, S. Pospisil¹³⁹, K. Potamianos⁴⁴, I.N. Potrap⁷⁷, C.J. Potter³¹, H. Potti¹¹,
 T. Poulsen⁹⁴, J. Poveda³⁵, T.D. Powell¹⁴⁶, M.E. Pozo Astigarraga³⁵, P. Pralavorio⁹⁹, S. Prell⁷⁶, D. Price⁹⁸,
 M. Primavera^{65a}, S. Prince¹⁰¹, M.L. Proffitt¹⁴⁵, N. Proklova¹¹⁰, K. Prokofiev^{61c}, F. Prokoshin^{144b},
 S. Protopopescu²⁹, J. Proudfoot⁶, M. Przybycien^{81a}, A. Puri¹⁷⁰, P. Puzo¹²⁹, J. Qian¹⁰³, Y. Qin⁹⁸,
 A. Quadt⁵¹, M. Queitsch-Maitland⁴⁴, A. Qureshi¹, P. Rados¹⁰², F. Ragusa^{66a,66b}, G. Rahal⁹⁵, J.A. Raine⁵²,
 S. Rajagopalan²⁹, A. Ramirez Morales⁹⁰, K. Ran^{15a}, T. Rashid¹²⁹, S. Raspovov⁵, M.G. Ratti^{66a,66b},
 D.M. Rauch⁴⁴, F. Rauscher¹¹², S. Rave⁹⁷, B. Ravina¹⁴⁶, I. Ravinovich¹⁷⁷, J.H. Rawling⁹⁸, M. Raymond³⁵,
 A.L. Read¹³¹, N.P. Readioff⁵⁶, M. Reale^{65a,65b}, D.M. Rebuzzi^{68a,68b}, A. Redelbach¹⁷⁴, G. Redlinger²⁹,
 R. Reece¹⁴³, R.G. Reed^{32c}, K. Reeves⁴², L. Rehnisch¹⁹, J. Reichert¹³⁴, D. Reikher¹⁵⁸, A. Reiss⁹⁷,
 A. Rej¹⁴⁸, C. Rembser³⁵, H. Ren^{15d}, M. Rescigno^{70a}, S. Resconi^{66a}, E.D. Resseguie¹³⁴, S. Rettie¹⁷²,
 E. Reynolds²¹, O.L. Rezanova^{120b,120a}, P. Reznicek¹⁴⁰, E. Ricci^{73a,73b}, R. Richter¹¹³, S. Richter⁴⁴,
 E. Richter-Was^{81b}, O. Ricken²⁴, M. Ridel¹³³, P. Rieck¹¹³, C.J. Riegel¹⁷⁹, O. Rifki⁴⁴, M. Rijssenbeek¹⁵²,
 A. Rimoldi^{68a,68b}, M. Rimoldi²⁰, L. Rinaldi^{23b}, G. Ripellino¹⁵¹, B. Ristic⁸⁷, E. Ritsch³⁵, I. Riu¹⁴,
 J.C. Rivera Vergara^{144a}, F. Rizatdinova¹²⁶, E. Rizvi⁹⁰, C. Rizzi¹⁴, R.T. Roberts⁹⁸, S.H. Robertson^{101,ad},
 D. Robinson³¹, J.E.M. Robinson⁴⁴, A. Robson⁵⁵, E. Rocco⁹⁷, C. Roda^{69a,69b}, Y. Rodina⁹⁹,
 S. Rodriguez Bosca¹⁷¹, A. Rodriguez Perez¹⁴, D. Rodriguez Rodriguez¹⁷¹, A.M. Rodríguez Vera^{165b},
 S. Roe³⁵, C.S. Rogan⁵⁷, O. Røhne¹³¹, R. Röhrlig¹¹³, C.P.A. Roland⁶³, J. Roloff⁵⁷, A. Romaniouk¹¹⁰,
 M. Romano^{23b,23a}, N. Rompotis⁸⁸, M. Ronzani¹²², L. Roos¹³³, S. Rosati^{70a}, K. Rosbach⁵⁰, N-A. Rosien⁵¹,
 B.J. Rosser¹³⁴, E. Rossi⁴⁴, E. Rossi^{72a,72b}, E. Rossi^{67a,67b}, L.P. Rossi^{53b}, L. Rossini^{66a,66b}, J.H.N. Rosten³¹,
 R. Rosten¹⁴, M. Rotaru^{27b}, J. Rothberg¹⁴⁵, D. Rousseau¹²⁹, D. Roy^{32c}, A. Rozanov⁹⁹, Y. Rozen¹⁵⁷,
 X. Ruan^{32c}, F. Rubbo¹⁵⁰, F. Rühr⁵⁰, A. Ruiz-Martinez¹⁷¹, Z. Rurikova⁵⁰, N.A. Rusakovich⁷⁷,
 H.L. Russell¹⁰¹, J.P. Rutherford⁷, E.M. Rüttinger^{44,m}, Y.F. Ryabov¹³⁵, M. Rybar³⁸, G. Rybkin¹²⁹, S. Ryu⁶,
 A. Ryzhov¹²¹, G.F. Rzehorž⁵¹, P. Sabatini⁵¹, G. Sabato¹¹⁸, S. Sacerdoti¹²⁹, H.F-W. Sadrozinski¹⁴³,
 R. Sadykov⁷⁷, F. Safai Tehrani^{70a}, P. Saha¹¹⁹, M. Sahinsoy^{59a}, A. Sahu¹⁷⁹, M. Saimpert⁴⁴, M. Saito¹⁶⁰,
 T. Saito¹⁶⁰, H. Sakamoto¹⁶⁰, A. Sakharov^{122,an}, D. Salamani⁵², G. Salamanna^{72a,72b},
 J.E. Salazar Loyola^{144b}, P.H. Sales De Bruin¹⁶⁹, D. Salihagic^{113,*}, A. Salnikov¹⁵⁰, J. Salt¹⁷¹,
 D. Salvatore^{40b,40a}, F. Salvatore¹⁵³, A. Salvucci^{61a,61b,61c}, A. Salzburger³⁵, J. Samarati³⁵, D. Sammel⁵⁰,
 D. Sampsonidis¹⁵⁹, D. Sampsonidou¹⁵⁹, J. Sánchez¹⁷¹, A. Sanchez Pineda^{64a,64c}, H. Sandaker¹³¹,
 C.O. Sander⁴⁴, M. Sandhoff¹⁷⁹, C. Sandoval²², D.P.C. Sankey¹⁴¹, M. Sannino^{53b,53a}, Y. Sano¹¹⁵,
 A. Sansoni⁴⁹, C. Santoni³⁷, H. Santos^{137a}, I. Santoyo Castillo¹⁵³, A. Santra¹⁷¹, A. Sapronov⁷⁷,
 J.G. Saraiva^{137a,137d}, O. Sasaki⁷⁹, K. Sato¹⁶⁶, E. Sauvan⁵, P. Savard^{164,aw}, N. Savic¹¹³, R. Sawada¹⁶⁰,
 C. Sawyer¹⁴¹, L. Sawyer^{93,al}, C. Sbarra^{23b}, A. Sbrizzi^{23a}, T. Scanlon⁹², J. Schaarschmidt¹⁴⁵, P. Schacht¹¹³,
 B.M. Schachtner¹¹², D. Schaefer³⁶, L. Schaefer¹³⁴, J. Schaeffer⁹⁷, S. Schaepe³⁵, U. Schäfer⁹⁷,
 A.C. Schaffer¹²⁹, D. Schaile¹¹², R.D. Schamberger¹⁵², N. Scharmberg⁹⁸, V.A. Schegelsky¹³⁵,
 D. Scheirich¹⁴⁰, F. Schenck¹⁹, M. Schernau¹⁶⁸, C. Schiavi^{53b,53a}, S. Schier¹⁴³, L.K. Schildgen²⁴,
 Z.M. Schillaci²⁶, E.J. Schioppa³⁵, M. Schioppa^{40b,40a}, K.E. Schleicher⁵⁰, S. Schlenker³⁵,
 K.R. Schmidt-Sommerfeld¹¹³, K. Schmieden³⁵, C. Schmitt⁹⁷, S. Schmitt⁴⁴, S. Schmitz⁹⁷,
 J.C. Schmoeckel⁴⁴, U. Schnoor⁵⁰, L. Schoeffel¹⁴², A. Schoening^{59b}, E. Schopf¹³², M. Schott⁹⁷,
 J.F.P. Schouwenberg¹¹⁷, J. Schovancova³⁵, S. Schramm⁵², A. Schulte⁹⁷, H-C. Schultz-Coulon^{59a},
 M. Schumacher⁵⁰, B.A. Schumm¹⁴³, Ph. Schune¹⁴², A. Schwartzman¹⁵⁰, T.A. Schwarz¹⁰³,
 Ph. Schwemling¹⁴², R. Schwienhorst¹⁰⁴, A. Sciandra²⁴, G. Sciolla²⁶, M. Scornajenghi^{40b,40a}, F. Scuri^{69a},
 F. Scutti¹⁰², L.M. Scyboz¹¹³, C.D. Sebastiani^{70a,70b}, P. Seema¹⁹, S.C. Seidel¹¹⁶, A. Seiden¹⁴³, T. Seiss³⁶,
 J.M. Seixas^{78b}, G. Sekhniaidze^{67a}, K. Sekhon¹⁰³, S.J. Sekula⁴¹, N. Semprini-Cesari^{23b,23a}, S. Sen⁴⁷,
 S. Senkin³⁷, C. Serfon¹³¹, L. Serin¹²⁹, L. Serkin^{64a,64b}, M. Sessa^{58a}, H. Severini¹²⁵, F. Sforza¹⁶⁷,
 A. Sfyrla⁵², E. Shabalina⁵¹, J.D. Shahinian¹⁴³, N.W. Shaikh^{43a,43b}, D. Shaked Renous¹⁷⁷, L.Y. Shan^{15a},
 R. Shang¹⁷⁰, J.T. Shank²⁵, M. Shapiro¹⁸, A.S. Sharma¹, A. Sharma¹³², P.B. Shatalov¹⁰⁹, K. Shaw¹⁵³,
 S.M. Shaw⁹⁸, A. Shcherbakova¹³⁵, Y. Shen¹²⁵, N. Sherafati³³, A.D. Sherman²⁵, P. Sherwood⁹²,

L. Shi^{155,as}, S. Shimizu⁷⁹, C.O. Shimmin¹⁸⁰, Y. Shimogama¹⁷⁶, M. Shimojima¹¹⁴, I.P.J. Shipsey¹³²,
 S. Shirabe⁸⁵, M. Shiyakova⁷⁷, J. Shlomi¹⁷⁷, A. Shmeleva¹⁰⁸, D. Shoaleh Saadi¹⁰⁷, M.J. Shochet³⁶,
 S. Shojaii¹⁰², D.R. Shope¹²⁵, S. Shrestha¹²³, E. Shulga¹¹⁰, P. Sicho¹³⁸, A.M. Sickles¹⁷⁰, P.E. Sidebo¹⁵¹,
 E. Sideras Haddad^{32c}, O. Sidiropoulou³⁵, A. Sidoti^{23b,23a}, F. Siegert⁴⁶, Dj. Sijacki¹⁶, J. Silva^{137a},
 M. Silva Jr.¹⁷⁸, M.V. Silva Oliveira^{78a}, S.B. Silverstein^{43a}, S. Simion¹²⁹, E. Simioni⁹⁷, M. Simon⁹⁷,
 R. Simoniello⁹⁷, P. Sinervo¹⁶⁴, N.B. Sinev¹²⁸, M. Sioli^{23b,23a}, I. Siral¹⁰³, S.Yu. Sivoklokov¹¹¹,
 J. Sjölin^{43a,43b}, P. Skubic¹²⁵, M. Slater²¹, T. Slavicek¹³⁹, M. Slawinska⁸², K. Sliwa¹⁶⁷, R. Slovak¹⁴⁰,
 V. Smakhtin¹⁷⁷, B.H. Smart⁵, J. Smiesko^{28a}, N. Smirnov¹¹⁰, S.Yu. Smirnov¹¹⁰, Y. Smirnov¹¹⁰,
 L.N. Smirnova¹¹¹, O. Smirnova⁹⁴, J.W. Smith⁵¹, M. Smizanska⁸⁷, K. Smolek¹³⁹, A. Smykiewicz⁸²,
 A.A. Snesarev¹⁰⁸, I.M. Snyder¹²⁸, S. Snyder²⁹, R. Sobie^{173,ad}, A.M. Soffa¹⁶⁸, A. Soffer¹⁵⁸, A. Søgaard⁴⁸,
 F. Sohns⁵¹, G. Sokhrannyi⁸⁹, C.A. Solans Sanchez³⁵, M. Solar¹³⁹, E.Yu. Soldatov¹¹⁰, U. Soldevila¹⁷¹,
 A.A. Solodkov¹²¹, A. Soloshenko⁷⁷, O.V. Solovyanov¹²¹, V. Solovyev¹³⁵, P. Sommer¹⁴⁶, H. Son¹⁶⁷,
 W. Song¹⁴¹, W.Y. Song^{165b}, A. Sopczak¹³⁹, F. Sopkova^{28b}, C.L. Sotiropoulou^{69a,69b}, S. Sottocornola^{68a,68b},
 R. Soualah^{64a,64c,j}, A.M. Soukharev^{120b,120a}, D. South⁴⁴, S. Spagnolo^{65a,65b}, M. Spalla¹¹³,
 M. Spangenberg¹⁷⁵, F. Spanò⁹¹, D. Sperlich¹⁹, T.M. Spieker^{59a}, R. Spighi^{23b}, G. Spigo³⁵, L.A. Spiller¹⁰²,
 D.P. Spiteri⁵⁵, M. Spousta¹⁴⁰, A. Stabile^{66a,66b}, R. Stamen^{59a}, S. Stamm¹⁹, E. Stanecka⁸², R.W. Stanek⁶,
 C. Stanescu^{72a}, B. Stanislaus¹³², M.M. Stanitzki⁴⁴, B. Stapf¹¹⁸, E.A. Starchenko¹²¹, G.H. Stark¹⁴³,
 J. Stark⁵⁶, S.H Stark³⁹, P. Staroba¹³⁸, P. Starovoitov^{59a}, S. Stärz¹⁰¹, R. Staszewski⁸², M. Stegler⁴⁴,
 P. Steinberg²⁹, B. Stelzer¹⁴⁹, H.J. Stelzer³⁵, O. Stelzer-Chilton^{165a}, H. Stenzel⁵⁴, T.J. Stevenson¹⁵³,
 G.A. Stewart³⁵, M.C. Stockton³⁵, G. Stoicea^{27b}, P. Stolte⁵¹, S. Stonjek¹¹³, A. Straessner⁴⁶,
 J. Strandberg¹⁵¹, S. Strandberg^{43a,43b}, M. Strauss¹²⁵, P. Strizenec^{28b}, R. Ströhmer¹⁷⁴, D.M. Strom¹²⁸,
 R. Stroynowski⁴¹, A. Strubig⁴⁸, S.A. Stucci²⁹, B. Stugu¹⁷, J. Stupak¹²⁵, N.A. Styles⁴⁴, D. Su¹⁵⁰, J. Su¹³⁶,
 S. Suchek^{59a}, Y. Sugaya¹³⁰, M. Suk¹³⁹, V.V. Sulin¹⁰⁸, M.J. Sullivan⁸⁸, D.M.S. Sultan⁵², S. Sultansoy^{4c},
 T. Sumida⁸³, S. Sun¹⁰³, X. Sun³, K. Suruliz¹⁵³, C.J.E. Suster¹⁵⁴, M.R. Sutton¹⁵³, S. Suzuki⁷⁹,
 M. Svatos¹³⁸, M. Swiatlowski³⁶, S.P. Swift², A. Sydorenko⁹⁷, I. Sykora^{28a}, M. Sykora¹⁴⁰, T. Sykora¹⁴⁰,
 D. Ta⁹⁷, K. Tackmann^{44,aa}, J. Taenzer¹⁵⁸, A. Taffard¹⁶⁸, R. Tafirout^{165a}, E. Tahirovic⁹⁰, N. Taiblum¹⁵⁸,
 H. Takai²⁹, R. Takashima⁸⁴, E.H. Takasugi¹¹³, K. Takeda⁸⁰, T. Takeshita¹⁴⁷, Y. Takubo⁷⁹, M. Talby⁹⁹,
 A.A. Talyshev^{120b,120a}, J. Tanaka¹⁶⁰, M. Tanaka¹⁶², R. Tanaka¹²⁹, B.B. Tannenwald¹²³, S. Tapia Araya¹⁷⁰,
 S. Tapprogge⁹⁷, A. Tarek Abouelfadl Mohamed¹³³, S. Tarem¹⁵⁷, G. Tarna^{27b,e}, G.F. Tartarelli^{66a}, P. Tas¹⁴⁰,
 M. Tasevsky¹³⁸, T. Tashiro⁸³, E. Tassi^{40b,40a}, A. Tavares Delgado^{137a,137b}, Y. Tayalati^{34e}, A.J. Taylor⁴⁸,
 G.N. Taylor¹⁰², P.T.E. Taylor¹⁰², W. Taylor^{165b}, A.S. Tee⁸⁷, R. Teixeira De Lima¹⁵⁰, P. Teixeira-Dias⁹¹,
 H. Ten Kate³⁵, J.J. Teoh¹¹⁸, S. Terada⁷⁹, K. Terashi¹⁶⁰, J. Terron⁹⁶, S. Terzo¹⁴, M. Testa⁴⁹,
 R.J. Teuscher^{164,ad}, S.J. Thais¹⁸⁰, T. Theveneaux-Pelzer⁴⁴, F. Thiele³⁹, D.W. Thomas⁹¹, J.P. Thomas²¹,
 A.S. Thompson⁵⁵, P.D. Thompson²¹, L.A. Thomsen¹⁸⁰, E. Thomson¹³⁴, Y. Tian³⁸, R.E. Ticse Torres⁵¹,
 V.O. Tikhomirov^{108,ap}, Yu.A. Tikhonov^{120b,120a}, S. Timoshenko¹¹⁰, P. Tipton¹⁸⁰, S. Tisserant⁹⁹,
 K. Todome¹⁶², S. Todorova-Nova⁵, S. Todt⁴⁶, J. Tojo⁸⁵, S. Tokár^{28a}, K. Tokushuku⁷⁹, E. Tolley¹²³,
 K.G. Tomiwa^{32c}, M. Tomoto¹¹⁵, L. Tompkins^{150,r}, K. Toms¹¹⁶, B. Tong⁵⁷, P. Tornambe⁵⁰, E. Torrence¹²⁸,
 H. Torres⁴⁶, E. Torró Pastor¹⁴⁵, C. Tosciri¹³², J. Toth^{99,ac}, F. Touchard⁹⁹, D.R. Tovey¹⁴⁶, C.J. Treado¹²²,
 T. Trefzger¹⁷⁴, F. Tresoldi¹⁵³, A. Tricoli²⁹, I.M. Trigger^{165a}, S. Trincaz-Duvoid¹³³, W. Trischuk¹⁶⁴,
 B. Trocmé⁵⁶, A. Trofymov¹²⁹, C. Troncon^{66a}, M. Trovatelli¹⁷³, F. Trovato¹⁵³, L. Truong^{32b},
 M. Trzebinski⁸², A. Trzupek⁸², F. Tsai⁴⁴, J.C-L. Tseng¹³², P.V. Tsiareshka^{105,aj}, A. Tsirigotis¹⁵⁹,
 N. Tsirintanis⁹, V. Tsiskaridze¹⁵², E.G. Tskhadadze^{156a}, I.I. Tsukerman¹⁰⁹, V. Tsulaia¹⁸, S. Tsuno⁷⁹,
 D. Tsybychev^{152,163}, Y. Tu^{61b}, A. Tudorache^{27b}, V. Tudorache^{27b}, T.T. Tulbure^{27a}, A.N. Tuna⁵⁷,
 S. Turchikhin⁷⁷, D. Turgeman¹⁷⁷, I. Turk Cakir^{4b,u}, R.J. Turner²¹, R.T. Turra^{66a}, P.M. Tuts³⁸,
 S. Tzamarias¹⁵⁹, E. Tzovara⁹⁷, G. Ucchielli⁴⁵, I. Ueda⁷⁹, M. Ughetto^{43a,43b}, F. Ukegawa¹⁶⁶, G. Unal³⁵,
 A. Undrus²⁹, G. Unei¹⁶⁸, F.C. Ungaro¹⁰², Y. Unno⁷⁹, K. Uno¹⁶⁰, J. Urban^{28b}, P. Urquijo¹⁰², G. Usai⁸,
 J. Usui⁷⁹, L. Vacavant⁹⁹, V. Vacek¹³⁹, B. Vachon¹⁰¹, K.O.H. Vadla¹³¹, A. Vaidya⁹², C. Valderanis¹¹²,

E. Valdes Santurio^{43a,43b}, M. Valente⁵², S. Valentini^{23b,23a}, A. Valero¹⁷¹, L. Valéry⁴⁴, R.A. Vallance²¹,
 A. Vallier⁵, J.A. Valls Ferrer¹⁷¹, T.R. Van Daalen¹⁴, H. Van der Graaf¹¹⁸, P. Van Gemmeren⁶,
 I. Van Vulpen¹¹⁸, M. Vanadia^{71a,71b}, W. Vandelli³⁵, A. Vaniachine¹⁶³, P. Vankov¹¹⁸, R. Vari^{70a},
 E.W. Varnes⁷, C. Varni^{53b,53a}, T. Varol⁴¹, D. Varouchas¹²⁹, K.E. Varvell¹⁵⁴, G.A. Vasquez^{144b},
 J.G. Vasquez¹⁸⁰, F. Vazeille³⁷, D. Vazquez Furelos¹⁴, T. Vazquez Schroeder³⁵, J. Veatch⁵¹,
 V. Vecchio^{72a,72b}, L.M. Veloce¹⁶⁴, F. Veloso^{137a,137c}, S. Veneziano^{70a}, A. Ventura^{65a,65b}, N. Venturi³⁵,
 V. Vercesi^{68a}, M. Verducci^{72a,72b}, C.M. Vergel Infante⁷⁶, C. Vergis²⁴, W. Verkerke¹¹⁸, A.T. Vermeulen¹¹⁸,
 J.C. Vermeulen¹¹⁸, M.C. Vetterli^{149,aw}, N. Viaux Maira^{144b}, M. Vicente Barreto Pinto⁵², I. Vichou^{170,*},
 T. Vickey¹⁴⁶, O.E. Vickey Boeriu¹⁴⁶, G.H.A. Viehhauser¹³², S. Viel¹⁸, L. Vigani¹³², M. Villa^{23b,23a},
 M. Villaplana Perez^{66a,66b}, E. Vilucchi⁴⁹, M.G. Vincter³³, V.B. Vinogradov⁷⁷, A. Vishwakarma⁴⁴,
 C. Vittori^{23b,23a}, I. Vivarelli¹⁵³, S. Vlachos¹⁰, M. Vogel¹⁷⁹, P. Vokac¹³⁹, G. Volpi¹⁴,
 S.E. von Buddenbrock^{32c}, E. Von Toerne²⁴, V. Vorobel¹⁴⁰, K. Vorobev¹¹⁰, M. Vos¹⁷¹, J.H. Vossebeld⁸⁸,
 N. Vranjes¹⁶, M. Vranjes Milosavljevic¹⁶, V. Vrba¹³⁹, M. Vreeswijk¹¹⁸, T. Šfiligoj⁸⁹, R. Vuillermet³⁵,
 I. Vukotic³⁶, T. Ženiš^{28a}, L. Živkovic¹⁶, P. Wagner²⁴, W. Wagner¹⁷⁹, J. Wagner-Kuhr¹¹², H. Wahlberg⁸⁶,
 S. Wahrmund⁴⁶, K. Wakamiya⁸⁰, V.M. Walbrecht¹¹³, J. Walder⁸⁷, R. Walker¹¹², S.D. Walker⁹¹,
 W. Walkowiak¹⁴⁸, V. Wallangen^{43a,43b}, A.M. Wang⁵⁷, C. Wang^{58b}, F. Wang¹⁷⁸, H. Wang¹⁸, H. Wang³,
 J. Wang¹⁵⁴, J. Wang^{59b}, P. Wang⁴¹, Q. Wang¹²⁵, R.-J. Wang¹³³, R. Wang^{58a}, R. Wang⁶, S.M. Wang¹⁵⁵,
 W.T. Wang^{58a}, W. Wang^{15c,ae}, W.X. Wang^{58a,ae}, Y. Wang^{58a,am}, Z. Wang^{58c}, C. Wanotayaroj⁴⁴,
 A. Warburton¹⁰¹, C.P. Ward³¹, D.R. Wardrope⁹², A. Washbrook⁴⁸, P.M. Watkins²¹, A.T. Watson²¹,
 M.F. Watson²¹, G. Watts¹⁴⁵, S. Watts⁹⁸, B.M. Waugh⁹², A.F. Webb¹¹, S. Webb⁹⁷, C. Weber¹⁸⁰,
 M.S. Weber²⁰, S.A. Weber³³, S.M. Weber^{59a}, A.R. Weidberg¹³², J. Weingarten⁴⁵, M. Weirich⁹⁷,
 C. Weiser⁵⁰, P.S. Wells³⁵, T. Wenaus²⁹, T. Wengler³⁵, S. Wenig³⁵, N. Wermes²⁴, M.D. Werner⁷⁶,
 P. Werner³⁵, M. Wessels^{59a}, T.D. Weston²⁰, K. Whalen¹²⁸, N.L. Whallon¹⁴⁵, A.M. Wharton⁸⁷,
 A.S. White¹⁰³, A. White⁸, M.J. White¹, R. White^{144b}, D. Whiteson¹⁶⁸, B.W. Whitmore⁸⁷, F.J. Wickens¹⁴¹,
 W. Wiedenmann¹⁷⁸, M. Wielers¹⁴¹, C. Wiglesworth³⁹, L.A.M. Wiik-Fuchs⁵⁰, F. Wilk⁹⁸, H.G. Wilkens³⁵,
 L.J. Wilkins⁹¹, H.H. Williams¹³⁴, S. Williams³¹, C. Willis¹⁰⁴, S. Willocq¹⁰⁰, J.A. Wilson²¹,
 I. Wingerter-Seez⁵, E. Winkels¹⁵³, F. Winklmeier¹²⁸, O.J. Winston¹⁵³, B.T. Winter⁵⁰, M. Wittgen¹⁵⁰,
 M. Wobisch⁹³, A. Wolf⁹⁷, T.M.H. Wolf¹⁸, R. Wolff⁹⁹, J. Wollrath⁵⁰, M.W. Wolter⁸², H. Wolters^{137a,137c},
 V.W.S. Wong¹⁷², N.L. Woods¹⁴³, S.D. Worm²¹, B.K. Wosiek⁸², K.W. Woźniak⁸², K. Wraight⁵⁵, M. Wu³⁶,
 S.L. Wu¹⁷⁸, X. Wu⁵², Y. Wu^{58a}, T.R. Wyatt⁹⁸, B.M. Wynne⁴⁸, S. Xella³⁹, Z. Xi¹⁰³, L. Xia¹⁷⁵, D. Xu^{15a},
 H. Xu^{58a,e}, L. Xu²⁹, T. Xu¹⁴², W. Xu¹⁰³, Z. Xu¹⁵⁰, B. Yabsley¹⁵⁴, S. Yacoob^{32a}, K. Yajima¹³⁰,
 D.P. Yallup⁹², D. Yamaguchi¹⁶², Y. Yamaguchi¹⁶², A. Yamamoto⁷⁹, T. Yamanaka¹⁶⁰, F. Yamane⁸⁰,
 M. Yamatani¹⁶⁰, T. Yamazaki¹⁶⁰, Y. Yamazaki⁸⁰, Z. Yan²⁵, H.J. Yang^{58c,58d}, H.T. Yang¹⁸, S. Yang⁷⁵,
 Y. Yang¹⁶⁰, Z. Yang¹⁷, W.-M. Yao¹⁸, Y.C. Yap⁴⁴, Y. Yasu⁷⁹, E. Yatsenko^{58c,58d}, J. Ye⁴¹, S. Ye²⁹,
 I. Yeletskikh⁷⁷, E. Yigitbasi²⁵, E. Yildirim⁹⁷, K. Yorita¹⁷⁶, K. Yoshihara¹³⁴, C.J.S. Young³⁵, C. Young¹⁵⁰,
 J. Yu⁸, J. Yu⁷⁶, X. Yue^{59a}, S.P.Y. Yuen²⁴, B. Zabinski⁸², G. Zacharis¹⁰, E. Zaffaroni⁵², R. Zaidan¹⁴,
 A.M. Zaitsev^{121,ao}, T. Zakareishvili^{156b}, N. Zakharchuk³³, S. Zambito⁵⁷, D. Zanzi³⁵, D.R. Zaripovas⁵⁵,
 S.V. Zeißner⁴⁵, C. Zeitnitz¹⁷⁹, G. Zemaitytė¹³², J.C. Zeng¹⁷⁰, Q. Zeng¹⁵⁰, O. Zenin¹²¹, D. Zerwas¹²⁹,
 M. Zgubić¹³², D.F. Zhang^{58b}, D. Zhang¹⁰³, F. Zhang¹⁷⁸, G. Zhang^{58a}, G. Zhang^{15b}, H. Zhang^{15c},
 J. Zhang⁶, L. Zhang^{15c}, L. Zhang^{58a}, M. Zhang¹⁷⁰, P. Zhang^{15c}, R. Zhang^{58a}, R. Zhang²⁴, X. Zhang^{58b},
 Y. Zhang^{15d}, Z. Zhang¹²⁹, P. Zhao⁴⁷, Y. Zhao^{58b,129,ak}, Z. Zhao^{58a}, A. Zhemchugov⁷⁷, Z. Zheng¹⁰³,
 D. Zhong¹⁷⁰, B. Zhou¹⁰³, C. Zhou¹⁷⁸, M.S. Zhou^{15d}, M. Zhou¹⁵², N. Zhou^{58c}, Y. Zhou⁷, C.G. Zhu^{58b},
 H.L. Zhu^{58a}, H. Zhu^{15a}, J. Zhu¹⁰³, Y. Zhu^{58a}, X. Zhuang^{15a}, K. Zhukov¹⁰⁸, V. Zhulanov^{120b,120a},
 A. Zibell¹⁷⁴, D. Ziemińska⁶³, N.I. Zimine⁷⁷, S. Zimmermann⁵⁰, Z. Zinonos¹¹³, M. Ziolkowski¹⁴⁸,
 G. Zobernig¹⁷⁸, A. Zoccoli^{23b,23a}, K. Zoch⁵¹, T.G. Zorbas¹⁴⁶, R. Zou³⁶, M. Zur Nedden¹⁹, L. Zwalski³⁵.

¹Department of Physics, University of Adelaide, Adelaide; Australia.

- ²Physics Department, SUNY Albany, Albany NY; United States of America.
- ³Department of Physics, University of Alberta, Edmonton AB; Canada.
- ^{4(a)}Department of Physics, Ankara University, Ankara; ^(b)Istanbul Aydin University, Istanbul; ^(c)Division of Physics, TOBB University of Economics and Technology, Ankara; Turkey.
- ⁵LAPP, Université Grenoble Alpes, Université Savoie Mont Blanc, CNRS/IN2P3, Annecy; France.
- ⁶High Energy Physics Division, Argonne National Laboratory, Argonne IL; United States of America.
- ⁷Department of Physics, University of Arizona, Tucson AZ; United States of America.
- ⁸Department of Physics, University of Texas at Arlington, Arlington TX; United States of America.
- ⁹Physics Department, National and Kapodistrian University of Athens, Athens; Greece.
- ¹⁰Physics Department, National Technical University of Athens, Zografou; Greece.
- ¹¹Department of Physics, University of Texas at Austin, Austin TX; United States of America.
- ^{12(a)}Bahcesehir University, Faculty of Engineering and Natural Sciences, Istanbul; ^(b)Istanbul Bilgi University, Faculty of Engineering and Natural Sciences, Istanbul; ^(c)Department of Physics, Bogazici University, Istanbul; ^(d)Department of Physics Engineering, Gaziantep University, Gaziantep; Turkey.
- ¹³Institute of Physics, Azerbaijan Academy of Sciences, Baku; Azerbaijan.
- ¹⁴Institut de Física d'Altes Energies (IFAE), Barcelona Institute of Science and Technology, Barcelona; Spain.
- ^{15(a)}Institute of High Energy Physics, Chinese Academy of Sciences, Beijing; ^(b)Physics Department, Tsinghua University, Beijing; ^(c)Department of Physics, Nanjing University, Nanjing; ^(d)University of Chinese Academy of Science (UCAS), Beijing; China.
- ¹⁶Institute of Physics, University of Belgrade, Belgrade; Serbia.
- ¹⁷Department for Physics and Technology, University of Bergen, Bergen; Norway.
- ¹⁸Physics Division, Lawrence Berkeley National Laboratory and University of California, Berkeley CA; United States of America.
- ¹⁹Institut für Physik, Humboldt Universität zu Berlin, Berlin; Germany.
- ²⁰Albert Einstein Center for Fundamental Physics and Laboratory for High Energy Physics, University of Bern, Bern; Switzerland.
- ²¹School of Physics and Astronomy, University of Birmingham, Birmingham; United Kingdom.
- ²²Centro de Investigaciones, Universidad Antonio Nariño, Bogota; Colombia.
- ^{23(a)}Dipartimento di Fisica e Astronomia, Università di Bologna, Bologna; ^(b)INFN Sezione di Bologna; Italy.
- ²⁴Physikalisches Institut, Universität Bonn, Bonn; Germany.
- ²⁵Department of Physics, Boston University, Boston MA; United States of America.
- ²⁶Department of Physics, Brandeis University, Waltham MA; United States of America.
- ^{27(a)}Transilvania University of Brasov, Brasov; ^(b)Horia Hulubei National Institute of Physics and Nuclear Engineering, Bucharest; ^(c)Department of Physics, Alexandru Ioan Cuza University of Iasi, Iasi; ^(d)National Institute for Research and Development of Isotopic and Molecular Technologies, Physics Department, Cluj-Napoca; ^(e)University Politehnica Bucharest, Bucharest; ^(f)West University in Timisoara, Timisoara; Romania.
- ^{28(a)}Faculty of Mathematics, Physics and Informatics, Comenius University, Bratislava; ^(b)Department of Subnuclear Physics, Institute of Experimental Physics of the Slovak Academy of Sciences, Kosice; Slovak Republic.
- ²⁹Physics Department, Brookhaven National Laboratory, Upton NY; United States of America.
- ³⁰Departamento de Física, Universidad de Buenos Aires, Buenos Aires; Argentina.
- ³¹Cavendish Laboratory, University of Cambridge, Cambridge; United Kingdom.
- ^{32(a)}Department of Physics, University of Cape Town, Cape Town; ^(b)Department of Mechanical Engineering Science, University of Johannesburg, Johannesburg; ^(c)School of Physics, University of the

Witwatersrand, Johannesburg; South Africa.

³³Department of Physics, Carleton University, Ottawa ON; Canada.

^{34(a)}Faculté des Sciences Ain Chock, Réseau Universitaire de Physique des Hautes Energies - Université Hassan II, Casablanca;^(b)Centre National de l'Energie des Sciences Techniques Nucleaires (CNESTEN), Rabat;^(c)Faculté des Sciences Semlalia, Université Cadi Ayyad, LPHEA-Marrakech;^(d)Faculté des Sciences, Université Mohamed Premier and LPTPM, Oujda;^(e)Faculté des sciences, Université Mohammed V, Rabat; Morocco.

³⁵CERN, Geneva; Switzerland.

³⁶Enrico Fermi Institute, University of Chicago, Chicago IL; United States of America.

³⁷LPC, Université Clermont Auvergne, CNRS/IN2P3, Clermont-Ferrand; France.

³⁸Nevis Laboratory, Columbia University, Irvington NY; United States of America.

³⁹Niels Bohr Institute, University of Copenhagen, Copenhagen; Denmark.

^{40(a)}Dipartimento di Fisica, Università della Calabria, Rende;^(b)INFN Gruppo Collegato di Cosenza, Laboratori Nazionali di Frascati; Italy.

⁴¹Physics Department, Southern Methodist University, Dallas TX; United States of America.

⁴²Physics Department, University of Texas at Dallas, Richardson TX; United States of America.

^{43(a)}Department of Physics, Stockholm University;^(b)Oskar Klein Centre, Stockholm; Sweden.

⁴⁴Deutsches Elektronen-Synchrotron DESY, Hamburg and Zeuthen; Germany.

⁴⁵Lehrstuhl für Experimentelle Physik IV, Technische Universität Dortmund, Dortmund; Germany.

⁴⁶Institut für Kern- und Teilchenphysik, Technische Universität Dresden, Dresden; Germany.

⁴⁷Department of Physics, Duke University, Durham NC; United States of America.

⁴⁸SUPA - School of Physics and Astronomy, University of Edinburgh, Edinburgh; United Kingdom.

⁴⁹INFN e Laboratori Nazionali di Frascati, Frascati; Italy.

⁵⁰Physikalisch Institut, Albert-Ludwigs-Universität Freiburg, Freiburg; Germany.

⁵¹II. Physikalisch Institut, Georg-August-Universität Göttingen, Göttingen; Germany.

⁵²Département de Physique Nucléaire et Corpusculaire, Université de Genève, Genève; Switzerland.

^{53(a)}Dipartimento di Fisica, Università di Genova, Genova;^(b)INFN Sezione di Genova; Italy.

⁵⁴II. Physikalisch Institut, Justus-Liebig-Universität Giessen, Giessen; Germany.

⁵⁵SUPA - School of Physics and Astronomy, University of Glasgow, Glasgow; United Kingdom.

⁵⁶LPSC, Université Grenoble Alpes, CNRS/IN2P3, Grenoble INP, Grenoble; France.

⁵⁷Laboratory for Particle Physics and Cosmology, Harvard University, Cambridge MA; United States of America.

^{58(a)}Department of Modern Physics and State Key Laboratory of Particle Detection and Electronics, University of Science and Technology of China, Hefei;^(b)Institute of Frontier and Interdisciplinary Science and Key Laboratory of Particle Physics and Particle Irradiation (MOE), Shandong University, Qingdao;^(c)School of Physics and Astronomy, Shanghai Jiao Tong University, KLPPAC-MoE, SKLPPC, Shanghai;^(d)Tsung-Dao Lee Institute, Shanghai; China.

^{59(a)}Kirchhoff-Institut für Physik, Ruprecht-Karls-Universität Heidelberg, Heidelberg;^(b)Physikalisch Institut, Ruprecht-Karls-Universität Heidelberg, Heidelberg; Germany.

⁶⁰Faculty of Applied Information Science, Hiroshima Institute of Technology, Hiroshima; Japan.

^{61(a)}Department of Physics, Chinese University of Hong Kong, Shatin, N.T., Hong Kong;^(b)Department of Physics, University of Hong Kong, Hong Kong;^(c)Department of Physics and Institute for Advanced Study, Hong Kong University of Science and Technology, Clear Water Bay, Kowloon, Hong Kong; China.

⁶²Department of Physics, National Tsing Hua University, Hsinchu; Taiwan.

⁶³Department of Physics, Indiana University, Bloomington IN; United States of America.

^{64(a)}INFN Gruppo Collegato di Udine, Sezione di Trieste, Udine;^(b)ICTP, Trieste;^(c)Dipartimento di Chimica, Fisica e Ambiente, Università di Udine, Udine; Italy.

- ^{65(a)}INFN Sezione di Lecce; ^(b)Dipartimento di Matematica e Fisica, Università del Salento, Lecce; Italy.
^{66(a)}INFN Sezione di Milano; ^(b)Dipartimento di Fisica, Università di Milano, Milano; Italy.
^{67(a)}INFN Sezione di Napoli; ^(b)Dipartimento di Fisica, Università di Napoli, Napoli; Italy.
^{68(a)}INFN Sezione di Pavia; ^(b)Dipartimento di Fisica, Università di Pavia, Pavia; Italy.
^{69(a)}INFN Sezione di Pisa; ^(b)Dipartimento di Fisica E. Fermi, Università di Pisa, Pisa; Italy.
^{70(a)}INFN Sezione di Roma; ^(b)Dipartimento di Fisica, Sapienza Università di Roma, Roma; Italy.
^{71(a)}INFN Sezione di Roma Tor Vergata; ^(b)Dipartimento di Fisica, Università di Roma Tor Vergata, Roma; Italy.
^{72(a)}INFN Sezione di Roma Tre; ^(b)Dipartimento di Matematica e Fisica, Università Roma Tre, Roma; Italy.
^{73(a)}INFN-TIFPA; ^(b)Università degli Studi di Trento, Trento; Italy.
⁷⁴Institut für Astro- und Teilchenphysik, Leopold-Franzens-Universität, Innsbruck; Austria.
⁷⁵University of Iowa, Iowa City IA; United States of America.
⁷⁶Department of Physics and Astronomy, Iowa State University, Ames IA; United States of America.
⁷⁷Joint Institute for Nuclear Research, Dubna; Russia.
^{78(a)}Departamento de Engenharia Elétrica, Universidade Federal de Juiz de Fora (UFJF), Juiz de Fora; ^(b)Universidade Federal do Rio De Janeiro COPPE/EE/IF, Rio de Janeiro; ^(c)Universidade Federal de São João del Rei (UFSJ), São João del Rei; ^(d)Instituto de Física, Universidade de São Paulo, São Paulo; Brazil.
⁷⁹KEK, High Energy Accelerator Research Organization, Tsukuba; Japan.
⁸⁰Graduate School of Science, Kobe University, Kobe; Japan.
^{81(a)}AGH University of Science and Technology, Faculty of Physics and Applied Computer Science, Krakow; ^(b)Marian Smoluchowski Institute of Physics, Jagiellonian University, Krakow; Poland.
⁸²Institute of Nuclear Physics Polish Academy of Sciences, Krakow; Poland.
⁸³Faculty of Science, Kyoto University, Kyoto; Japan.
⁸⁴Kyoto University of Education, Kyoto; Japan.
⁸⁵Research Center for Advanced Particle Physics and Department of Physics, Kyushu University, Fukuoka ; Japan.
⁸⁶Instituto de Física La Plata, Universidad Nacional de La Plata and CONICET, La Plata; Argentina.
⁸⁷Physics Department, Lancaster University, Lancaster; United Kingdom.
⁸⁸Oliver Lodge Laboratory, University of Liverpool, Liverpool; United Kingdom.
⁸⁹Department of Experimental Particle Physics, Jožef Stefan Institute and Department of Physics, University of Ljubljana, Ljubljana; Slovenia.
⁹⁰School of Physics and Astronomy, Queen Mary University of London, London; United Kingdom.
⁹¹Department of Physics, Royal Holloway University of London, Egham; United Kingdom.
⁹²Department of Physics and Astronomy, University College London, London; United Kingdom.
⁹³Louisiana Tech University, Ruston LA; United States of America.
⁹⁴Fysiska institutionen, Lunds universitet, Lund; Sweden.
⁹⁵Centre de Calcul de l’Institut National de Physique Nucléaire et de Physique des Particules (IN2P3), Villeurbanne; France.
⁹⁶Departamento de Física Teorica C-15 and CIAFF, Universidad Autónoma de Madrid, Madrid; Spain.
⁹⁷Institut für Physik, Universität Mainz, Mainz; Germany.
⁹⁸School of Physics and Astronomy, University of Manchester, Manchester; United Kingdom.
⁹⁹CPPM, Aix-Marseille Université, CNRS/IN2P3, Marseille; France.
¹⁰⁰Department of Physics, University of Massachusetts, Amherst MA; United States of America.
¹⁰¹Department of Physics, McGill University, Montreal QC; Canada.
¹⁰²School of Physics, University of Melbourne, Victoria; Australia.
¹⁰³Department of Physics, University of Michigan, Ann Arbor MI; United States of America.

- ¹⁰⁴Department of Physics and Astronomy, Michigan State University, East Lansing MI; United States of America.
- ¹⁰⁵B.I. Stepanov Institute of Physics, National Academy of Sciences of Belarus, Minsk; Belarus.
- ¹⁰⁶Research Institute for Nuclear Problems of Byelorussian State University, Minsk; Belarus.
- ¹⁰⁷Group of Particle Physics, University of Montreal, Montreal QC; Canada.
- ¹⁰⁸P.N. Lebedev Physical Institute of the Russian Academy of Sciences, Moscow; Russia.
- ¹⁰⁹Institute for Theoretical and Experimental Physics of the National Research Centre Kurchatov Institute, Moscow; Russia.
- ¹¹⁰National Research Nuclear University MEPhI, Moscow; Russia.
- ¹¹¹D.V. Skobeltsyn Institute of Nuclear Physics, M.V. Lomonosov Moscow State University, Moscow; Russia.
- ¹¹²Fakultät für Physik, Ludwig-Maximilians-Universität München, München; Germany.
- ¹¹³Max-Planck-Institut für Physik (Werner-Heisenberg-Institut), München; Germany.
- ¹¹⁴Nagasaki Institute of Applied Science, Nagasaki; Japan.
- ¹¹⁵Graduate School of Science and Kobayashi-Maskawa Institute, Nagoya University, Nagoya; Japan.
- ¹¹⁶Department of Physics and Astronomy, University of New Mexico, Albuquerque NM; United States of America.
- ¹¹⁷Institute for Mathematics, Astrophysics and Particle Physics, Radboud University Nijmegen/Nikhef, Nijmegen; Netherlands.
- ¹¹⁸Nikhef National Institute for Subatomic Physics and University of Amsterdam, Amsterdam; Netherlands.
- ¹¹⁹Department of Physics, Northern Illinois University, DeKalb IL; United States of America.
- ^{120(a)}Budker Institute of Nuclear Physics and NSU, SB RAS, Novosibirsk;^(b)Novosibirsk State University Novosibirsk; Russia.
- ¹²¹Institute for High Energy Physics of the National Research Centre Kurchatov Institute, Protvino; Russia.
- ¹²²Department of Physics, New York University, New York NY; United States of America.
- ¹²³Ohio State University, Columbus OH; United States of America.
- ¹²⁴Faculty of Science, Okayama University, Okayama; Japan.
- ¹²⁵Homer L. Dodge Department of Physics and Astronomy, University of Oklahoma, Norman OK; United States of America.
- ¹²⁶Department of Physics, Oklahoma State University, Stillwater OK; United States of America.
- ¹²⁷Palacký University, RCPTM, Joint Laboratory of Optics, Olomouc; Czech Republic.
- ¹²⁸Center for High Energy Physics, University of Oregon, Eugene OR; United States of America.
- ¹²⁹LAL, Université Paris-Sud, CNRS/IN2P3, Université Paris-Saclay, Orsay; France.
- ¹³⁰Graduate School of Science, Osaka University, Osaka; Japan.
- ¹³¹Department of Physics, University of Oslo, Oslo; Norway.
- ¹³²Department of Physics, Oxford University, Oxford; United Kingdom.
- ¹³³LPNHE, Sorbonne Université, Paris Diderot Sorbonne Paris Cité, CNRS/IN2P3, Paris; France.
- ¹³⁴Department of Physics, University of Pennsylvania, Philadelphia PA; United States of America.
- ¹³⁵Konstantinov Nuclear Physics Institute of National Research Centre "Kurchatov Institute", PNPI, St. Petersburg; Russia.
- ¹³⁶Department of Physics and Astronomy, University of Pittsburgh, Pittsburgh PA; United States of America.
- ^{137(a)}Laboratório de Instrumentação e Física Experimental de Partículas - LIP;^(b)Departamento de Física, Faculdade de Ciências, Universidade de Lisboa, Lisboa;^(c)Departamento de Física, Universidade de Coimbra, Coimbra;^(d)Centro de Física Nuclear da Universidade de Lisboa, Lisboa;^(e)Departamento de Física, Universidade do Minho, Braga;^(f)Departamento de Física Teórica y del Cosmos, Universidad de

- Granada, Granada (Spain);^(g)Dep Física and CEFITEC of Faculdade de Ciências e Tecnologia, Universidade Nova de Lisboa, Caparica; Portugal.
- ¹³⁸Institute of Physics of the Czech Academy of Sciences, Prague; Czech Republic.
- ¹³⁹Czech Technical University in Prague, Prague; Czech Republic.
- ¹⁴⁰Charles University, Faculty of Mathematics and Physics, Prague; Czech Republic.
- ¹⁴¹Particle Physics Department, Rutherford Appleton Laboratory, Didcot; United Kingdom.
- ¹⁴²IRFU, CEA, Université Paris-Saclay, Gif-sur-Yvette; France.
- ¹⁴³Santa Cruz Institute for Particle Physics, University of California Santa Cruz, Santa Cruz CA; United States of America.
- ¹⁴⁴^(a)Departamento de Física, Pontificia Universidad Católica de Chile, Santiago;^(b)Departamento de Física, Universidad Técnica Federico Santa María, Valparaíso; Chile.
- ¹⁴⁵Department of Physics, University of Washington, Seattle WA; United States of America.
- ¹⁴⁶Department of Physics and Astronomy, University of Sheffield, Sheffield; United Kingdom.
- ¹⁴⁷Department of Physics, Shinshu University, Nagano; Japan.
- ¹⁴⁸Department Physik, Universität Siegen, Siegen; Germany.
- ¹⁴⁹Department of Physics, Simon Fraser University, Burnaby BC; Canada.
- ¹⁵⁰SLAC National Accelerator Laboratory, Stanford CA; United States of America.
- ¹⁵¹Physics Department, Royal Institute of Technology, Stockholm; Sweden.
- ¹⁵²Departments of Physics and Astronomy, Stony Brook University, Stony Brook NY; United States of America.
- ¹⁵³Department of Physics and Astronomy, University of Sussex, Brighton; United Kingdom.
- ¹⁵⁴School of Physics, University of Sydney, Sydney; Australia.
- ¹⁵⁵Institute of Physics, Academia Sinica, Taipei; Taiwan.
- ¹⁵⁶^(a)E. Andronikashvili Institute of Physics, Iv. Javakhishvili Tbilisi State University, Tbilisi;^(b)High Energy Physics Institute, Tbilisi State University, Tbilisi; Georgia.
- ¹⁵⁷Department of Physics, Technion, Israel Institute of Technology, Haifa; Israel.
- ¹⁵⁸Raymond and Beverly Sackler School of Physics and Astronomy, Tel Aviv University, Tel Aviv; Israel.
- ¹⁵⁹Department of Physics, Aristotle University of Thessaloniki, Thessaloniki; Greece.
- ¹⁶⁰International Center for Elementary Particle Physics and Department of Physics, University of Tokyo, Tokyo; Japan.
- ¹⁶¹Graduate School of Science and Technology, Tokyo Metropolitan University, Tokyo; Japan.
- ¹⁶²Department of Physics, Tokyo Institute of Technology, Tokyo; Japan.
- ¹⁶³Tomsk State University, Tomsk; Russia.
- ¹⁶⁴Department of Physics, University of Toronto, Toronto ON; Canada.
- ¹⁶⁵^(a)TRIUMF, Vancouver BC;^(b)Department of Physics and Astronomy, York University, Toronto ON; Canada.
- ¹⁶⁶Division of Physics and Tomonaga Center for the History of the Universe, Faculty of Pure and Applied Sciences, University of Tsukuba, Tsukuba; Japan.
- ¹⁶⁷Department of Physics and Astronomy, Tufts University, Medford MA; United States of America.
- ¹⁶⁸Department of Physics and Astronomy, University of California Irvine, Irvine CA; United States of America.
- ¹⁶⁹Department of Physics and Astronomy, University of Uppsala, Uppsala; Sweden.
- ¹⁷⁰Department of Physics, University of Illinois, Urbana IL; United States of America.
- ¹⁷¹Instituto de Física Corpuscular (IFIC), Centro Mixto Universidad de Valencia - CSIC, Valencia; Spain.
- ¹⁷²Department of Physics, University of British Columbia, Vancouver BC; Canada.
- ¹⁷³Department of Physics and Astronomy, University of Victoria, Victoria BC; Canada.
- ¹⁷⁴Fakultät für Physik und Astronomie, Julius-Maximilians-Universität Würzburg, Würzburg; Germany.

¹⁷⁵Department of Physics, University of Warwick, Coventry; United Kingdom.

¹⁷⁶Waseda University, Tokyo; Japan.

¹⁷⁷Department of Particle Physics, Weizmann Institute of Science, Rehovot; Israel.

¹⁷⁸Department of Physics, University of Wisconsin, Madison WI; United States of America.

¹⁷⁹Fakultät für Mathematik und Naturwissenschaften, Fachgruppe Physik, Bergische Universität Wuppertal, Wuppertal; Germany.

¹⁸⁰Department of Physics, Yale University, New Haven CT; United States of America.

¹⁸¹Yerevan Physics Institute, Yerevan; Armenia.

^a Also at Borough of Manhattan Community College, City University of New York, NY; United States of America.

^b Also at California State University, East Bay; United States of America.

^c Also at Centre for High Performance Computing, CSIR Campus, Rosebank, Cape Town; South Africa.

^d Also at CERN, Geneva; Switzerland.

^e Also at CPPM, Aix-Marseille Université, CNRS/IN2P3, Marseille; France.

^f Also at Département de Physique Nucléaire et Corpusculaire, Université de Genève, Genève; Switzerland.

^g Also at Departament de Fisica de la Universitat Autonoma de Barcelona, Barcelona; Spain.

^h Also at Departamento de Física Teorica y del Cosmos, Universidad de Granada, Granada (Spain); Spain.

ⁱ Also at Departamento de Física, Instituto Superior Técnico, Universidade de Lisboa, Lisboa; Portugal.

^j Also at Department of Applied Physics and Astronomy, University of Sharjah, Sharjah; United Arab Emirates.

^k Also at Department of Financial and Management Engineering, University of the Aegean, Chios; Greece.

^l Also at Department of Physics and Astronomy, University of Louisville, Louisville, KY; United States of America.

^m Also at Department of Physics and Astronomy, University of Sheffield, Sheffield; United Kingdom.

ⁿ Also at Department of Physics, California State University, Fresno CA; United States of America.

^o Also at Department of Physics, California State University, Sacramento CA; United States of America.

^p Also at Department of Physics, King's College London, London; United Kingdom.

^q Also at Department of Physics, St. Petersburg State Polytechnical University, St. Petersburg; Russia.

^r Also at Department of Physics, Stanford University; United States of America.

^s Also at Department of Physics, University of Fribourg, Fribourg; Switzerland.

^t Also at Department of Physics, University of Michigan, Ann Arbor MI; United States of America.

^u Also at Giresun University, Faculty of Engineering, Giresun; Turkey.

^v Also at Graduate School of Science, Osaka University, Osaka; Japan.

^w Also at Hellenic Open University, Patras; Greece.

^x Also at Horia Hulubei National Institute of Physics and Nuclear Engineering, Bucharest; Romania.

^y Also at II. Physikalischs Institut, Georg-August-Universität Göttingen, Göttingen; Germany.

^z Also at Institucio Catalana de Recerca i Estudis Avancats, ICREA, Barcelona; Spain.

^{aa} Also at Institut für Experimentalphysik, Universität Hamburg, Hamburg; Germany.

^{ab} Also at Institute for Mathematics, Astrophysics and Particle Physics, Radboud University Nijmegen/Nikhef, Nijmegen; Netherlands.

^{ac} Also at Institute for Particle and Nuclear Physics, Wigner Research Centre for Physics, Budapest; Hungary.

^{ad} Also at Institute of Particle Physics (IPP); Canada.

^{ae} Also at Institute of Physics, Academia Sinica, Taipei; Taiwan.

^{af} Also at Institute of Physics, Azerbaijan Academy of Sciences, Baku; Azerbaijan.

^{ag} Also at Institute of Theoretical Physics, Ilia State University, Tbilisi; Georgia.

- ah* Also at Instituto de Física Teórica de la Universidad Autónoma de Madrid; Spain.
- ai* Also at Istanbul University, Dept. of Physics, Istanbul; Turkey.
- aj* Also at Joint Institute for Nuclear Research, Dubna; Russia.
- ak* Also at LAL, Université Paris-Sud, CNRS/IN2P3, Université Paris-Saclay, Orsay; France.
- al* Also at Louisiana Tech University, Ruston LA; United States of America.
- am* Also at LPNHE, Sorbonne Université, Paris Diderot Sorbonne Paris Cité, CNRS/IN2P3, Paris; France.
- an* Also at Manhattan College, New York NY; United States of America.
- ao* Also at Moscow Institute of Physics and Technology State University, Dolgoprudny; Russia.
- ap* Also at National Research Nuclear University MEPhI, Moscow; Russia.
- aq* Also at Physics Dept, University of South Africa, Pretoria; South Africa.
- ar* Also at Physikalisches Institut, Albert-Ludwigs-Universität Freiburg, Freiburg; Germany.
- as* Also at School of Physics, Sun Yat-sen University, Guangzhou; China.
- at* Also at The City College of New York, New York NY; United States of America.
- au* Also at The Collaborative Innovation Center of Quantum Matter (CICQM), Beijing; China.
- av* Also at Tomsk State University, Tomsk, and Moscow Institute of Physics and Technology State University, Dolgoprudny; Russia.
- aw* Also at TRIUMF, Vancouver BC; Canada.
- ax* Also at Universita di Napoli Parthenope, Napoli; Italy.
- * Deceased